GDL/GMF-91-01

Turbulent Premixed Hydrogen/Air Flames

by

S. Kwon, M.-S. Wu, J.F. Driscoll and G.M. Faeth

15 February 1991

Prepared for:

Department of the Navy

Office of Naval Research

Ocean Engineering Division, Code:1121

800 N. Quincy Street

Arlington, Virginia 22217-5000

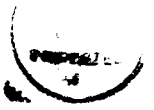

Contract No. N00014-87-K-0698

Steven E. Ramberg

Scientific Program Officer

SECURITY CLASSIFICATION OF THIS PAGE (When Data Entered)

REPORT DOCUMENTATION PAGE		READ INSTRUCTIONS BEFORE COMPLETING FORM
1. REPORT NUMBER	2. GOVT ACCESSION NO.	3. RECIPIENT'S CATALOG NUMBER
4. TITLE (and Subtitle) Turbulent Premixed Hydrogen-Air Flames		5. TYPE OF REPORT & PERIOD COVERED Final Report 8/1/87 to 12/31/90
		6. PERFORMING ORG. REPORT NUMBER GDL/GMF-91-01
7. AUTHOR(s) S. Kwon, M.-S. Wu, F.F. Driscoll and G.M. Faeth		8. CONTRACT OR GRANT NUMBER(s) N00014-87-K-0698
9. PERFORMING ORGANIZATION NAME AND ADDRESS Department of Aerospace Engineering The University of Michigan Ann Arbor, MI 48109-2140		10. PROGRAM ELEMENT, PROJECT, TASK AREA & WORK UNIT NUMBERS
11. CONTROLLING OFFICE NAME AND ADDRESS Office of Naval Research 800 North Quincy Street Arlington, VA 22217-5000		12. REPORT DATE April 1991
		13. NUMBER OF PAGES
14. MONITORING AGENCY NAME & ADDRESS(if different from Controlling Office)		15. SECURITY CLASS. (of this report) Unclassified
		15a. DECLASSIFICATION/DOWNGRADING SCHEDULE

16. DISTRIBUTION STATEMENT (of this Report)

Approved for public release; distribution unlimited.

17. DISTRIBUTION STATEMENT (of the abstract entered in Block 20, if different from Report)

18. SUPPLEMENTARY NOTES

19. KEY WORDS (Continue on reverse side if necessary and identify by block number)

Turbulent combustion, premixed flames, turbulent gas jets, isotropic turbulence, flame instabilities, numerical simulation

20. ABSTRACT (Continue on reverse side if necessary and identify by block number)

The properties of turbulent premixed flames were investigated both theoretically and experimentally. Attention was limited to hydrogen/air mixtures burning as either turbulent jet flames or as freely propagating flames in isotropic turbulence. The research has application to a variety of premixed turbulent combustion processes: underwater metal

DD FORM 1 JAN 73 1473 EDITION OF 1 NOV 65 IS OBSOLETE

S/N 0102-LF-014-6601

SECURITY CLASSIFICATION OF THIS PAGE (When Data Entered)

cutting at great depth, primary combustors for high-speed airbreathing propulsion systems, afterburners, fuel/air explosions, and spark-ignition internal combustion engines.

Studies of premixed turbulent hydrogen/air jet flames involved combustion within the nearly homogeneous potential core region for jet Reynolds numbers of 7000-40000. Measurements included the following: laser light sheet imaging for flame surface statistics, conditional laser velocimetry for gas turbulence properties, Rayleigh scattering for unreactedness, and flash schlieren photography for flow visualization. Predictions of flame structure were undertaken using both contemporary turbulence models and stochastic simulation. The stochastic simulation was developed during the present study and involved use of statistical time series techniques to simulate unburned gas velocities along the flame surface combined with a two-dimensional flame advection and propagation algorithm. Major findings of this phase of the investigation are as follows: (1) effects of preferential diffusion are relevent for flames at high Reynolds numbers, retarding and enhancing the distortion of the flame surface by turbulence for stable and unstable conditions, respectively; (2) local turbulent burning velocity, flame brush thickness and the fractal dimension of the flame surface all increase with distance from the flameholder, with larger rates of increase at larger turbulence intensities; (3) estimates of flame properties using contemporary turbulence models were only fair because these methods cannot account for effects of preferential diffusion, distance from the flameholder and finite laminar flame speeds; and (4) the stochastic simulation duplicated measured trends of flame surface fproperties for neutral preferential diffusion conditions (the only case considered) but underestimated effects of turbulence (particularly near the flame tip) due to the limitations of a two-dimensional simulation.

Work on freely propagating flames was limited to neutral preferential diffusion conditions. Experiments were carried out for spark ignited flames in isotropic turbulence within a fan stirred reaction vessel with turbulence Reynolds numbers in the range 1900-4200. Measurements included the following: laser light sheet imaging for flame surface statistics, two-point laser velocimetry for unburned gas turbulence properties, and flash schlieren photography for flow visualization. Predictions of flame structure were limited to the two-dimensional stochastic simulation. Major findings of this phase of the investigation are as follows: (1) local turbulent burning velocity, flame brush thickness and the fractal dimension of the flame surface all increased with time (distance) from the point of ignition, with larger rates of increase at larger turbulence intensities; (2) existing correlations of turbulent burning velocities and flame surface fractal dimensions are incomplete because they don't account for effects of time (distance) from the point of ignition; and (3) estimates of flame surface properties based on the two-dimensional simulation were reasonably good, using the artifice of doubling the velocity fluctuations to account for the limitations of a two-dimensional simulation.

Definitive evaluation of the stochastic simulation technique will require extension to a three-dimensional algorithm. Fortunately, extension to three dimensions is tractable, even for high Reynolds number flames, due to the computational efficiency of the velocity simulation.

ACKNOWLEDGEMENTS

The authors wish to thank the General Motors Corporation for the donation of the fan-stirred combustion chamber and E.G. Groff and T. Fansler of the General Motors Research Laboratories for useful discussions concerning the research. We also wish to acknowledge the assistance of the staff of the Gas Dynamics Laboratories of the Department of Aerospace Engineering: R.D. Glass, W. Eaton, G. Gould and T. Griffin for help with the experiments; and S. Bauerle for help with publications.

TABLE OF CONTENTS

LIST OF TABLES

LIST OF FIGURES

NOMENCLATURE

A_L	mean flame surface area
A_T	average surface area of wrinkled flame
D_2	fractal dimension of intersection of flame surface with a plane
D_3	fractal dimension of flame surface
d	burner exit diameter
ℓ_i	integral length scale based on velocity components i
ℓ_K	Kolmogorov scale
L_C	flame length based on a time-averaged unreactedness of 0.5
$O_2/(O_2+N_2)$	volumetric fraction of O_2 in nonfuel gas
P_L	mean flame perimeter
P_T	average perimeter of wrinkled flame
r_f	flame radius
Re_d	Reynolds number based on burner exit conditions, $\bar{u}_{o,\,avg}\, d/\nu_o$
Re_T	Reynolds number of turbulence, $\bar{u}_o'\, \ell_{uo}/\nu_o$
S_L	laminar burning velocity
S_T	turbulent burning velocity
$S_{T,eff}$	effective turbulent burning velocity
u	streamwise velocity
v	crosstream velocity
x	streamwise distance

Greek Symbols

α	thermal diffusivity
δ_L	laminar flame thickness
ε	ruler length for fractal property measurement

ν	kinematic viscosity
ϕ	fuel-equivalence ratio

Subscripts

avg	mean burner exit value
b,u	burned and unburned gas property
o	burner exit condition

Superscripts

$(\bar{})$,$(\bar{})'$	mean and r.m.s. fluctuating property

1. INTRODUCTION

This investigation considered the properties of turbulent premixed flames both theoretically and experimentally. Attention was limited to combustion of mixtures of hydrogen, oxygen and nitrogen because of interest in using premixed hydrogen/oxygen flames for underwater metal cutting processes at great depth where high pressures cause normally laminar cutting flames to become turbulent. However, the research also has application to a variety of other premixed turbulent combustion process; for example: primary combustors for high-speed airbreathing propulsion systems, afterburners, fuel/air explosions and spark-ignition internal combustion engines.

This is a final report of accomplishments during the investigation. The present report is brief, additional details can be found in other articles, papers and theses generated during the course of the work, see Table 1 for a summary. The articles by Wu et al. (1990, 1991a, b) and Kwon et al. (1991) are appended to provide a convenient reference. Finally, Kwon (1991) and Wu (1991) provide detailed descriptions of the research as well as complete tabulations of data.

The investigation was divided into two phases, one considering turbulent jet flames because they approximate the configuration of flames used in flame-cutting processes, the other considering freely-propagating flames in isotopic turbulence because this fundamental configuration simplifies the interpretation of results needed to gain a better understanding of turbulence/flame interaction. Highlights of each of these phases of the research are considered, in turn, in the following closing with a summary of the major conclusions of the study.

2. TURBULENT JET FLAMES

2.1 Introduction

Turbulent premixed flames are an important fundamental combustion problem with numerous practical applications; therefore, they have received significant attention in the past, see Wu et al. (1990, 1991a,b) and references therein for review of past work. Nevertheless, experimental and theoretical progress in the field has been limited. The main difficulties are that existing measurements either involve complex flows that are difficult to interpret or compute accurately, or they involve moderate Reynolds numbers where the degree of development of turbulence and the intrusion of buoyancy are not representative of turbulent flames. The objective of the present phase of the investigation was to help address these limitations by measuring the structure of turbulent hydrogen/air jet flames at high Reynolds numbers typical of practical applications. Hydrogen/air flames were studied due to their relevance to metal cutting and propulsion applications. Hydrogen/air flames also are of interest because they place unusual stress on concepts of modeling turbulent flames, e.g., they have unusually high laminar flame speeds and are subject to diffusive-thermal instabilities from the preferential diffusion of hydrogen. Thus, to help quantify the significance of these phenomena, the measurements were used to evaluate predictions of the process. All work was limited to the thin flamelet regime defined by Bray (1980), where the flame thickness is smaller than the smallest (Kolmogorov) scales of the turbulence, because this regime is most relevant to practical applications.

Hydrodynamic and diffusive-thermal (preferential diffusion) instabilities are the two main mechanisms of instability of premixed flames (Clavin, 1985). However, hydrodynamic instability is weak and has only been observed in special circumstances (Groff, 1982); therefore, it is generally agreed that preferential diffusion is responsible for

Table 1. Summary of Publications

Journal Articles:

Wu, M.-S., Kwon, S., Driscoll, J.F. and Faeth, G.M. (1990) Turbulent premixed hydrogen/air flames at high Reynolds numbers. Combust. Sci. Tech. 73, 327-350.

Wu, M.-S., Kwon, S., Driscoll, J.F. and Faeth, G.M. (1991) Preferential diffusion effects on the surface structure of turbulent premixed hydrogen/air flames. Combust. Sci. Tech., in press.

Kwon, S., Wu, M.-S., Driscoll, J.F. and Faeth, G.M. (1991) Flame surface properties of premixed flames in isotopic turbulence: measurements and numerical simulations. Combust. Flame, in press.

Wu, M.-S., Kwon, S., Driscoll J.F. and Faeth, G.M. (1991) Evaluation of stochastic simulations of premixed turbulent jet flames. Combust. Sci. Tech., submitted.

Papers:

Wu, M.-S., Kwon, S., Driscoll, J.F. and Faeth, G.M. (1988) Turbulent premixed hydrogen/air flames. Proceedings of the Twenty-First Fall Technical Meeting, Eastern Section of the Combustion Institute, Pittsburgh, pp. 2.1-2.4.

Wu, M.-S., Kwon, S., Driscoll, J.F. and Faeth, G.M. (1990) Visualization and analysis of the structure of high Reynolds number hydrogen-air premixed flames. AIAA 28th Aerospace Sciences Meeting, Reno, AIAA Paper No. 90-0161.

Kwon, S., Wu, M.-S., Driscoll, J.F. and Faeth, G.M. (1990) Flame surface properties of neutrally stable premixed flames in isotopic turbulence. Proceedings of the Twenty-Third Fall Technical Meeting, Eastern Section of the Combustion Institute, Pittsburgh, pp. 116-1 to 116-4.

Wu, M.-S., Kwon, S., Driscoll, J.F. and Faeth, G.M. (1991) Stochastic simulation of neutrally-stable premixed turbulent jet flames: measurements and predictions. Proceedings of the 1991 Spring Technical Meeting, Central States Section of the Combustion Institute, Pittsburgh, in press.

Theses:

Wu, M.-S. (1991) The surface structure of turbulent premixed hydrogen/air rim-stabilized flames at high Reynolds numbers. Ph.D. thesis, The University of Michigan, Ann Arbor.

Kwon, S. (1991) Flame surface properties of neutrally stable premixed flames in isotropic turbulence. Ph.D. thesis, The University of Michigan, Ann Arbor.

most observations of laminar flame instability. Within the thin flamelet regime, preferential diffusion instability involves the interaction between diffusion of a faster-diffusing reactant and the variation of laminar burning velocity with fuel-equivalence ratio (Manton et al., 1952). Reactants are consumed within a thin reaction zone so that the faster-diffusing reactant accumulates near bulges in the flame surface extending toward the reactants and is depleted from bulges extending toward the products. Thus, when the laminar burning velocity increases/decreases with increasing concentration of the faster-diffusing reactant, the bulges grow/decay and the flame is unstable/stable. Hydrogen is the faster-diffusing reactant in hydrogen/air flames, while the maximum laminar burning velocity is reached at a fuel-equivalence ratio (ϕ) of 1.8; therefore, these flames are stable/unstable for ϕ greater or less than 1.8.

Effects of preferential-diffusion instability have largely been studied to explain the instabilities of laminar flames, however, they also affect turbulent flames. Clavan and coworkers (1985) have studied this phenomenon for turbulent flames having large scale and low turbulence intensity. They found that turbulent distortion of the flame surface was chaotically enhanced for unstable conditions, while the flame acted like a high-pass filter, damping low-frequency deflections, for stable conditions. These studies involved only weak turbulence however, so that investigation of corresponding effects for practical turbulent flames is of significant interest.

Exact numerical simulation of premixed turbulent flames is too computationally intensive to be feasible for the foreseeable future (Pope, 1990); therefore, turbulence models and approximate numerical simulations have received significant attention (Bray, 1980; Pope, 1990). Among the turbulence models, Cant and Bray (1988) report a relatively advanced method that can allow for flame quenching by large levels of turbulent distortion (flame stretch); however, this approach has not been evaluated using measurements. Similarly, approximate numerical simulations have been described that models, remove many of the ad hoc features of turbulence (Ashurst and Barr, 1983; Ghoniem et al., 1980, 1983); however, these methods are still too computationally intensive to allow their evaluation using measurements from large Reynolds number turbulent flames.

The objectives of the present investigation were designed to help fill some of the existing gaps in the literature. Measurements were undertaken to provide the turbulence properties of the unreacted gas, and flame surface statistics, for high Reynolds number turbulent premixed round jet flames. These results were used to assess the relevance of preferential-diffusion phenomena for high Reynolds number flames and to evaluate predictions of the process. Two predictive methods were examined: (1) the contemporary turbulence model of Cant and Bray (1988), and (2) an approximate numerical simulation developed during the present investigation that has sufficient computational efficiency to be tractable for high Reynolds number turbulent flames.

2.2 Experimental Methods

Apparatus. The test apparatus consisted of a round coaxial burner where the outer burner flame provided a hot environment to stabilize the inner burner flame (which was the flame that was studied). The burners injected vertically upward with the inner burner flow being fully-developed turbulent pipe flow from a tube having an 11 mm inside diameter. The burners operated at atmospheric pressure with the exhaust products removed through a hood. Instruments were mounted rigidly so that the burner was traversed horizontally and vertically to access various points within the inner burner flame.

Instrumentation. Measurements involved flash schlieren photography for flow visualization, laser velocimetry to measure gas velocities and turbulence properties,

Rayleigh scattering to measure the extent of reaction and flame tomography to measure flame surface statistics. Flash schlieren photography is a well-known technique so only the other methods will be discussed in the following.

A dual-beam forward scatter laser-velocimeter (LV) was used to measure conventional time-averaged mean and fluctuating velocities in the flow, as well as conditional velocities and turbulence properties in the unreacted gas. Frequency shifting was used, when necessary, to control directional bias and ambiguity. The optical plane of the laser beams was rotated to measure streamwise and radial velocities. For overall flow measurements, the flow was seeded with aluminum oxide particles having a nominal diameter of 1 μm. Conditional velocity properties were found by seeding the flow with oil droplets having a nominal diameter of 1 μm: these drops vaporized at the flame front so that velocities were only measured in the unreacted gas.

The Rayleigh scattering arrangement was similar to Driscoll and Gulati (1988). The 488 nm line of an argon-ion laser was focussed at a point in the flame and the scattered light from the point was observed using a photodetector. The Rayleigh scattered light from the dense unreacted gas was much stronger than from the combustion products. Thus, the output was a telegraph signal yielding the fraction of time when reactants were present (the unreactedness) and the time-averaged frequency of shifting between reacted and unreacted states. All other statistical properties of a telegraph signal can be found from these two properties.

Flame tomography was used to find flame surface statistics. This involved seeding the reactants with oil drops having a nominal diameter of 1 μm which burned out in the flame front similar to the conditional LV measurements. The drops were illuminated with a 200 μm thick laser light sheet from a pulsed dye laser. The laser light scattered from the drops was photographed normal to the light sheet with the short duration of the pulsed laser (1μs) acting to stop the flow so that the edge of the drop containing region (the flame sheet) could be resolved. These records were processed using an image analyzer system to yield mean and fluctuating flame radius, the perimeter of the flame and the fractal dimensions of the flame surface (see Mantzaras et al. (1989) and Mandelbrodt (1982) for a discussion of fractal properties of flame surfaces). Orienting the optical system in the vertical and horizontal directions yielded corresponding flame surface properties.

Test Conditions. Two series of tests were conducted yielding a wide range of test conditions. Table 2 is a summary of test conditions for the second series which was used to evaluate effects of preferential diffusion and the performance of the approximate numerical simulation. All tests were in the thin flamelet regime where the smallest turbulent length scales (the Kolmogorov scales) are comparable or greater than the flame thickness. The tests involved ϕ = 0.8, 1.8 and 3.6, which are in the unstable, neutral and stable preferentral-diffusion regimes. The unstable and stable flame conditions involve identical laminar flame speeds and jet exit conditions so that differences between the properties of the flames provides direct evidence of effects of preferential diffusion. That such effects were observed can be seen directly from the flame lengths, L_c, summarized in Table 2; clearly, L_c is consistently shorter for the unstable than the stable flame showing that stable conditions reduce distortion of the flame surface by turbulence (and correspondingly the turbulent flame speed) so that longer flames are needed to complete the reaction.

Table 2. Summary of Turbulent Jet Flame Tests[a]

$\bar{u}_{o,avg}/S_L$	0.9			2.5		
ϕ	0.8	1.8	3.6	0.8	1.8	3.6
Preferential Diffusion Regime	Unstable	Neutral	Stable	Unstable	Neutral	Stable
$\bar{u}_{o,avg}$ (m/s)	20.4	31.1	20.4	55.0	88.0	58.3
$\bar{u}_{o,avg}$ (m/s)	2.0	3.1	2.0	5.5	8.8	5.8
S_L (m/s)[b]	2.2	3.5	2.3	2.2	3.5	2.3
$Re_d=\bar{u}_{o,avg}d/\nu_o$	11300	13900	7000	30600	39200	20000
$Re_T=\bar{u}_{o,avg}\,\ell_{uo}/\nu_o$	313	389	194	861	1104	562
L_c/d	2.6	2.6	2.8	4.0	5.3	7.7
$\ell_K(\mu m)$	42	35	60	20	16	27
$\delta_L=\alpha_o/S_L(\mu m)$	19	17	35	19	17	35
Flame regime[c]	Wrinkled thin flamelets			Mixing-limited thin flamelets		

[a]Round jet burner (d = 11 mm) directed vertically upward with ℓ_{uo} = 3.1 mm
[b]Laminar flame speeds from Andrews and Bradley (1973).
[c]Based on definitions from Bray (1980).

2.3 Theoretical Methods

Turbulence Model. Theoretical methods evaluated using the new measurements were based on procedures of turbulence models and approximate numerical simulation. The turbulence model involved a Favre-averaged formulation along the lines of Cant and Bray (1988) with some features drawn from earlier work in this laboratory, see Wu et al. (1990) for specific details. Major assumptions were as follows: boundary-layer approximations apply, steady (in the mean) axisymmetric flow with no swirl, low Mach number flow with negligible potential and kinetic energy changes, negligible radiant energy exchange, equal exchange coefficients of all species and heat, high Reynolds number flow so that laminar transport is negligible in comparison to turbulent transport, negligible effects of buoyancy on turbulence properties and infinitely-thin flame sheet separating the burned and unburned gases. These assumptions are either representative of the conditions of the experiments or are typical of contemporary turbulence models of premixed flames.

Initial conditions for the computations, at the burner exit, were taken to be fully-developed turbulent pipe flow having properties drawn from references cited in Hinze (1975). The formulation of Cant and Bray (1988) accounts for quenching due to turbulent

distortion of the flame surface, parameters needed for this approach involved laminar flame speeds from Andrews and Bradley (1973), specific recommendations from Cant and Bray (1988), and a fit of present measurements at one test condition — see Wu et al. (1990).

Approximate Numerical Simulation. Turbulent flame propagation was numerically simulated using statistical time series simulation of the velocity field of the unburned gas combined with a flame advection and propagation algorithm. The simulation of the velocity field was based on conventional statistical time-series methods (Box and Jenkins, 1976) but extended similar to earlier work in this laboratory (Kounalakis et al., 1991; Parthesarathy and Faeth, 1990) to treat a multidimensional process, see Kwon (1991) for a derivation of the procedure for two-and three-dimensional time-dependent velocity fields. The flame advection and propagation algorithm was taken from the MIMOC computer program of Ghoniem et al. (1983), which is limited to a two-dimensional time-dependent simulation. This is a major limitation for treating fundamentally three-dimensional time-dependent turbulence, however, assessing the present approach is justified before undertaking the significant extension required to treat three-dimensional effects.

Other major assumptions of the approximate numerical simulations are as follows: constant-pressure turbulent deflagration wave, infinitely-thin flame sheet, turbulence properties of the unburned gas are stationary and are unaffected by the presence of the flame, the flame is neutrally-stable with negligible effects of quenching (i.e., relative to the unburned gas, the flame propagates normal to its surface at the laminar burning velocity). The assumptions of constant pressure, thin flames, neutral stability, attachment points near the burner rim and turbulence properties unaffected by the flame were all conditions of the experiments used to evaluate these simulations. Neglecting quenching was also reasonable because the flames were at the maximum laminar burning velocity condition, well away from flammability limits, and values of the relative turbulence intensity, $\bar{u}'/S_L$, were relatively small.

Statistical simulations of the velocity field can be designed to satisfy any number of the statistical properties of turbulence but priorities must be set to control computation and computer memory requirements. Thus, present calculations were limited to simulating mean velocities, Gaussian probability density functions of velocity fluctuations, and temporal and spatial correlations. The correlations were approximated by exponential functions because this yields a Markov-like simulation that vastly simplifies computations (Box and Jenkins, 1976; Kwon et al., 1991). It was also assumed that correlations between the important nearest neighbors in space and time were locally homogeneous and could be decomposed as products of correlations in each coordinate direction. Under these approximations, the simulation of velocity fluctuations at a particular point only involves results at the seven nearest neighbors while still satisfying correlations over all space and time (exactly for homogeneous isotropic turbulence, and within 30 percent for locally-homogeneous turbulence).

2.4 Results and Discussion

Experimental Observations. Measurements of the velocity field within the unreacted gas indicated that flow properties approximated turbulent pipe flow at corresponding radial positions. This behavior follows because the present flames were relatively short so that the unreacted gas was largely within the potential core-like region of the flow. Additionally, variations of turbulence properties were not large over this region and approximated locally homogeneous flow (Wu et al., 1991a).

Initial flow visualizations using flash schlieren photography exhibited effects of preferential-diffusion (Wu et al., 1990). Aside from the flame length observations discussed

in connection with Table 2, the flame surfaces for stable conditions were much smoother than for unstable conditions when other properties were comparable. This implies that the preferential diffusion mechanism acts to suppress/enhance turbulent distortion of the flame surface even for high-Reynolds flames. These observations could be quantified by computing average turbulent burning velocities for the entire flame surface, $S_{T,eff}$. The resulting values of $S_{T,\,eff}/S_L$ are plotted as a function of effective relative turbulence intensities in Fig. 1. Values of S_L in these correlations are drawn from the measurements of Andrews and Bradley (1973). Results plotted in Fig. 1 are for ϕ = 0.8, 1.0, 1.8 and 3.6 for Re_d in the range 7000-40000. The results indicate that effective turbulent flame speeds fall on two branches: a neutral-unstable branch involving ϕ = 0.8, 1.0 and 1.8 and a stable branch involving ϕ = 3.57. The stable branch has substantially less response to increased turbulence levels (i.e., a smaller slope) than the neutral-unstable branch. Furthermore, even within the neutral-unstable branch, unstable conditions are somewhat more responsive to increased turbulence levels than the neutral condition. These trends clearly imply that diffusive-thermal phenomena retard turbulent distortion of the flame surface for stable conditions (thus reducing $S_{T,eff}$) and, to a lesser degree, enhance distortion for unstable conditions (yielding higher values of $S_{T,eff}$) for high Reynolds number turbulent flames. After finding this behavior, review of earlier measurements in the literature revealed similar trends for other fuels like H_2 - CH_4 /air, propane/air and iso-octane/air flames, as discussed by Wu et al. (1991a), see Abdel-Gayed et al. (1984) for a typical example. Thus, this behavior is not solely caused by the unusually high mass diffusivities of hydrogen but is also characteristic of any reactant mixture where the mass diffusivities of all species are not the same.

The effect of both preferential diffusion and the development of distortion of the flame surface with increasing distance from the flameholder can bee seen from the results illustrated in Fig. 2. This involves plots of flame surface area ratios, A_T/A_L, for unstable, neutral and stable conditions (burner exit conditions and laminar flame speeds are identical for the unstable and stable conditions, ϕ = 0.8 and 3.6). As discussed by Gouldin (1987), A_T/A_L is proportional to S_T/S_L at at modest stretch rates for neutral conditions, and approximately so for unstable and stable conditions. First of all, A_T/A_L is seen to progressively increase from values of unity at the flameholder (corresponding to laminar combustion) with increasing distance from the burner exit. This behavior is somewhat analogous to turbulent dispersion of particles where increased distance from the point of introduction of the particles allows the action of turbulence to increase the lateral spread of the particles. Also similar to effects of turbulent dispersion, the rate of increase of A_T/A_L is increased as the turbulence intensity increases. Effects of preferential diffusion can be seen by comparing results for ϕ = 0.8 and 3.6 which have identical values of $\overline{u}'/S_L$. The unstable flame generally has larger values of A_T/A_L at a given distance from the burner exit, reflecting the enhanced distortion of the flame surface for unstable conditions. However, the effect of growth of flame surface area with distance from the flameholder plays a role as well; for example, the stable flame extends farthest from the burner exit, due to lower levels of distortion near the burner, but eventually exhibits higher values of A_T/A_L than the rest at large distances from the burner exit.

A popular measure of the degree of wrinkeldness of flame tomographs is the fractal dimension, D_2 (Gouldin, 1987) which can be measured as described by Mandelbrot (1982). Results obtained from horizontal light sheet images are plotted in Fig. 3 for the same flame conditions as Fig. 2. Values of D_2 are seen to be influenced by height above the burner, $\overline{u}'_{o,avg}/S_L$ and effects of preferential diffusion instability, similar to A_T/A_L in Fig. 2. For all conditions, D_2 progressively increases with increasing distance from the burner exit. Near the burner exit, D_2 approaches unity, which is the value representative of a smooth grometrical surface (Mandelbrot, 1982) — corresponding to laminar like conditions mentioned earlier. This follows since the point of attachment is fixed along the periphery of

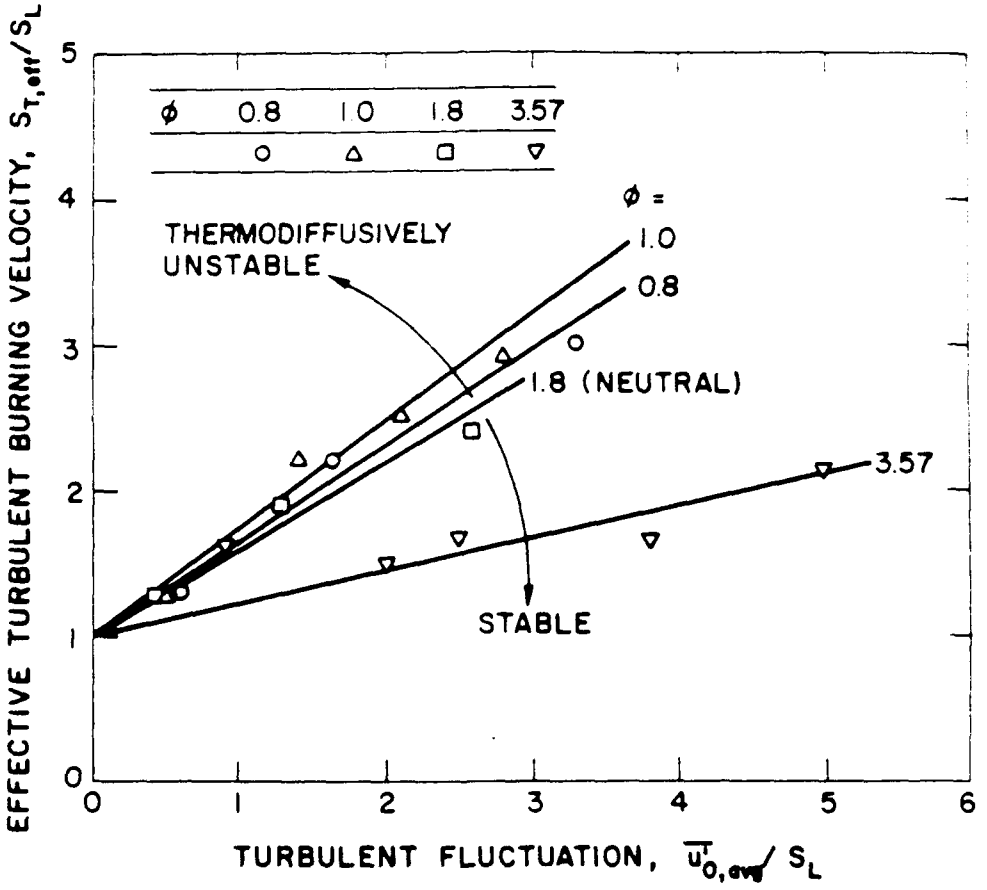

Fig. 1 Effective turbulent burning velocity of jet flames as a function of relative velocity fluctuations. From Wu et al. (1990).

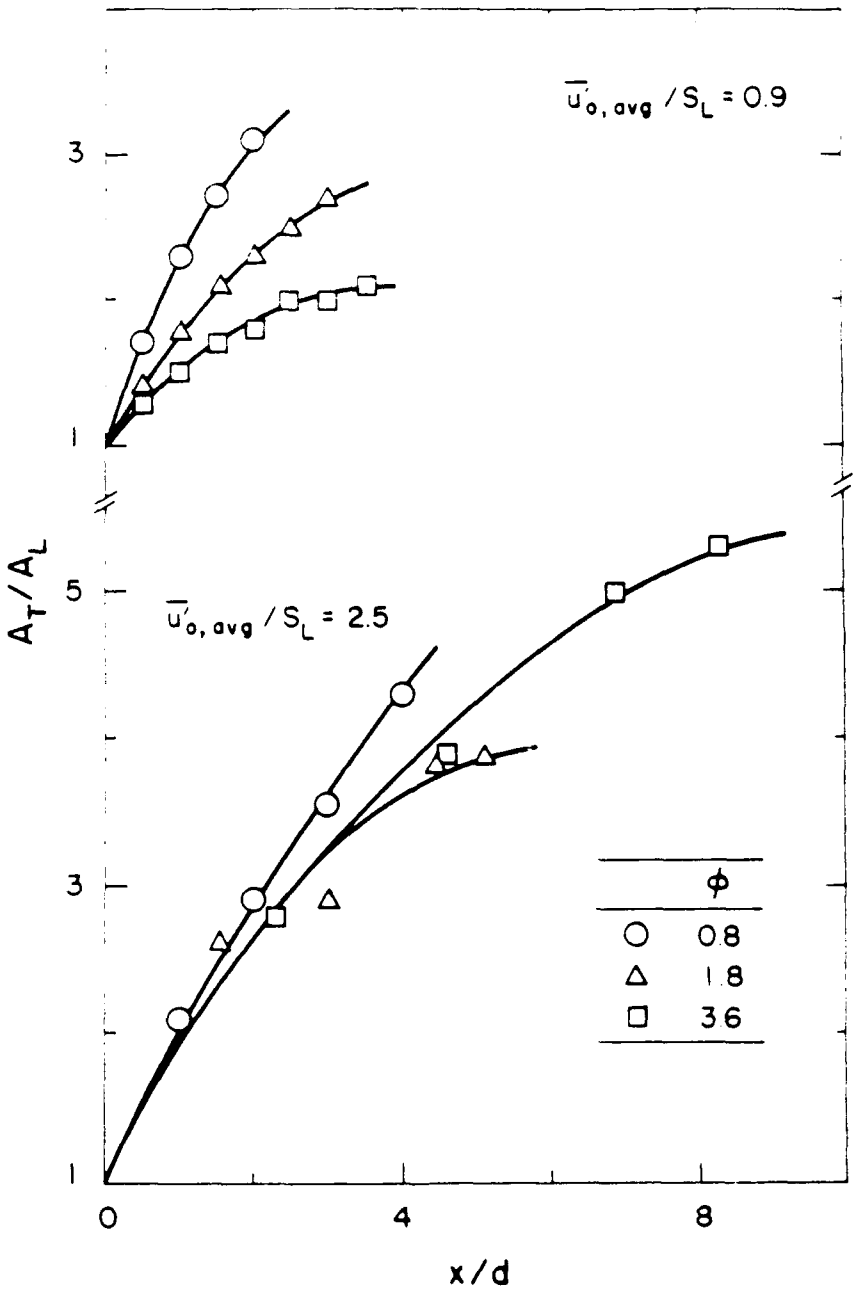

Fig. 2 Ratio of the turbulent to mean flame area as a function of distance from the flame holder for jet flames. From Wu et al. (1991a).

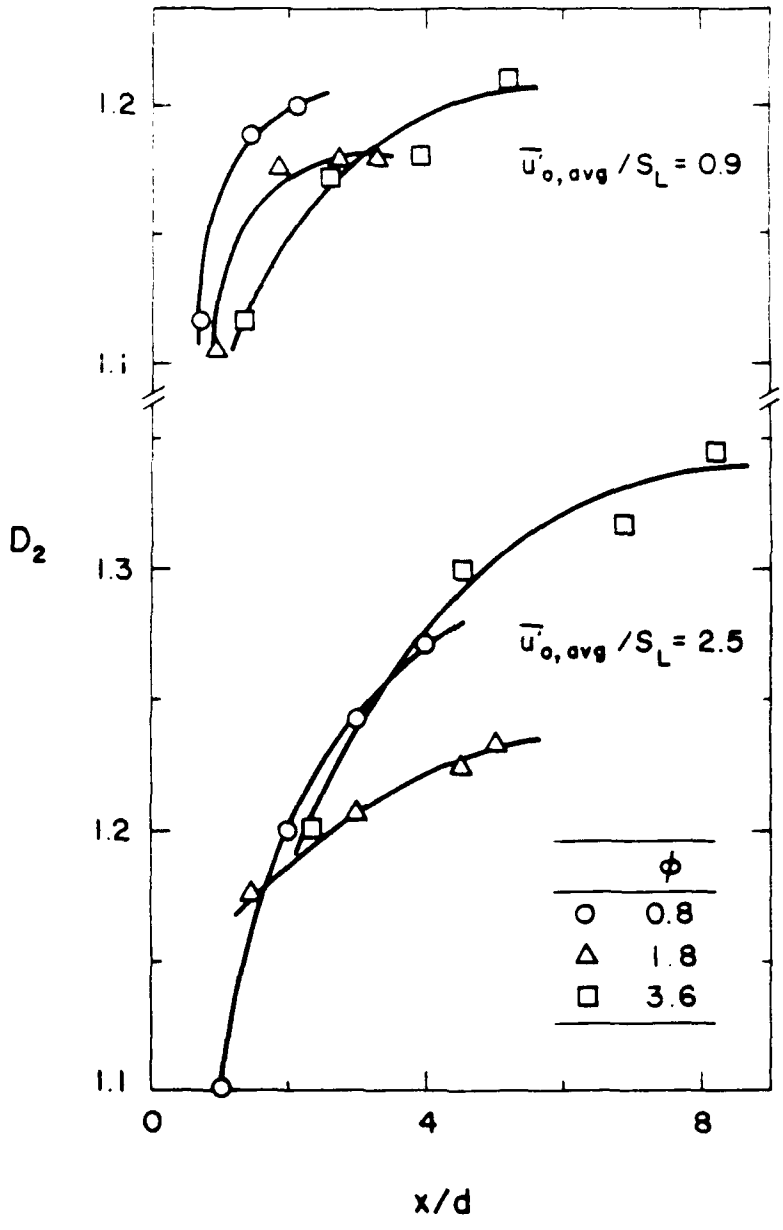

Fig. 3 Variation of fractal dimension, D_2, of flame surface with distance from the flame holder for jet flames. From Wu et al. (1991a).

the burner passage exit and the turbulence does not have sufficient distance (time) to distort the flame surface from this boundary condition. The subsequent increase of D_2 with distance is limited by two factors: the finite extent of the flame, so that the largest values of D_2 are associated with the longest flames; and the maximum distortion of surfaces in turbulent flows, which appears to be in the range D_2 = 1.3 - 1.4 (Gouldin, 1987; Mantzaras et al., 1989, Wu et al., 1991a). Notably, results for the longest flame in Fig. 3 appear to be approaching the limiting values of D_2 in spite of a relatively low value of $\overline{u}'_{o,avg}/S_L$ and the fact that this flame is stable. Effects of preferential diffusion also are are evident from the results plotted in Fig. 3. This is seen most readily for $\overline{u}'_{o,avg}/S_L$ = 0.9 where the initial rate of growth of D_2 is more rapid for ϕ = 3.6 (stable).

Taken together, present observations of the development of flame surface distortion and preferential diffusion preclude notions that flame surface properties on based solely on local conditions and only involve passive propagation of the flame at a fixed laminar flame speed (except for conditions where effects of quenching are small at the singular neutral preferential diffusion state). Thus, early correlations of S_T/S_L and D_2 (or $D_3 = D_2 + 1$) solely as a function of $\overline{u}'/S_L$ were found (Abdel-Gayed et al., 1984; Mantzaras et al. 1989) because $\overline{u}'/S_L$ influences the rate of growth of these properties for limited ranges of flame sizes, however, effects of development of flame surface distortion with distance clearly are important as well. Additionally, preferential diffusion affects of the rate of growth of these properties, contributing to apparent scatter of such correlations even for fixed values of $\overline{u}'/S_L$ and flame sizes. Additionally, the growth of surface distortion with distance from a flameholder, even when turbulence properties remain nearly constant, obviously invalidates concepts that local properties alone affect turbulent combustion rates — ideas which are implicit in turbulence models of combustion that have been proposed thus far. That these effects have been observed in high Reynolds number flames implies that they are not just artifacts of laboratory experiments but must be considered in any useful theory or model of turbulent premixed combustion.

Theoretical Results. In view of the observations that were just discussed, it is not surprising that the comparison between predictions using the Cant and Bray (1988) turbulence model and present measurements were not very satisfying (Wu et al., 1990). Even after choosing one empirical parameter to fit measurements and predictions at a particular condition, the model was not very effective for predicting the trends of the results. The intrinsic difficulties are that the model does not account for effects of distance from the flameholder and preferential diffusion. Another problem is that existing turbulence models implicitly ignore effects of laminar flame speeds (implying that $\overline{u}'/S_L$ very large) which is not appropriate for both present test conditions and many practical applications. Finally, although the Cant and Bray (1988) approach allows for effects of local quenching, these effects were not large for present test conditions; therefore, this aspect of their approach was not really tested. Taken together, contemporary turbulence models will require extensive additional development to become effective for practical turbulent flames, in spite of extensive work on them in the past.

Due to the limited promise of turbulence models of premixed turbulent flames, the bulk of present theoretical work was devoted to approximate numerical simulations (Wu et al., 1991b). As a first step, considerations were limited to neutral-stability conditions and a two-dimensional time dependent simulation, as noted earlier. Simulated flame properties duplicated measured trends of the variation of flame surface properties and mean unreactedness with distance from the burner exit and relative turbulence intensity. However, effects of turbulence were underestimated — particularly near the flame tip — due to the limitations of a two-dimensional simulation (i.e., due to out of plane deflection of the thin region of unreacted gas near the flame tip). The simulations of freely propagating flames were less subject to this problem due to the relatively large-diameter

flame balls that were considered; therefore, evaluation of the approximate numerical simulation will be discussed in connection with these results in the next section. Nevertheless, present computations have established the computational feasibility of three-dimensional time dependent approximate simulations — even for high Reynolds number flames — so that the method clearly merits additional development.

3. TURBULENT FREELY-PROPAGATING FLAMES

3.1 Introduction

An experimental and theoretical study of free turbulent premixed flames at neutrally-stable preferential diffusion conditions is discribed. This problem is of interest because the constraints of flame holding and the complications of effects of preferential diffusion are absent, while the flame is subjected to the simplest hydrodynamic state of turbulence. The experiments involved hydrogen/air/nitrogen mixtures ignited within a fan-stirred combustion chamber. Measurements included flame tomography to find flame surface statistics and two-point laser velocimetry to find the turbulence properties of the unburned gas. Test conditions were in the wrinkled thin flamelet regime with turbulence Reynolds numbers in the range 0-4195, which are representative of the intense flames found in practical applications. Flame surface properties were numerically simulated using time-series simulation techniques (Box and Jenkins, 1976) with the simulations being evaluated using the new measurements.

Earlier measurements of premixed flames in isotropic turbulence have been reported, see Abdel-Gayed et al. (1984) and Kwon et al. (1991) for a discussion recent work along these line. The main distinction between the present measurements and earlier work is a greater emphasis on the evolution of measured flame surface statistical properties during propagation from the point of ignition and the absence of preferential diffusion effects. Additionally, it is hoped that the small rates of flame stretch in comparison to extinction conditions, the simple and well-characterized turbulence field, and the information on flame surface development, will be useful for developing and evaluating models of the process. As discussed in connection with the turbulent jet flames, the present approximate numerical simulation represents a significant departure from methods reported in the past — e.g., Ashurst and Barr (1983), Ghoniem et al. (1980, 1983), Pope (1990) — that has significant potential to treat practical turbulent premixed flames due to its computational efficiency.

3.2 Experimental Methods

Apparatus. The fan-stirred combustion chamber was developed by Groff (1987) based on an original concept of Semenov (1965). A similar arrangement was used by Abdel-Gayed et al. (1984). The chamber is quasi-spherical with a 260 mm crossectional diameter at the center. Optical access was provided by two 92 mm diameter windows in the end wall and two 10 mm diameter windows in the side walls (each pair of windows mounted opposite one another). The isotropic turbulent field was generated by four fans mounted at 90° intervals along the periphery of the chamber with the fan flows directed toward the walls. Fansler and Groff (1990) show that this arrangement provides an istropic flow field in the central region of the chamber.

The combustible mixture was prepared by filling the chamber with hydrogen, nitrogen and air to appropriate partial pressure levels and then mixing the gas with the fans. The mixture was ignited by a spark at the center of the chamber. Measurements were limited to the period where the pressure increase within the chamber was small so that the

flames corresponded to constant pressure deflagration waves in an unreacted turbulent gas having constant properties.

Instrumentation. Measurements involved laser velocimetry to find the flow properties of the unreacted gas and flame tomography to find flame surface statistics. Both measurements involved adding small kerosene drops (nominal diameter less than 1 μm) to the unreacted gas; these drops disappeared at the flame surface as discussed earlier.

The laser velocimetry system was a dual-beam forward-scatter arrangement that provided both single-and two-point velocity statistics. Both measurements used frequency shifting to control directional bias and ambiguity with the laser beams rotated to measure velocity components in orthogonal (vertical and horizontal) directions. The single-point measurements were straight-forward and involved directing the laser beams and observing the measuring volume (in the forward scatter direction) through the large windows. The two-point measurements involved directing the laser beams at a small angle through the small windows to provide a measuring volume that was 70 mm long. Two points within this measuring volume were observed with two traversable detectors through the large windows to provide two-point measurements.

The flame tomography measurements were similar to the jet flames. A pulsed-dye laser was used to form a thin light sheet (200 μm thick) directed through one of the small side windows. The light sheet was observed normal to its plane from the one of the large windows using a 35 mm SLR camera whose exposure was controlled by the short duration of the laser pulse (1-2 μs). The boundary between the unburned and burned gas could be observed due to the absence of scattering from drops within the burned gas. This boundary was analyzed similar to the turbulent jet flames to find flame surface statistics.

Test Conditions. Test conditions for freely-propagating flames are summarized in Table 3. All tests were at $\phi = 1.8$, which is the neutral preferential-diffusion condition. Values of S_L were varied by varying the degree of dilution with nitrogen to yield $\bar{u}'/S_L$ in the range 0.48-1.60. The turbulence was well developed with turbulence Reynolds numbers in the range 1965-4195, representative of high intensity practical premixed turbulent flames. Characteristic flame thicknesses were generally an order of magnitude smaller than the Kolmogorov scale of the turbulence, which is characteristic of the thin flamelet regime.

3.3 Theoretical Methods

Turbulent flame propagation was numerically simulated using the flame advection and propagation algorithm from the MIMOC routine (Ghoniem et al., 1983), combined with a statistical time series simulation of flow velocities in the unburned gas. As noted earlier, MIMOC can only provide a two-dimensional time dependent simulation of flame surface motion. This is a major limitation but it was desired to evaluate the simplified simulation before extending it to treat three-dimensional effects.

Other major assumptions of the approximate numerical simulation are as follows: constant pressure deflagration wave; infinitely-thin flame sheet with constant unburned and burned gas scalar properties; stationary homogeneous isotropic turbulence in the unburned gas, unaffected by the presence of the flame; neutrally-stable flame with negligible effects of quenching, i.e., relative to the gas, the flame propagates normal to its surface at a constant laminar burning velocity; and mean velocity field in the unburned gas was found assuming that the flame acts like a spherically symmetric volumetric source. The constant pressure and thin flamelet assumptions are conditions of the experiments. The assumption that the turbulence properties of the unburned gas are not affected by the flame is an open

issue, although existing measurements suggest that the volumetric expansion of flame passively convects the turbulent field of the unburned gas away from the ignition source (Kwon et al., 1991). Neutral stability is a condition of the experiments while effects of quenching are not large because the present flames were well away from extinction conditions and had modest values of $\overline{u}'/S_L$. Finally, the volumetric source approximation yielded an excellent representation of mean velocities in the unreacted gas measured by laser velocimetry during turbulent flame propagation (Kwon et al., 1991).

Table 3. Summary of Turbulent Freely-Progagating Flame Tests[a]

$O_2/(O_2 + N_2)$	0.210	0.210	0.150	0.150	0.125
$\overline{u}'/S_L$	0.48	0.90	0.80	1.60	1.00
$\overline{u}'$(m/s)	1.2	2.4	1.2	2.4	1.2
S_L (m/s)[b]	2.5	2.5	1.5	1.5	1.2
$Re_T = \overline{u}'_o \, \ell_{uo}/\nu_o$	1965	3930	2095	4195	2320
ℓ_K (μm)	21	12	13	8	12
$\delta_L = \alpha_o/S_L$ (μm)	1.8	1.8	2.8	2.8	3.3

[a] Hydrogen, air and nitrogen mixtures at neutral preferential-diffusion conditions (ϕ = 1.8), in the thin flamelet regime, at 3 atm. and 298 ± 3K. The longitudinal integral length scale of the turbulence was 12.5 mm.
[b]From Lewis and von Elbe (1961).

The statistical simulation of the velocity field of the unburned gas was similar to the approach discribed for the jet flames. The computations simulated mean velocities, Gaussian PDF's of velocity fluctuations and temporal and spatial correlations. Cross correlations are zero and the locally-homogeneous approximation is not needed for isotropic turbulence. The temporal and spatial correlations were approximated as exponential functions: this is reasonably accurate for temporal and longitudinal spatial correlations but does not represent the negative portion of the Frenkiel function shape of the transverse correlation (Hinze, 1975; Tennekes and Lumley, 1972). Nevertheless, the approximation was adopted for the transverse spatial correlation as well, because the significant portion, where the values of the correlation are near unity, is approximately exponential. Similarly, because the high correlation region is of major interest, correlations were decomposed as products of correlations along each coordinate direction as discussed in connection with the jet flame simulation.

Under these approximations, the simulation of velocity fluctuations at a particular point only involves the seven nearest neighbors of the point in space and time for a two-dimensional time-dependent simulation (the 15 nearest neighbors for a three-dimensional time-dependent simulation). This arrangement provides a Markov-like process that simulates the decay of correlations, taken to be exponential functions, for all space and time. Kwon (1991) discusses evaluation of numerical accuracy of the method: for 4000 realizations, r.m.s. fluctuations were accurate within 5% and temporal and spatial

correlations were accurate with 30% (within two integral scales). A larger number of realizations would reduce the uncertainties of simulated properties.

A typical realization of the fluctuating velocity field for conditions where no flame is present is illustrated in Fig. 4. The effect of allowing for spatial and temporal correlations is evident from the cell-like structure with cell sizes comparable to integral scales; in contrast, simulation of only probability density functions yields a nonphysical random structure with points close to one another having velocities in different directions. In fact, the simulation of Fig. 4 bears a striking resemblance to the instantaneous turbulent velocity fields measured by Reuss et al. (1990) using particle-image velocimetry.

3.4 Results and Discussion

Unburned Gas Properties. The turbulence properties of the unburned gas were measured for all conditions used during testing. These measurements were completed in the absence of flame propagation. Within ±30mm from the center of the chamber, the results showed mean velocities less than 10% of velocity fluctuations, $\bar{v}'/\bar{u}'$ generally within 10% of unity, and variations of $\bar{u}'$ and $\bar{v}'$ with position less than 10%. Velocity fluctuations were proportional to the fan speed and relatively independent of the pressure. Spatial and temporal correlations approximated exponential functions, except for the crosstream spatial correlation at large distances as discussed earlier. The spatial integral scale based on streamwise fluctuations was 12.5 mm, relatively independent of position and fan speed, within ± 30 mm from the center of the chamber. Temporal integral scales were inversely proportional to the fan speed.

Measurements of mean radial velocities in the flow were obtained by ensemble averaging single-channel measurements made in the presence of propagating flames. These results yielded a excellent correlation with estimates for potential flow from a volumetric source, as follows (Kwon et al., 1991):

$$\bar{u} / (S_T (\rho_u / \rho_b - 1)) = (\bar{r}_f / r)^2 \qquad (1)$$

Results of Eq. (1) as well as the direct measurements of turbulence properties were used in the simulation to estimate flame surface properties.

Flame Surface Statistics. Typical flame tomographs for the present neutrally stable conditions at $\bar{u}'/S_L = 1.6$, which is the highest value considered, are illustrated in Fig. 5. The tomographs are for $\bar{r}_f = 15$, 30 and 45 mm. The results show a progressive increase of flame surface distortion with increasing radius (or time of propagation). This behavior is analogous to the progressively increasing distortion of the flame surface of premixed turbulent jet flames with increasing distance from the flameholder that was discussed earlier.

Simulated flame surfaces at $\bar{u}'/S_L = 1.6$ (the experimental value) and 3.2 also are illustrated in Fig. 5. Both simulations represent the trend that flame surface distortion increases with mean radios (time). The main effect of increasing $\bar{u}'/S_L$ is to increase the degree of distortion of the surface at particular values of $\bar{r}_f$ so that the larger $\bar{u}'/S_L$ yields a more irregular surface with finer-grained distortion. Both simulations are qualitatively similar to the flame tomographs, however, the small-scale distortions are better represented by the results for $\bar{u}'/S_L = 3.2$ (which is twice the experimental value). This is reasonable, because a two-dimensional simulation is expected to underestimate effects of true three-dimensional turbulent distortion. More quantitative assessment of the simulations will be undertaken in the following.

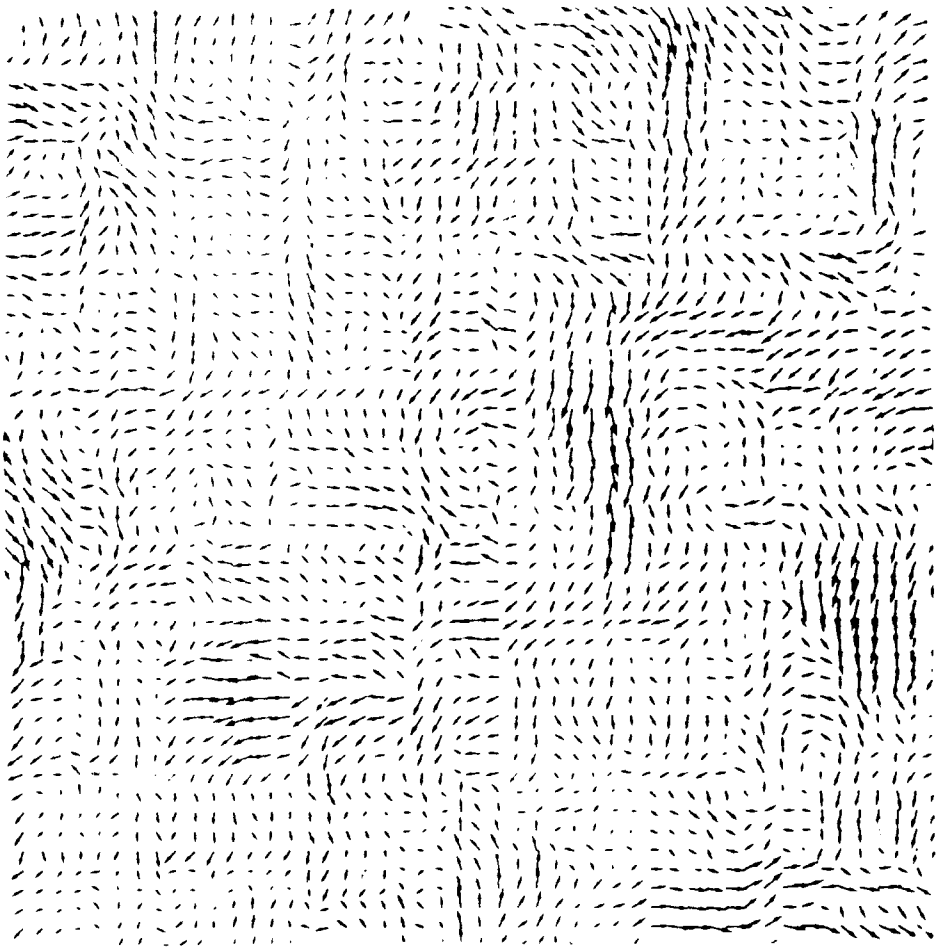

Fig. 4 Typical simulation of velocity fluctuation in istropic turbulence.

Measured and simulated values of the fractal dimension, $D_3 = D_2 + 1$, are plotted as a function of $\bar{r}_f$ in Fig. 6. At small $\bar{r}_f$, D_3 is nearly 2.0 which is representative of a smooth spherical spark kernel. The subsequent increase is due to progressive deformation of the flame surface by turbulence, somewhat analogous to the behavior of D_3 for turbulent jet flames with increasing distance from the flame holder. However, maximum values of D_3, are not large, generally less than 2.15. This is caused by the limited propagation time of present tests, which only corresponds to 0.4-1.3 times the integral time scale or distances of propagation into the unreacted gas mixture on the order of one spatial integral scale (the larger displacements of $\bar{r}_f$ being caused by effects of volumetric expansion). While the D_3 illustrated in Fig. 6 show monotonic growth in the early stages of flame growth that were observed, it is expected that D_3 would eventually approach values in the range 2.3-2.4 that are characteristic of passive isoclinic surfaces in isotropic turbulent fields. However, measurements at larger values of $\bar{r}_f$, or smaller spatial and temporal integral scales, are needed to confirm this behavior. The results do show, however, that the rate of increase of D_3 with distance increases as $\bar{u}'/S_L$ increases. Thus, correlations of D_3 as a function of $\bar{u}'/S_L$ have been found for flames of particular sizes (Mantzaras et al., 1987)but clearly do not account for the important effect of distance from the point of ignition.

Simulated values of D_3 in Fig 6 also exhibit a progressive increase with increasing flame radius. However, use of the experimental value of $\bar{u}'/S_L$ yields simulated values of D_3 that are significantly smaller than the measurements for each value of $\bar{r}_f$. However, doubling $\bar{u}'/S_L$ for the simulation yields a reasonably good estimate of the variation of D_3 with $\bar{r}_f$. A probable reason for this deficiency is that out of plane distortions of the flame surface, which should contribute to its irregularity, are suppressed by two-dimensional simulations.

Another measure of the distortion of flame surfaces by turbulence was found by measuring the perimeters of the flame surfaces. For present conditions, flame wrinkles are not large and it is reasonable to assume that surface properties are isotropic so that the wrinkled surface can be related to the perimeter as follows (Wu et al., 1991a):

$$A_T / A_L = 2 (P_T / P_L) - 1 \qquad (2)$$

Additionally, for neutral preferential diffusion conditions and modest stretch rates, A_T/A_L is a measure of S_T/S_L as noted earlier.

Measured and simulated values of P_T/P_L are plotted as a function of $\bar{r}_f$ in Fig 7. The measurements show that P_T/P_L is near unity for small values of $\bar{r}_f$, which is representative of the nearly smooth spherical spark kernel in this region. Similar to D_3, however, P_T/P_L progressively increases with increasing $\bar{r}_f$, with the rate of increase being more rapid as $\bar{u}'/S_L$ increases. Whether P_T/P_L, and thus S_T/S_L, eventually approaches an asymptotic value, even though D_3 reaches an asymptotic value, is a major open issue for premixed turbulent flames — tests involving longer progation times are needed to help resolve this important property. Associating P_T/P_L with S_T/S_L indicates that it increases with $\bar{r}_f$, with $\bar{u}'/S_L$ largely controlling the rate of increase, for laboratory scale measurements like those illustrated in Fig. 7. Thus, correlations of S_T/S_L solely as a function of $\bar{u}'/S_L$ are only appropriate for particular values of $\bar{r}_f$, as recently shown by Trautwein et al. (1990).

Because D_3 and P_T/P_L are closely related flame surface features, the comparison between measured and simulated values of P_T/P_L in Fig. 7 is similar to results for D_3 in Fig. 6. In general, the simulations yield the correct trends of P_T/P_L with increasing $\bar{r}_f$ and $\bar{u}'/S_L$ but quantitative agreement is only achieved by using values of $\bar{u}'/S_L$ roughly twice

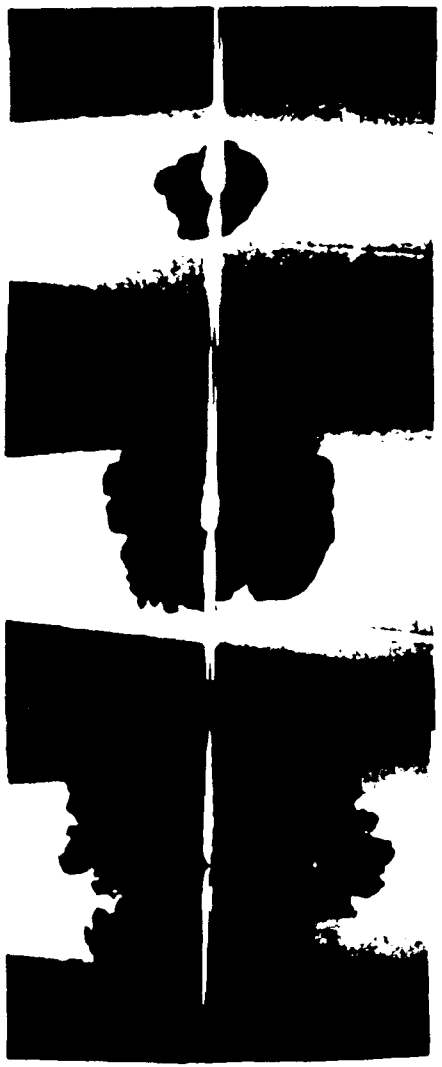

$u'/S_L = 1.6$ $u'/S_L = 1.6$ (SIM.) $u'/S_L = 3.2$ (SIM.)

Fig. 5 Observed and simulated flame surface images for freely-propagating flames: $O_2/(N_2+O_2) = 0.15$; $\bar{r}_f$ = 15, 30 and 45 mm. From Kwon et al. (1991).

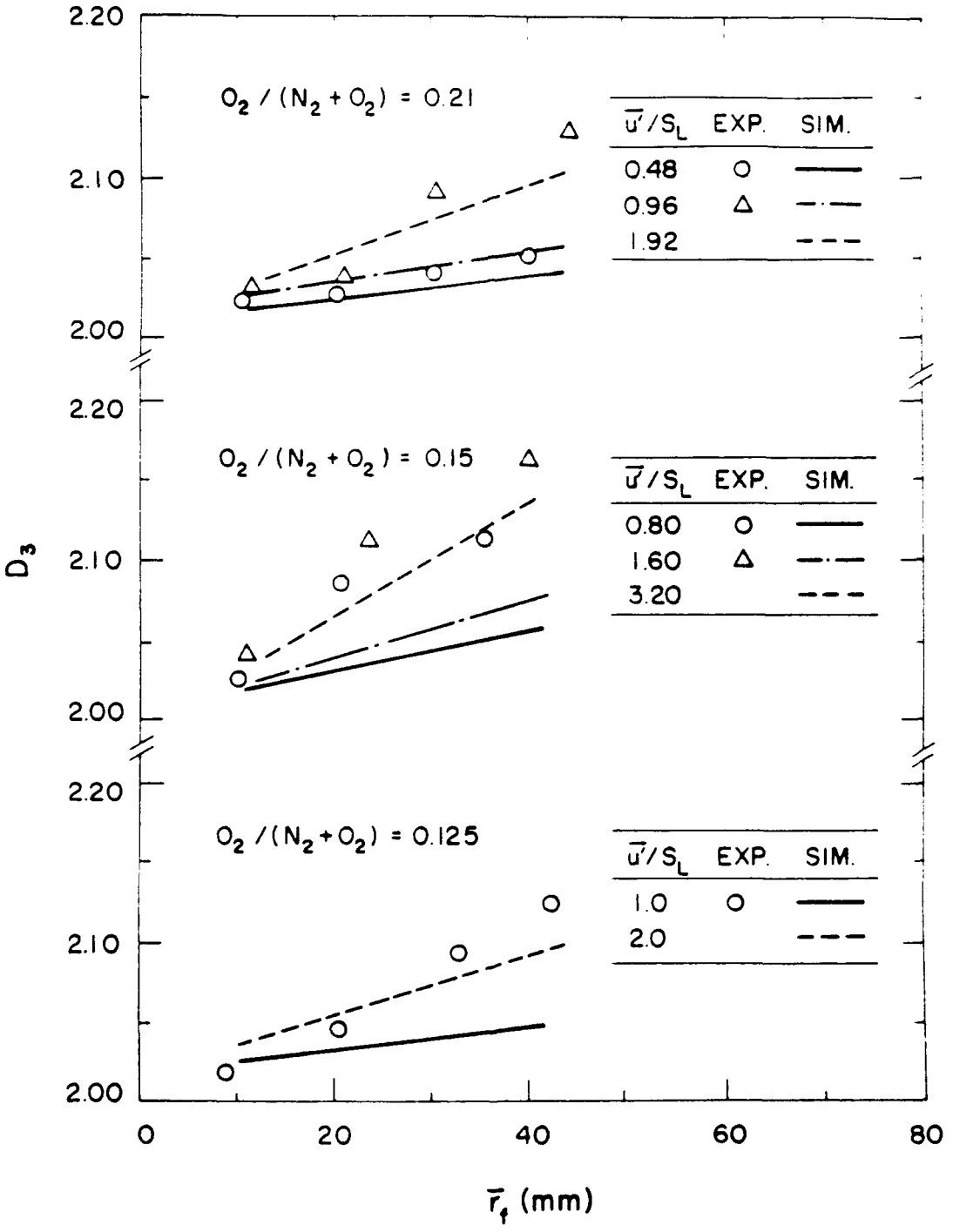

Fig. 6 Observed and simulated fractal dimension, D_3, of the flame surface as a function of flame radius for freely-propagating flames. From Kwon et al. (1991).

the experimental values. As before, the limitations of a two-dimensional simulation are the most probable cause of this difficulty.

4. CONCLUSIONS

A theoretical and experimental study of the properties of turbulent premixed hydrogen/oxygen/nitrogen flames was completed, considering both jet and freely-propagating flames at turbulence Reynolds numbers in the range 280-4200. The main conclusions of the study can be summarized as follows:

1. Effects of preferential diffusion are significant for high Reynolds number flames, acting to reduce/increase rates distortion of the flame surface (and correspondingly the local turbulent burning velocity) for stable/unstable conditions. Behavior at unstable conditions is of greatest interest for hydrogen/air or oxygen flames, used for propulsion or flame cutting applications, because lean or stoichiometric mixture ratios are used for these applications which is within the unstable regime. In contrast, behavior at stable conditions is of greatest interest for heavy-hydrocarbon/air flames,used for propulsion or automotive applications, because the relevant lean mixture ratios fall in the stable regime for these fuels.

2. Spatial variations of flame surface properties were quantified. As the distance from the flameholder or point of ignition increased, even though unburned gas turbulence properties were relatively constant, the following properties increased in value: flame surface area normalized by the mean flame area (and thus the local turbulent burning velocity), flame brush thickness, and the fractal dimension of the flame surface. However, at large distances, the fractal dimension approached values appropriate for isoclinic surfaces in isotropic turbulence, e.g., $D_3 = 2.3$-2.4, while approach to the flame tip limits the maximum value of the other properties for jet flames. These effects imply that turbulent premixed flames are geometry specific while the spatial variations imply that models or correlations of turbulent flame properties based on local properties alone, which don't specifically account for distance from the flameholder or point of ignition, are intrinsically incomplete, i.e., there is no basis for use of the local conditions hypothesis for the combustion rates of turbulent premixed flames.

3. Increasing values of turbulent fluctuations relative to the laminar burning velocity, $\overline{u}'/S_L$, tend to increase the rate of distortion of the flame surface with distance from the flameholder or point of ignition and also increases levels of fine-grained roughness of the flame surface. Thus, correlations of turbulent burning velocity and flame surface fractal dimension solely as a function of $\overline{u}'/S_L$ can be found because they reflect this rate of increased over limited ranges of flame dimensions. Nevertheless, such correlations are incomplete unless they account for development of flame surface properties with distance from the flameholder or point of ignition.

4. Estimates of turbulent jet flame properties based on a contemporary turbulence model due to Cant and Bray (1988), which allows for effects of flame stretch, yielded only fair agreement with measurements. The difficulties are attributed to effects of preferential diffusion and finite laminar burning velocities which are not considered in the model, and the use of the local conditions hypothesis which is intrinsically incomplete, as noted earlier.

5. The present two-dimensional numerical simulation successfully predicted the trends of flame properties with distance from the flameholder, or point of ignition, and $\overline{u}'/S_L$. Quantitatively accurate predictions near the base of the jet flames, or for freely

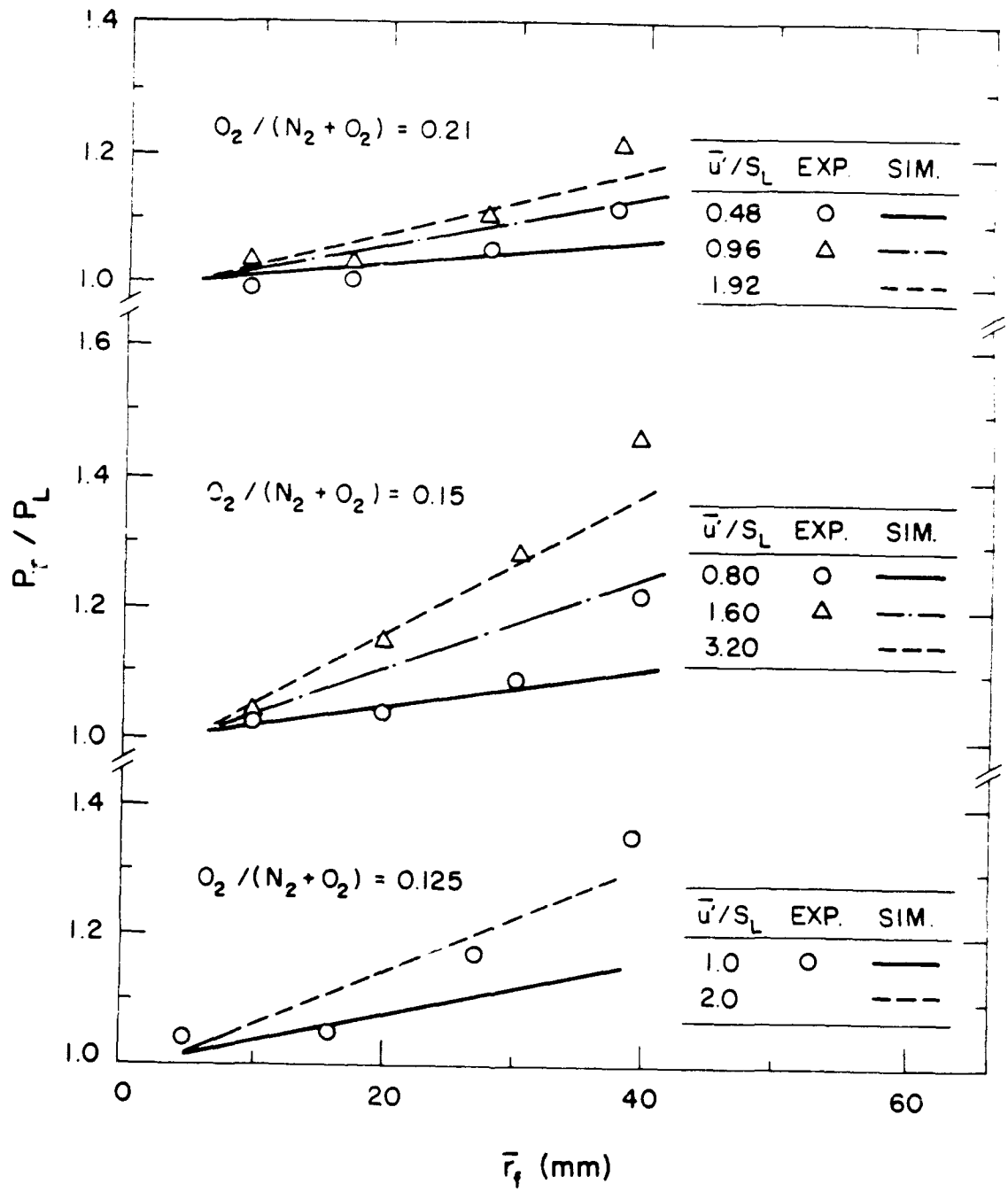

Fig. 7 Observed and simulated turbulent to mean flame perimeter as a function of flame radius for freely-propagating flames. From Kwon et al. (1991).

propagating flames having diameters larger than the integral length scale, could be obtained by the artifice of doubling $\overline{u}'/S_L$ in order to compensate for the limitations of a two-dimensional simulation of three-dimensional turbulence. However, the generality of this artifice is unknown and it is less effective where motion of the flame as a whole is significant, i.e., near the tip of jet flames or when the flame kernel is small for freely propagating flames.

6. Three-dimensional time-dependent simulations are needed to definitively evaluate the effectiveness of the present numerical simulations. Fortunately, extension to three dimensions is tractable, even for practical high Reynolds number flames, due to the computational efficiency of the present velocity simulation. Issues of modification of unburned gas turbulence properties by the flame, quenching and preferential diffusion still must be assessed. The present stochastic simulation provides a promising framework to consider these effects because the instantaneous flame surface is simulated, from which local flame curvature, stretch and flow acceleration can be found.

REFERENCES

Abdel-Gayed, R.G., Bradley, D., Hamid, M.N. and Laws, M. (1984) Lewis number effects on turbulent burning velocity. *Twentieth Symposium (International) on Combustion,* The Combustion Institute, Pittsburgh, pp. 505-512.

Andrews, G.E. and Bradley, D. (1973) Determination of burning velocity by double ignition in a closed vessel. *Combust. Flame* 20:77-89.

Ashurst, W.T. and Barr, P.K. (1983) Stochastic calculation of laminar wrinkled flame propagation via vortex dynamics. *Comb. Sci. Tech.* 34:227-256 .

Box, G.P., and Jenkins, G.M. (1976) *Time Series Analysis*, Holden-Day, San Francisco, CA, pp. 47-66.

Bray, K.N.C. (1980) Turbulent flows with premixed reactants. In P.A. Libby and F.A. Williams (Eds.), *Turbulent Reacting Flows,* Springer-Verlag, Berlin, pp. 115-183.

Cant, R.S. and Bray, K.N.C. (1988) Strained laminar flamelet calculations of premixed turbulent combustion in a closed vessel. *Twenty-Second Symposium (International) on Combustion*, Pittsburgh, pp. 791-799.

Clavin, P. (1985) Dynamic behavior of premixed flame fronts in laminar and turbulent flows. *Prog. Energy Combustion. Sci.* 11:1-59.

Driscoll, J. F. and Gulati, A. (1988) Measurement of various terms in the turbulent kinetic energy balance within a flame and comparison with theory. *Combust. Flame* 72:131-152.

Ghoniem, A.F., Chorin, A.J. and Oppenheim, A.K. (1980) Numerical modeling of turbulent combustion of premixed gases. *Eighteenth Symposium (International) on Combustion,* The Combustion Institute, Pittsburgh, pp. 1375-1383.

Ghoniem, A.F., Marek, C.J. and Oppenheim, A.K. (1983) Modeling interface motion of combustion (MIMOC), NASA TP-2132

Gouldin, F.C. (1987) An application of fractals to modeling premixed turbulent flames. *Combust. Flame* 68:249-266.

Groff, E.G. (1987) An experimental evaluation of an entrainment flame-propagation model. *Combust. Flame* 67:153-162.

Groff, E.G. (1982) The cellular nature of confined spherical propane-air flames. *Combust. Flame* 48:51-62.

Hinze, J.O. (1975) *Turbulence*, McGraw-Hill, New York, 2nd Ed., Chapt. 3.

Kounalakis, M.E., Sivathanu, Y.R. and Faeth, G.M. (1991) Infrared radiation statistics of non-luminous turbulent diffusion flames. *J. Heat Trans.*, in press.

Kwon, S., Wu, M.-S., Driscoll, J. F. and Faeth, G. M. (1991) Flame surface properties of premixed flames in isotropic turbulence: measurements and numerical simulations. *Combust. Flame*, in press.

Lewis, B. and von Elbe, G. (1961) *Combustion, Flames and Explosions of Gases*, 2nd Ed., Academic Press, New York, , pp. 381-384.

Mandelbrot, B.B. (1982) *The Fractal Geometry of Nature*. W. H. Freeman, San Francisco.

Manton, J., von Elbe, G. and Lewis, B. (1952) Nonisotropic propagation of combustion waves in explosive gas mixtures and development of cellular flames. *J. Chem. Phys.* 20:153-158.

Mantzaras, J., Felton, P.G. and Bracco, F.V. (1989) Fractals and turbulent premixed engine flames. *Combust. Flame* 77:295-310 .

Parthasarathy, R.N. and Faeth, G.M. (1990) Turbulent dispersion of particles in self-generated homogeneous turbulence. *J. Fluid Mech.* 22:515-537.

Pope, S.B. (1990) Computations of turbulent combustion: progress and challenges. *Twenty-Third Symposium (International) on Combustion*, The Combustion Institute, Pittsburgh, in press.

Reuss, D.L., Barkley, M., Felton, P.G., Landreth, C.C. and Adrian, R.J. (1990) Velocity, vorticity, and strain-rate ahead of a flame in an engine using particle image velocimetry. SAE Paper No. 900053.

Semenov, E.S. (1965) Measurements of turbulence characteristics in a closed volume with artificial turbulence. *Comb. Expl. Shock Waves* 1:57-62.

Tennekes, H. and Lumley, J.L. (1972) *Turbulence*, M.I.T. Press, Cambridge, pp. 67-70.

Trautwein, S.E., Grundo, A. and Adomeit, G. (1990) The influence of turbulence intensity and laminar flame speed on turbulent flame propagation under engine like conditions. *Twenty-Third Symposium (International) on Combustion*, The Combustion Institute, Pittsburgh, in press.

Wu, M.-S., Kwon, S., Driscoll, J.F. and Faeth, G.M. (1990) Turbulent premixed hydrogen/air flames at high Reynolds numbers. *Combust. Sci. Tech.* 73:327-350.

Wu, M.-S., Kwon, S., Driscoll, J.F. and Faeth, G.M. (1991a) Preferential diffusion effects on the surface structure of turbulent premixed hydrogen/air flames. *Combust. Sci. Tech.*, in press.

Wu, M.S., Kwon, S., Driscoll, J.F. and Faeth, G.M. (1991b) Evaluation of stochastic simulations of premixed turbulent jet flames *Combust. Sci. Tech.*, submitted.

APPENDIX A: WU ET AL. (1990)

Combust. Sci. and Tech. 1990 Vol. 73 pp. 327-350
Photocopying permitted by license only

Turbulent Premixed Hydrogen/Air Flames at High Reynolds Numbers

M. S. WU, S. KWON, P. E. DRISCOLL and G. M. FAETH *Department of Aerospace Engineering, The University of Michigan, Ann Arbor, Michigan 48109-2140*

(*Received July 24, 1989; in final form April 23, 1990*)

Abstract Measurements of mean and fluctuating reaction progress variable and streamwise velocities are reported for turbulent premixed hydrogen/air flames burning at relatively high Reynolds numbers (up to 18000, based on streamwise r.m.s. velocity fluctuations and integral length scales). A round jet geometry was used with the flame surrounded by a hot combustion gas environment at atmospheric pressure. Mixing-limited combustion was achieved; values of r.m.s. velocity fluctuations, normalized by the laminar burning velocity (u'/S_L), exceeded 15 in some instances. Test conditions included fuel equivalence ratios of 0.3–3.6 and burner exit Reynolds numbers (based on exit diameter) of 7000–40000 with fully developed turbulent pipe flow at the burner exit. It was found that effects of diffusive-thermal (preferential diffusion) phenomena were important, for both stable (fuel equivalence ratios greater than 1.8) and unstable conditions, even at the present high Reynolds numbers, for example, flame surfaces were more spiked and effective turbulent burning velocities for unstable conditions were twice as large as burning velocities for stable conditions having comparable normalized turbulence levels (u'/S_L). The measurements were used to evaluate contemporary turbulence models of premixed flames that are based on the laminar flamelet concept and which allow for effects of flame stretch; predictions yielded only fair agreement with measurements, partly due to the fact that the models ignore effects of finite laminar flame speeds and diffusive-thermal (preferential diffusion) phenomena that are found to be particularly important for hydrogen/air flames.

NOMENCLATURE

a	acceleration of gravity
c	reaction progress variable
C_i	constants in turbulence model
d	burner exit diameter
g	constant in reaction rate expression
G	generic property
I_q	flamelet quench integral
k	turbulence kinetic energy
l	integral length scale
l_K	Kolmogorov length scale
L_c	flame length based on $\bar{c}_c = 0.5$
r	radial distance
Re	burner exit Reynolds number
S_L	laminar burning velocity
$S_{T,\text{eff}}$	effective turbulent burning velocity
S_{c_i}	source term in governing equations
u	streamwise velocity
x	streamwise distance
v	radial velocity

Address Correspondence to G. M. Faeth, 218 Aerospace Engineering Building, The University of Michigan, Ann Arbor, MI 48109-2140

Greek Letters

α	thermal diffusivity
δ_l	laminar flame thickness
ε	rate of dissipation of turbulence kinetic energy
ε_q	rate of dissipation at quenching condition
μ_t	turbulent viscosity
ν	kinematic viscosity
ρ	density
σ	standard deviation of log normal distribution
σ_t	turbulent Prandtl/Schmidt number
$\lvert\sigma_s\rvert$	crossing angle factor
τ	heat release parameter
ϕ	fuel-equivalence ratio

Subscripts

avg	average value
c	centerline value
o	burner exit condition

Superscripts

$\tilde{(\ )}$	Favre-averaged mean property
$\bar{(\ )}$, $(\ )'$	time-averaged mean and r.m.s. fluctuating property

INTRODUCTION

Turbulent premixed flames are an important fundamental combustion problem with numerous practical applications; therefore, they have received significant attention in the past. Nevertheless, Libby *et al.* (1986) point out that additional measurements are needed to develop and evaluate theories of turbulent premixed flames. The main problems are that existing measurements either involve complex flow configurations that are difficult to compute accurately, or moderate Reynolds numbers where the degree of development of the turbulence and the intrusion of buoyancy may not be representative of practical flames. The objective of the present investigation was to help address these limitations by measuring the structure of turbulent hydrogen/air jet flames at high Reynolds numbers. Hydrogen/air flames were studied since they are of interest for several advanced propulsion and metal cutting applications and they place unusual stress on concepts of modeling turbulent flames, *e.g.*, they have unusually high laminar flame speeds and are subject to diffusive-thermal instabilities due to preferential diffusion of hydrogen. Thus, to help quantify the potential significance of these phenomena, the measurements were also used to evaluate predictions of contemporary turbulence models of the process.

Hydrodynamic and diffusive-thermal instabilities are the two main mechanisms of instability of premixed flames when effects of buoyancy are small (Williams, 1989). However, while hydrodynamic instability has been observed in special circumstances (Groff, 1982), it is generally agreed that most observations of laminar flame instability can be traced to diffusive-thermal effects (Markstein, 1951). The preferential-diffusion mechanism that is associated with diffusive-thermal instability is particularly relevant to the behavior of hydrogen/air flames due to the unusually high mass diffusivity of

hydrogen in comparison to other stable species in flames (Williams, 1985). Preferential diffusion involves the interaction between transverse diffusion of a faster-diffusing reactant and the variation of the laminar flame speed with the unreacted gas composition (Manton *et al*., 1952). Since the flame serves as a sink for reactants, the faster-diffusing species accumulates near upstream-pointing bulges in the flame surface and is depleted from downstream-pointing bulges. For fuel equivalence ratios at which the laminar flame speed increases with increasing concentration of the fast-diffusing constituent, the bulges grow and the flame is unstable. Hydrogen is the faster-diffusing constituent for hydrogen/air flames, therefore, these flames are unstable for fuel-equivalence ratios less than 1.8, at which the maximum laminar flame speed is reached (Andrews and Bradley, 1973; Lewis and von Elbe, 1961). Indeed, Andrews and Bradley (1973) and Halstead *et al*. (1974) have observed that certain fuel-lean hydrogen/air flames are unstable. The hydrogen/air system is somewhat unique in this respect: most other fuel/air systems have *maximum laminar flame speeds near a* fuel-equivalence ratio of unity, and most other fuels (except for methane) are heavier than air and are unstable for fuel-rich conditions.

Although diffusive-thermal phenomena have been primarily studied to explain instabilities of premixed flames propagating in laminar environments, they can still influence flames in turbulent environments where the flame surface is distorted by turbulent fluctuations. Clavin and coworkers have studied these effects using asymptotic analysis and measurements in turbulent flows having large scale and low intensity (Boyer *et al*., 1980; Clavin, 1985; Clavin and Williams, 1979, 1982; Searby and Clavin, 1986). Turbulent deflections of the flame surface were found to be chaotically enhanced for unstable conditions, in contrast, the flame acted like a high-pass filter, damping low-frequency turbulent deflections of its surface for stable conditions. The conditions of these studies involved only weak turbulence, however, and are rather far removed from highly-turbulent premixed flames; therefore, the importance of diffusive-thermal phenomena for practical turbulent flames, as shown in the following, has not been established previously.

Rigorous asymptotic analysis or exact numerical simulations have not progressed to the point where they can treat practical turbulent premixed flames; therefore, turbulence models have received significant attention (see Bray (1980), Cant and Bray (1988), Jones and Whitelaw (1982), Libby *et al* (1986) and references cited therein). These methods are generally limited to high Reynolds number turbulent flows at the laminar-flamelet limit where the reaction zone is thin compared to the smallest length scales of the turbulence. Initial work involved either eddy breakup ideas or thin laminar flamelets at the mixing-controlled limit where effects of the details of laminar flamelet structure are small (Bray, 1980). Recent methods, however, consider effects of quenching due to flame stretch — an important turbulence/chemistry interaction at high Reynolds numbers (Cant and Bray, 1988). Nevertheless, existing methods tacitly ignore effects of finite laminar flame speeds and diffusive-thermal phenomena that may be important in some instances. Furthermore, these methods involve many other approximations and empiricisms that have not yet been evaluated by comparison with measurements.

In summary, it is important to assess whether diffusive-thermal effects, which are known to be important at low Reynolds numbers, are also important at high Reynolds numbers. Do they enhance turbulent burning velocities for unstable conditions, decrease turbulent burning velocities at stable conditions, and are these effects significant enough so that they should be considered in models of turbulent premixed flames? Thus, the main objectives of the present investigation were to measure the structure of premixed hydrogen/air jet flames (which are likely to exhibit diffusive-thermal (preferential diffusion) phenomena) at high Reynolds numbers, and to use

these results to evaluate the predictions of contemporary turbulence models along the lines of Bray (1980) and Cant and Bray (1988). Test conditions were as follows: $0.3 \leq \phi \leq 3.57$, which involves both unstable and stable regimes for preferential diffusion instability; $7000 \leq Re \leq 40000$, which insures reasonably well-developed turbulence over the test range; $0.4 \leq \bar{u}'_{x=0}/S_l \leq 15.5$, to vary the relative importance of laminar and turbulent flame propagation effects; and $4 \leq \bar{u}_{x=0}/S_l \leq 155$, so that the boundary-layer approximations could be used to analyze the flow, since mean flame angles with respect to the streamwise direction were relatively small. Measurements included flash-Schlieren photography for flow visualization, Rayleigh scattering for the extent of reaction, and laser velocimetry for streamwise velocities. Some limited observations of premixed hydrogen/air flames were also undertaken in a fan-stirred bomb in order to gain insight concerning diffusive-thermal behavior.

The paper begins with descriptions of experimental and theoretical methods. Results of flow visualization in the fan-stirred bomb and the jet flames are then discussed. The paper concludes with consideration of measurements of the extent of reaction and velocities, and their comparison with predictions.

EXPERIMENTAL METHODS

Apparatus

Jet burner. Figure 1 is a sketch of the jet burner. A coaxial design was used, consisting of an inner round jet burner having a diameter of 11 mm and a tube length-to-diameter ratio of 50, to yield nearly fully developed turbulent pipe flow at the burner exit, and an outer burner having a diameter of 98 mm with the outer flame stabilized much like a flat-flame burner above a bed of beads and screens. The burners operated at atmospheric pressure with combustion products removed by a hood whose inlet was 1 m above the burner exit. Instruments were mounted rigidly, therefore, the burner was traversed in the radial (positioning accuracy of 10 μm) and vertical (positioning accuracy of 1000 μm) directions to measure flame structure.

All measurements were limited to the jet flame of the inner burner, while the outer burner flame only served to provide a hot environment to stabilize and reduce rates of entrainment of the jet flame. Since the velocities and mixture ratios of the outer and inner burners were not the same (as discussed later), there was a mixing layer between the two flows as sketched in Figure 1. The mixing layer was well outside the location of the jet flame of the inner burner, however, and had no observable influence on its flow and combustion properties (visualizations and measurements providing evidence of this behavior will be discussed later).

Hydrogen (99.95% purity) was supplied from commercial cylinders while dry air (dew point less than 240 K) was obtained from laboratory supplies. All gas flow rates were measured with rotameters, yielding a maximum uncertainty of fuel-equivalence ratios less than 12% at $\phi = 0.3$ with the proportionately lower values at higher fuel-equivalence ratios. The gases were mixed in a manifold and then flowed through long lines (length-to-diameter ratios of ca. 400) to achieve uniform mixtures at the burner inlets. In order to control flash-back, which was problematical due to the high flame speeds of hydrogen/air mixtures, flame arrestor screens were installed in the reactant lines of both burners at a location of 50 diameters upstream of the burner exit.

Fan-stirred bomb. The fan-stirred bomb is described by Groff (1987). It is similar to

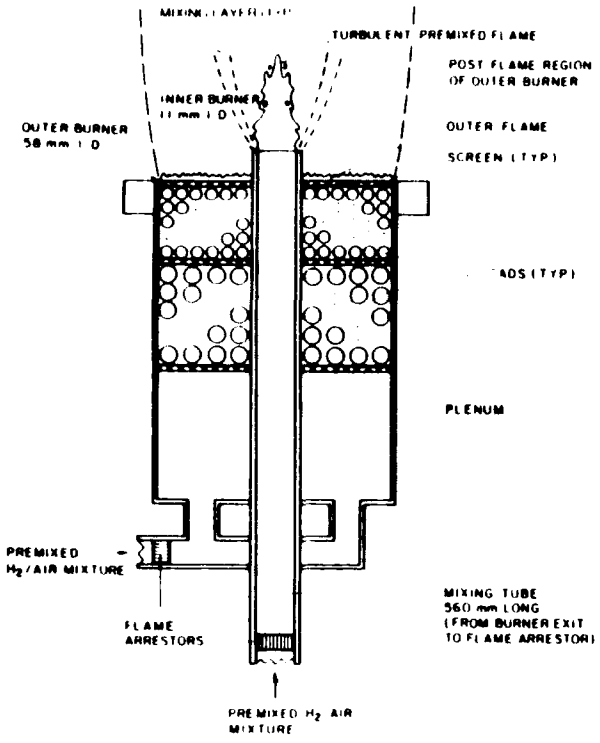

FIGURE 1 Sketch of the jet burner

the arrangement used earlier by Semenov (1965) and Bradley and coworkers (Abdel-Gayed *et al*., 1976, 1984; Andrews and Bradley, 1973). The chamber is quasi-spherical with a volume of 10 600 cc and a 260 mm crosssectional diameter at the center. Optical access is provided by two 92 mm diameter quartz windows mounted opposite one another. Turbulence was generated by four fans (8 bladed, blade diameter of 135 mm, pitch of 45°) located at 90° intervals around the periphery of the vessel. The fans directed their flow toward the center of the vessel and operated at rotational speeds up to 2400 rpm.

The hydrogen and air sources were the same as the jet flame experiments. The proper partial pressures of hydrogen and air were mixed together using the fans and the flame was spark ignited at the center of the vessel using electrodes extending from the top and bottom. The spark gap was roughly 3 mm while the sparks had a duration of 0.5 ms and stored energies of 0.3 mJ.

Fansler (1989) measured the properties of the turbulent field produced by the fans using laser velocimetry. The turbulence is nearly isotropic over a region having a diameter of 80 mm at the center of the vessel. Mean velocities are negligible while velocity fluctuations vary linearly with fan speed over the present test range (0.44 m/s at 600 rpm and 1.84 m/s at 2400 rpm) relatively independent of pressure. Hot-wire measurements during the present investigation confirmed these results at atmospheric pressure, within experimental uncertainties.

Flow visualization. Flash Schlieren photographs and cinematography were used to visualize the jet and bomb flames, respectively. Both arrangements used 102 mm diameter parabolic reflectors, having focal lengths of 1220 mm, to collimate the light beam and focus it on the knife edge. The light source for the jet flames was a Xenon Corp., Model 457, Pulsar Flashlamp, yielding 10 J per pulse with a 1 μs flash duration. The flash duration was short enough to stop the flame and flame luminousity was not a problem, therefore, single photographs were taken in a darkened room using an open-camera shutter with Type 52 Polaroid film (100 × 125 mm, fine-grained ASA 400).

The light source for the fan-stirred bomb was an EG&G Model 3CP4 flash lamp with a PS-450 power supply having with a light intensity of 1 mJ/flash and a flash duration of 1 μs. The lamp was synchronized with the motion-picture camera. The flash-Schlieren photographs were recorded with a 16 mm high-speed camera operating at roughly 1000 pictures per second, using Tri-X negative film.

Rayleigh scattering. The arrangement for the Rayleigh scattering measurements was similar to Gulati and Driscoll (1986). For hydrogen/air flames, Rayleigh-scattered light is a unique function of reactedness, within an accuracy of 3.7%. To measure the Rayleigh scattered light, the blue line of an argon-ion laser (488 nm with 2W of optical power) was focussed with a 80 mm focal length lens. The scattered light was collected at 90° from the laser beam using an f1.2 camera lens having a focal length of 85 mm. The collected light was then focussed on a photomultiplier tube (RCA 4526) through a laser-line filter (10 nm optical bandpass at 488 nm). The optical configuration yielded a measuring volume having a diameter of 250 μm and a length of 500 μm.

The output of the photomultiplier was amplified and low-pass filtered before digitization using a 14 bit A/D converter. The resulting signal was sampled at 50 kHz and stored as samples of 4096 records on a minicomputer. Since the hydrogen/air flames are thin, temporal records approximated telegraph signals as the measuring volume crossed between burned and unburned gas. At each location, the background signal and flame radiation were measured and found to contribute 6% to the Rayleigh signal and were subtracted. Shot noise also was determined at each location using a previously-measured calibration curve that related shot noise to the mean signal level. The shot noise contribution to the r.m.s. signal fluctuations was typically 8% and was subtracted; it does not contribute to the mean signal level. Several sets of records were processed to yield statistically-significant time-averaged mean and fluctuating reactiveness (defined as the fraction of time that burned gas was present). Uncertainties (95% confidence) of these measurements were dominated by gradient broadening and the finite number of samples that were processed; they are estimated to be less than 10%.

Laser velocimetry. The arrangement of the laser velocimetry system was modified slightly from Gulati and Driscoll (1986). A dual-beam forward-scatter arrangement was used based on the green line of an argon-ion laser (514.5 nm with 2 W of optical power). The optical arrangement yielded a measuring volume having a diameter of 200 μm and a length of 870 μm. The region where measurements were made involved relatively-high velocities (10–120 m/s) and relatively low turbulence intensities (less than 30%); therefore, it was not necessary to use frequency shifting to control directional bias and ambiguity.

TABLE I

Turbulent Jet Flame Test Conditions

ϕ	$\bar{u}_o$ (m/s)ᵃ	$\bar{u}_o/S_L$	L_f/d
$Re = 7000$, $Re_l = 280$			
0.30	10.9	[illegible]	6.1
0.65	12.1 (13.0)	0.7	
0.80	12.6	0.6	2.1
1.00	13.3	0.5	1.9
1.80	15.7	0.4	1.7
3.57	20.4	0.9	[illegible]
$Re = 20000$, $Re_l = 800$			
0.00	27.9 (28.5)		
0.30	31.0	[illegible]	[illegible]
0.80	36.0	1.6	3.7
1.00	37.9	1.4	3.2
1.80	45.0	1.3	3.3
3.57	58.3	[illegible]	2.7
$Re = 40000$, $Re_l = 1800$			
0.30	62.1	15.5	8.5
0.65	69.1 (66.0)	3.7	
0.80	77.0	3.3	5.4
1.00	75.8	2.8	4.8
1.80	90.0	2.6	5.3
3.57	116.4	5.0	11.7

Concentric tube burner: inner tube 11 mm inside diameter × 1 mm thick; outer tube 58 mm inside diameter × 3 mm thick. Outer flame: $\phi = 0.3$, $Re = 3400$, $\bar{u}_o = 1$ m/s. Hydrogen (99.98% purity)/air flames at atmospheric pressure.

ᵃ Based on measured flow rate. Numbers in parentheses denote LDA data averaged over burner exit. S_L from Andrews and Bradley (1973); $u'_{o,max}/\bar{u}_{o}$ taken to be 10%.

The jet flow was seeded with aluminum oxide particles having a nominal diameter of 1 μm. The Doppler signals were processed with a burst counter and stored on a minicomputer. Mean and fluctuating velocities were then computed as ensemble averages, ignoring effects of velocity bias, since these effects were found to be small. Uncertainties (95% confidence) of these measurements were dominated by finite sampling times; they are estimated to be less than 2% for mean velocities and 14% for velocity fluctuations.

Test conditions

Turbulent jet flame test conditions are summarized in Table I. Measurements were completed for jet Reynolds numbers ($Re = \bar{u}_o d/\nu_o$) of 7000, 20000 and 40000. These conditions correspond to turbulent Reynolds numbers ($Re_l = u'_{o,max} l/\nu_o$) of 280, 800 and 1800, where $l = 0.4d$, assuming fully developed turbulent pipe flow at the burner exit (Laufer, 1954). Fuel equivalence ratios were in the range 0.3–3.57 so that unstable ($\phi < 1.8$) and stable ($\phi > 1.8$) diffusive thermal conditions were considered. Values of $\bar{u}_o/S_L$ were in the range 0.44–15.52, to vary the relative importance of laminar and turbulent flame propagation effects. Additionally, $u'_{o,max}/\bar{u}_{o}$ at the burner exit was roughly 10%, so that $u'_{o,max}/S_L$ varied in the range 4–155; this generally yielded conditions where mean flame angles with respect to the streamwise direction were small so that the boundary layer approximations could be used to simplify predictions. Normalized flame lengths, L_f/d (based on the distance along the axis where $\xi = 0.5$) were in the range 1.7–11.7, and burner exit Richardson numbers were small (10^{-5}–10^{-3}); therefore, properties of the unburned gas were generally dominated by burner exit conditions. In the following, ϕ and Re will be used to identify particular flame results. However, it should be recognized that other fundamental flame properties ($u'_{o,max}/S_L$, $\bar{u}_{o}/S_L$, Re_l, etc.) vary when these parameters are changed, as summarized in Table I.

It was originally planned to operate the outer burner flame at the same fuel-equivalence ratio as the inner burner flame in order to provide an adiabatic combustion-gas environment for the inner flame that was being studied. However, this was found to be unnecessary. Present test conditions were well within the flammability limits for hydrogen/air flames; therefore, the properties of the outer flame had negligible influence on the structure of the inner flame, e.g., the structure of the inner flame did not change even when the outer flame was turned off completely for present test conditions. This followed even for fuel-rich conditions, since eventual oxidation of the fuel rich combustion products of the inner flame occurred in a diffusion flame within the mixing layer that was well separated from the inner premixed flame (except at the point of flame attachment near the burner exit), e.g., the diameter of the inner flame was in the range 0–d while the diameter of the mixing layer was in the range d–$3d$. Additionally, velocities within the unburned inner flame gases, that primarily control the structure of the inner flame, were little influenced by the ambient environment and generally preserved burner exit conditions for the present high Reynolds number inner burner flows (these results will be discussed later). Nevertheless, rather than operating the inner burner in an air environment, the outer burner was operated at $\phi = 0.3$ with an average burner exit velocity of 1 m/s for all test conditions. This preserved an adiabatic ambient environment for tests nearest flammability limits ($\phi = 0.3$), where the inner flame had largest diameters, and improved flow visualization and reduced entrainment rates to the inner flame, while controlling the costs of operating the outer burner over a lengthy test program.

Present test conditions are summarized on a flow regime map along the lines of Bray (1980) in Figure 2. Average jet exit conditions are used to define u' and l on the plots since the flames were dominated by unburned gas properties as noted earlier. Present tests are largely in the mixing limited thin flamelet regime ($\bar{u}' > S_L$,

Present test conditions are summarized on a flow regime map along the lines of Bray (1980) in Figure 2. Average jet exit conditions are used to define u' and l on the plots since the flames were dominated by unburned gas properties as noted earlier. Present tests are largely in the mixing limited thin flamelet regime ($u' > S_L$, $\delta_L < l_K$). However, results at higher Reynolds numbers for $\phi = 0.3$ are in the mixing limited thickened flame regime ($u' > S_L$, $\delta_L > l_K$) while measurements for $\phi > 0.8$ and $Re = 7000$ are in the wrinkled thin flamelet regime due to relatively low turbulence intensities and relatively high laminar flame speeds at these conditions.

Measured time averaged mean and fluctuating velocities near the burner exit are plotted as a function of radial distance in Figure 3. These measurements were made at $x/d = 0.18$, which was the position nearest the exit that could be completely traversed by the laser velocimetry system. Results are illustrated at all three Reynolds numbers for various values of ϕ; however, varying ϕ had little effect on the measurements. Measurements illustrated for $\phi = 0$ show that the flow was symmetric. Present mean velocity profiles are in good agreement with Nikuradse (1932) except near the edge of the flow where the developing mixing layer between the jet exit and the measuring location affects present measurements. Present measurements of turbulence intensities are somewhat higher than those of Laufer (1954), even in the region that is not affected by the mixing layer; however, these differences decrease as jet Reynolds numbers increase toward the value of 500000 used by Laufer (1954). In general, the results illustrated in Figure 3 suggest that present burner exit conditions approximate fully developed turbulent pipe flow at comparable Reynolds numbers.

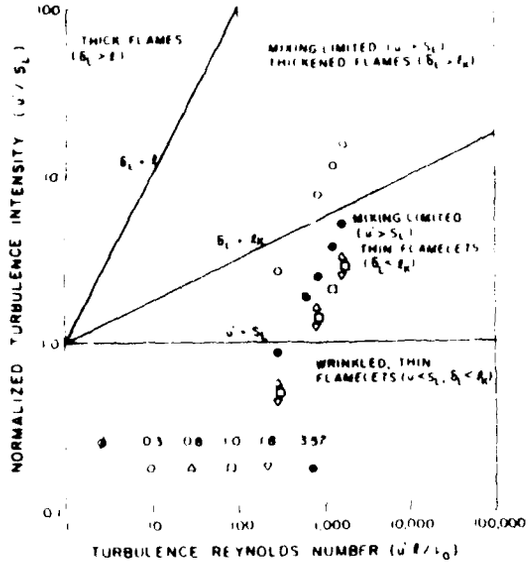

FIGURE 2 Turbulent flame regimes of the measurements

THEORETICAL METHODS

General description

Flame length and statistical properties were predicted using a Favre averaged turbulence model that is similar to that of Bray (1980) and Cant and Bray (1988), with some specific features from earlier work in this laboratory (Jeng and Faeth, 1984; Lee *et al.*, 1988). A major assumption was that the boundary layer approximations apply. Even though the present flames were relatively short, this assumption was reasonable since the ratio of the radius of the burner to the location where the flames reached the axis (roughly $2L_f$) was generally less than 0.1. This implies that mean flame angles with respect to the streamwise direction were relatively small. Furthermore, measurements (to be discussed later) showed that increases of streamwise velocity fluctuations in the region of the flames, which is indicative of significant streamwise turbulent transport (Bray *et al.*, 1985), were only significant for the two shortest flames studied ($Re_0 = 7000$ and $\phi = 1.0$ and 1.8; see Table 1). Thus, streamwise turbulent transport, which often involves effects of counter gradient diffusion, could be ignored while radial transport was treated using gradient diffusion approximations based on earlier calibrations for constant- and variable-density turbulent round jets (Jeng and Faeth, 1984).

Other major assumptions of the formulation are as follows: (1) steady (in the mean) axisymmetric flow with no swirl, (2) low Mach number flow with negligible potential and kinetic energy changes, and negligible viscous dissipation in the mean, (3) negligible effects of radiant energy exchange, (4) equal exchange coefficients of all

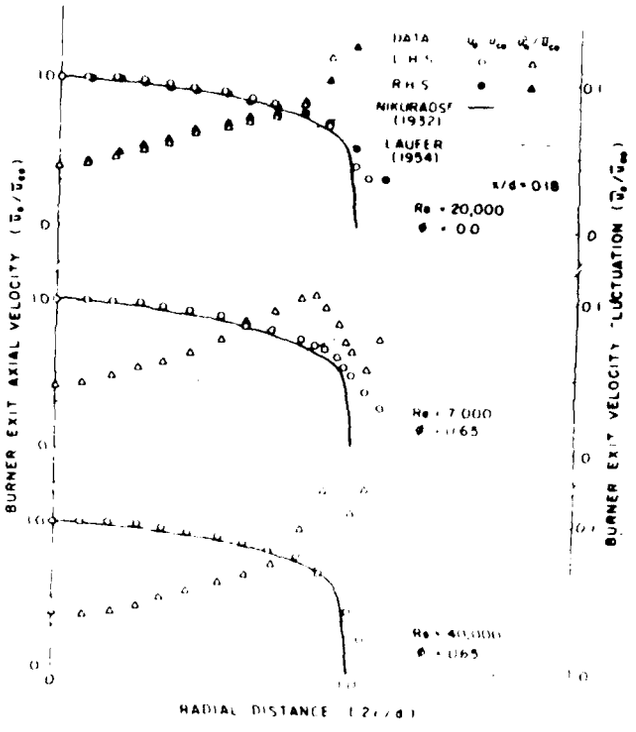

FIGURE 3 Streamwise mean and r.m.s. fluctuating velocities at the burner exit

species and heat, (5) high Reynolds numbers so that laminar transport is negligible in comparison to turbulent transport, (6) negligible direct effects of buoyancy on turbulence properties, and (7) instantaneous separation of the flow field into regions of burned and unburned gas by an infinitely thin flame. These assumptions are either representative of the conditions of the experiments or are typical of current turbulence models of premixed flames. For example, high burner exit velocities and short flame lengths imply small radiation numbers and thus negligible effects of radiant energy exchange. The assumption of equal exchange coefficients is widely used for turbulent flow while laminar transport, which would not satisfy this approximation due to the large mass diffusivity of the hydrogen, is not very important (aside from transport within the laminar flamelets that is not associated with bulk mixing) for Reynolds numbers on the order of 10^4. Furthermore, burner exit Richardson numbers are small (10^{-5} to 10^{-3}) and the flames are short, therefore, direct effects of buoyancy on turbulence properties are small. Finally, present test conditions are generally within the thin-flamelet regime as discussed in connection with Figure 2.

Formulation

Under these assumptions, Bray (1980) shows that flow properties can be found by solving governing equations for conservation of mass, momentum, and reaction

TABLE II
Source Terms in the Governing Equations

G	S								
1	0								
u	[illegible]								
[illegible]	[illegible]								
k	[illegible]								
[illegible]	[illegible]								
[illegible]	[illegible]								
[illegible]	[illegible]								
C_μ	[illegible]	[illegible]	[illegible]	[illegible]	σ_k	[illegible]	[illegible]	[illegible]	[illegible]
0.09	1.44	1.8[illegible]	1.8[illegible]	[illegible]	1.0	1.[illegible]	1.0	[illegible]	1.8
ϕ		[illegible]		0.8		1.0		1.8	[illegible]
[illegible]		0.4		[illegible]		[illegible]		[illegible]	2.[illegible]
[illegible] $\times 10^{[illegible]}$		0.4[illegible]		[illegible]		504		1050	14[illegible]

[a] From Andrews and Bradley (1973).
[b] [illegible]

progress variable, in conjunction with second order turbulence model equations for turbulence kinetic energy and its rate of dissipation. The governing equations then take the following general form (Bray, 1980; Jeng and Faeth, 1984; Lee *et al.*, 1988)

$$\frac{\partial}{\partial x}(\rho u G) + \frac{1}{r}\frac{\partial}{\partial r}(r\rho v G) = \frac{1}{r}\frac{\partial}{\partial r}\left(r\frac{\mu_t}{\sigma_G}\frac{\partial G}{\partial r}\right) + S_G \qquad (1)$$

where $G = 1$ (for conservation of mass), u, [illegible], k and ϵ. The turbulent viscosity was found as usual

$$\mu_t = C_\mu \rho k^2/\epsilon \qquad (2)$$

The boundary conditions for Eq. (1) involve symmetry at the axis and a constant property ambient environment, e.g.

$$r = 0, \frac{\partial G}{\partial r} = 0; \quad r \to \infty, \; G = 0 (G \neq [illegible]), [illegible] = 1 \qquad (3)$$

Since test results showed that the inner premixed flame considered during these computations was not affected by the properties of the outer burner flame, ambient gas properties of the inner flame were taken to be its combustion products. Initial conditions were defined at the burner exit where the flow was assumed to be fully-developed turbulent pipe flow, therefore, distributions of u, k and ϵ were obtained from Nikuradse (1932) and Laufer (1954), noting that time- and Favre-averaged quantities are identical for constant density flows and $\tilde{c} = 0$ by definition at the burner exit. The sensitivity of the predictions to variations of initial conditions, and to other parameters of the formulation, was examined and will be taken up later.

The source terms appearing in Eq. (1), S_G, are summarized in Table II, along with all empirical constants. Except for S_c, all source terms and empirical constants are identical to earlier computations for axisymmetric turbulent flows in the laboratory (Jeng and Faeth, 1984; Lee *et al.*, 1988). These empirical constants were selected to match predictions and measurements for various constant- and variable-density noncombusting single phase round jets and have yielded good predictions of the structure of turbulent jet diffusion flames (Jeng and Faeth, 1984); however, these values are not very different from early proposals of k–ϵ turbulence models (Lockwood and Naguib, 1975).

Turbulent reaction was treated in two ways: (1) the mixing limited approach used by Lee *et al.* (1988), and (2) the recent approach of Cant and Bray (1988) which provides for effects of flame stretch. The mixing limited approach is based on Bray (1980) for thin laminar flames [illegible] the laminar flame speed is small in comparison to velocity fluctuations. This yields the following source term for $\tilde{c}$

$$S_c = C_c \rho \epsilon [illegible] / k \qquad (4)$$

where $C_c = 1.8[illegible]$ from Lee *et al.* (1988).

The approach of Cant and Bray (1988) is far more complex and is summarized in Table II. Values of the laminar flame speed are needed; these were obtained from Andrews and Bradley (1973) and are listed in Table II. Other parameters are discussed by Cant and Bray (1988); [illegible] and [illegible] were based on their suggestions while matching predictions and measurements at [illegible] and $Re = 40000$. Matching other conditions was not possible without adopting values of [illegible], and [illegible] that were either beyond the ranges recommended by Cant and Bray (1988) or were not consistent with the measured laminar flame properties of Andrews and Bradley (1973).

Under the thin flame approximation the flow only has instantaneous burned and unburned gas states. The unburned state is an initial condition; the burned state was found by assuming thermodynamic equilibrium for adiabatic constant-pressure combustion at atmospheric pressure using the Gordon and McBride (1971) code. Under the thin flame approximation, c has a double delta probability density function and all mean and fluctuating scalar properties (including c) are only functions of their values in the burned and unburned gas and $\tilde{c}$; see Bray (1980) or Lee *et al.* (1988) for specific formulas.

Calculations

The calculations employed the GENMIX algorithm of Spalding (1978). Present results involved 30 radial grid nodes with streamwise step sizes limited to less than 3% of the current flow width or a 5% increase of the mass flow rate of the jet, whichever was smaller. Doubling the number of grid nodes changed predictions less than 1%; therefore, numerical accuracy generally exceeds expected uncertainties of other aspects of the predictions.

The sensitivity of the predictions to variations of parameters in the formulation was also studied. The most sensitive parameters were k_0, ϵ_0 and C_c, where 50% increases of these quantities caused [illegible]20, 20 and [illegible]7% variations in predicted values of L_f. Since k_0 and ϵ_0 are known reasonably well for fully developed turbulent pipe flow, while C_c was selected to match one set of measurements, these results suggest that the predictions are relatively insensitive to parameters in comparison to the limitations of turbulence modeling itself.

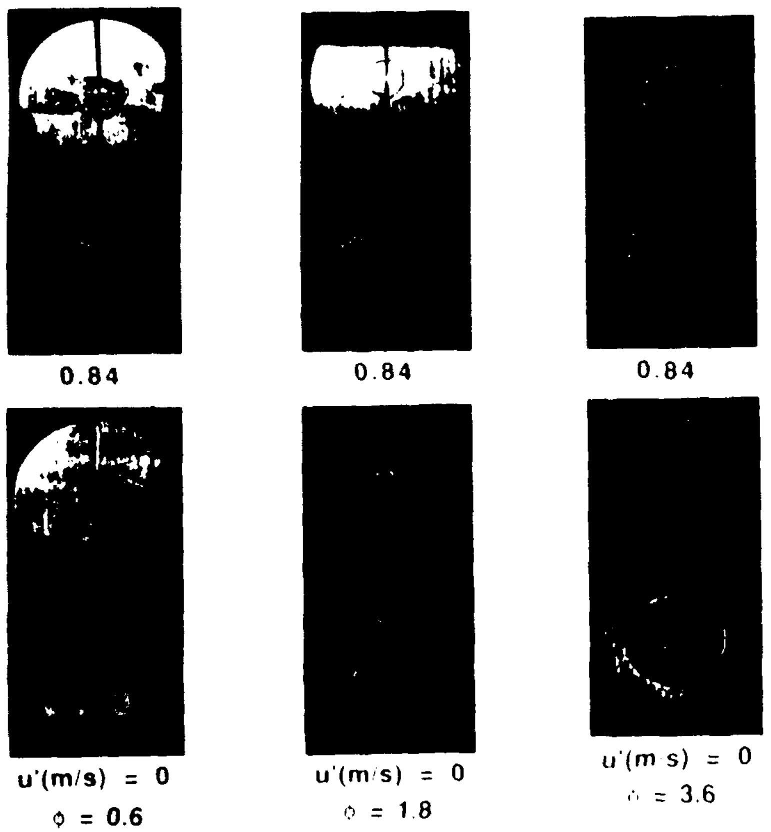

FIGURE 4. Flash Schlieren photographs of the flame within the fan-stirred bomb. Note: ϕ = 0.6, 1.8 and 3.6 correspond to unstable, neutral, and stable preferential diffusion conditions, respectively.

RESULTS AND DISCUSSION

Flow Visualization

Flash Schlieren photographs of combustion within the fan-stirred bomb provide a useful indication of diffusive thermal effects since both quiescent and turbulent conditions could be observed. Some representative results are illustrated in Figure 4. Photographs of the flame at two instants after ignition are illustrated for unstable (ϕ = 0.6), neutral (ϕ = 1.8) and stable (ϕ = 3.6) conditions at both quiescent and turbulent ($\bar{u}'$ = 0.84 m/s) conditions. At quiescent conditions, the flame surface is relatively smooth for neutral and stable conditions but becomes spontaneously wrinkled shortly after ignition for unstable conditions. When the reactants are turbulent, the turbulence causes a wrinkled flame surface for all conditions; the presence of

turbulence significantly increases the degree of distortion of the flame surface even for unstable conditions. However, diffusive thermal effects, analogous to those found by Clavin and coworkers (Clavin, 1985), can be seen by comparing the photographs for neutral and stable conditions. Neutral conditions presumably reflect the behavior of passive distortion of the flame surface by turbulence since diffusive thermal effects are absent and effects of flame stretch are small due to modest turbulence levels and the high laminar flame speed. Thus, comparing this baseline result with the photographs for stable conditions suggests that diffusive thermal effects have acted to reduce the distortion of the flame surface by turbulence for stable conditions. The results were similar for other test conditions: diffusive thermal effects *generally reduced* flame distortion by turbulence for stable conditions (ϕ > 1.8) and enhanced distortion for unstable conditions (ϕ < 1.8), although the degree of enhancement was generally less apparent.

It was also possible to identify similar diffusive thermal effects from the flash-Schlieren photographs of the turbulent jet flames. Some representative results for ϕ = 1.3, 1.8 and 3.57 and *Re* = 2000, 20000 and 40000 are illustrated in Figure 5. Taking ϕ = 1.8 as the neutral condition, where diffusive thermal effects are minimized, it is clear that the flame surface for stable conditions (ϕ = 3.57) is wrinkled to a lesser degree at comparable Reynolds numbers. In contrast, the flame surfaces for unstable conditions (ϕ = 1.0) are somewhat more irregular (spiked), and have a greater number of detached islands of unreacted gas than is observed for neutral conditions at the same Reynolds number. Thus, diffusive thermal effects appear to be important for all fuel equivalence ratios (except possibly near the neutral condition) even at relatively *high* Reynolds numbers.

The photographs of Figure 5 also show that the flame lengths increase dramatically as *Re* increases and are shortest near ϕ = 1.8 where the laminar flame speed is a maximum (this is most evident for *Re* = 2000). This behavior will be discussed subsequently, based on the more quantitative measurements of reaction progress variable. Nevertheless, predictions based on the mixing controlled turbulent reaction expression (Eq. (4)) could not reproduce these trends, yielding flame lengths, L_f, of ca. 10 for all test conditions. Therefore, only the Cant and Bray (1988) approach will be considered in the following in order to reduce cluttering of the plots with obviously ineffective predictions.

Finally, the Schlieren photographs of Fig. 5 help quantify the location of the mixing layer between the inner and outer burner flames for present test conditions. The layer can be seen most clearly for *Re* = 2000 and 20000, where it appears as a dark shaded area emanating from the left hand side of the burner exit (a corresponding but less distinct light shaded area appears at the right side of the photographs). As noted earlier, the primary jet burner flames are well inside the location of the mixing layer.

Unreactedness

Mean and fluctuating values of the reaction progress variable are simply related, since this variable yields a telegraph signal for the thin flamelet conditions of present tests; this implies that [illegible]. This relationship was satisfied by measurements over the present test range within 15%; therefore, *the following discussion will be limited to* $\bar{c}$. Measured and predicted time-averaged unreactedness along the axis of the jet flames, (1 − $\bar{c}$), are illustrated in *Figure 6* for *Re* = 2000, 20000 and 40000 at unstable (ϕ = 0.3, 0.8, 1.0), neutral (ϕ = 1.8) and stable (ϕ = 3.56) conditions with respect to diffusive thermal effects. *Predictions are based on the Cant and Bray (1988)*

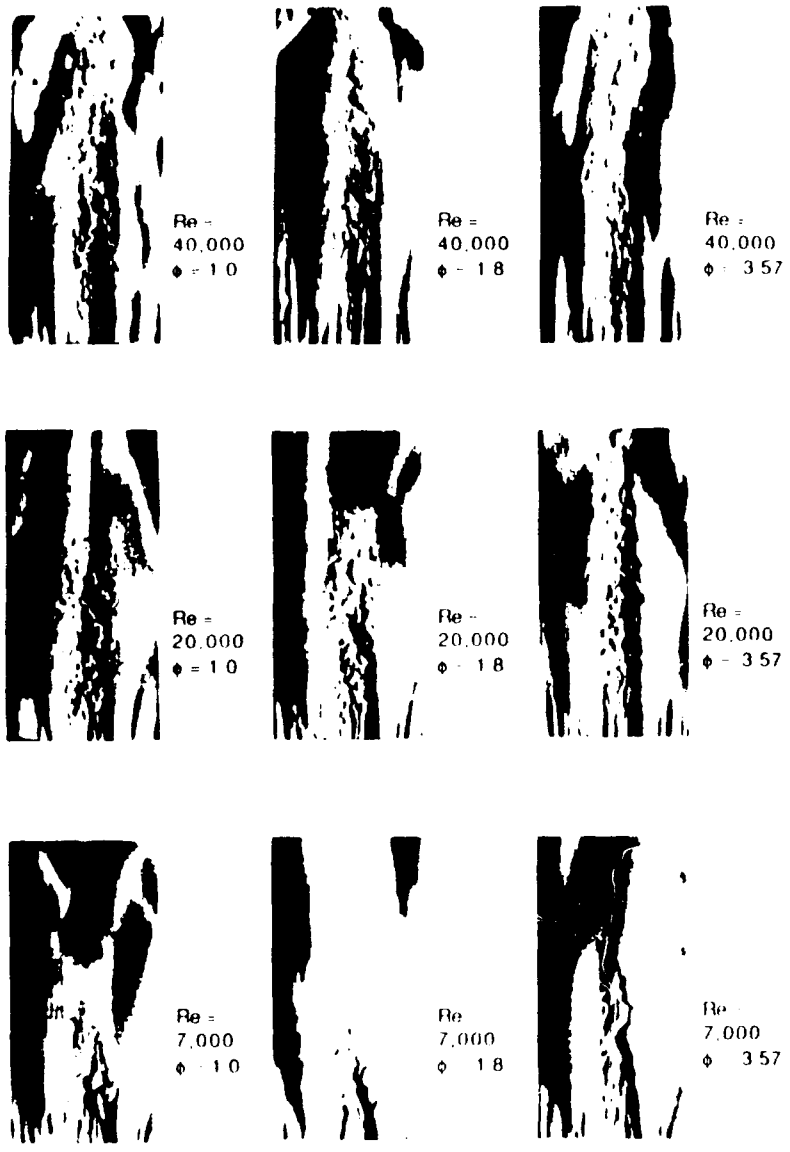

FIGURE 5 Flash Schlieren photographs of jet flames. Note $\phi = 1.0$, 1.8, and 3.57 correspond to unstable, neutral, and stable preferential diffusion conditions, respectively.

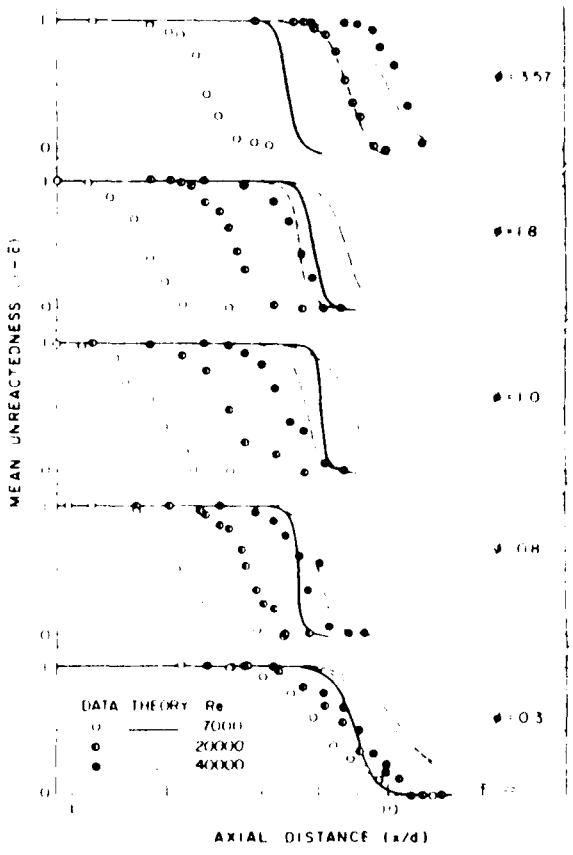

FIGURE 6 Mean unreactedness along the burner axis.

turbulent reaction model with parameters selected to match predictions and measurements at $\phi = 3.57$ and $Re = 40000$, as noted earlier.

A significant trend of the results illustrated in Figure 6 is that flame lengths increase with increasing Re for all values of ϕ. The increase is greatest for $\phi = 1.8$ where the laminar flame speed is relatively large in comparison to levels of turbulent fluctuations, e.g., $\tilde{u}_{rms}/S_l$ is in the range of 0.4–2.6 at this value of ϕ which places most of these results in or near the wrinkled thin flamelet regime ($\tilde{u}' > S_l$) illustrated in Figure 2. At these conditions, the turbulent burning velocity is dominated by laminar effects and only increases slightly due to increased turbulent velocity fluctuations (since $\tilde{u}'/S_l$ is relatively small) as $\tilde{u}_{rms}$ (and thus Re) increases, even though $\tilde{u}'_{rms}/\tilde{u}_{rms}$ is nearly constant for present test conditions. As a result, the flame stabilizes at a shallower angle with respect to the streamwise direction as $\tilde{u}_{rms}$ (and thus Re)

increases and the flame length increases accordingly. Similarly, Re has the smallest effect on flame length at $\phi = 0.3$ where the laminar flame speed is relatively small in comparison to levels of turbulent fluctuations (e.g., $u_{rms}/S_L = 6.4$ at this value of ϕ which places these results well into the mixing limited thin flamelet regime ($u' > S_L$) illustrated in Figure 2. At these conditions, the turbulent burning velocity is dominated by turbulent effects and increases nearly proportional to increased turbulent velocity fluctuations as u_{rms} (and thus Re) increases, since u_{rms}/u_{rms_0} is nearly constant. In this case, the increased turbulent burning velocity nearly compensates for the increased burner exit velocity so that the flame position is nearly independent of u_{rms} (and thus Re). By definition, the flame length should be nearly independent of Re as mixing-limited conditions are approached. Thus, in view of the behavior seen in Figure 6, the order of magnitude estimate of the boundary between the wrinkled and the mixing-limited thin-flamelet regimes illustrated in Figure 2 would be improved by locating it at $u' \approx 3S_L$.

In addition to direct effects of laminar flame speeds, the results illustrated in Figure 6 also exhibit effects of diffusive-thermal phenomena. For example, the flame length for $\phi = 3.57$ and $Re = 40{,}000$ is longer than the rest, even the results approaching the mixing-controlled limit at $\phi = 0.3$ where the laminar flame speed is much lower. This suggests that diffusive-thermal phenomena at the stable condition are acting to reduce the distortion of the flame surface so that the required area to complete reaction can only be achieved by an increased flame length. Certainly quenching effects do not offer an explanation for this trend since the laminar flame speed for $\phi = 3.57$ is nearly an order of magnitude greater than $\phi = 0.3$, which should reverse the trend seen in Figure 6. Similarly, flame lengths for $\phi = 0.8$ and 1.0 are shorter than the neutral condition, $\phi = 1.8$, even though their laminar flame speeds are smaller; this suggests that diffusive-thermal phenomena at unstable conditions are acting to increase wrinkling of the flame surface so that the required area to complete reaction can be achieved in a shorter flame length. Naturally, u_{rms}/S_L also plays a role in the required flame length, as discussed earlier; present results will be viewed directly in these terms later.

The combined effects of u_{rms}/S_L varying in the range 0.4–15.5 and diffusive thermal phenomena, for the present measurements, are not explicitly considered in the Cant and Bray (1988) combustion model. Thus, it is not surprising that there is only fair agreement between measurements and predictions illustrated in Figure 6. The main deficiency of the predictions is that the effect of Reynolds number is underestimated. Furthermore, since diffusive-thermal effects are not considered in the model, fitting the results at a stable condition ($\phi = 3.57$) causes predictions for neutral and unstable conditions to overestimate flame lengths. Finally, predictions are rather sensitive to the fit of the quenching correction; this causes flame lengths to reach a minimum at intermediate Re for some conditions (see $\phi = 1.0$ and 1.8) which is not observed experimentally. It appears that substantial extension of models of turbulent reaction in premixed flames will be required to treat many of the trends observed for hydrogen/air flames.

The measured and predicted radial variation of unreactedness are illustrated in Figure 7 for $\phi = 0.8$, 1.8 and 3.57 and $Re = 40{,}000$. Results for other test conditions, however, were similar. The coordinates are highly normalized; therefore, the measurements exhibit a crude similarity at each x/l. This follows from the roughly triangular shape of the mean flame position in a plane through its axis, which is somewhat reflected by the flash Schlieren photographs of Figure 4. For all flames have the same base dimension and thus roughly the same width at equal fractions of their height. The predictions are in fair agreement with the measurements at $x/l = 0.25$ and 1.0;

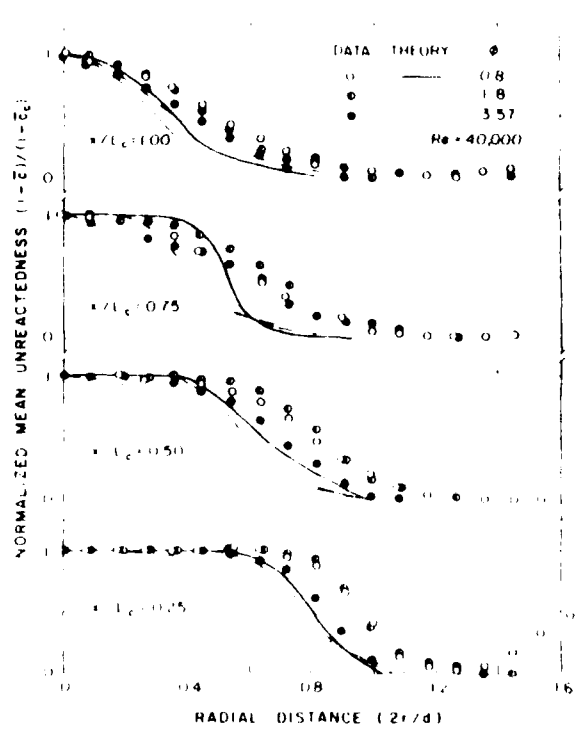

FIGURE 7. Radial profiles of mean unreactedness.

however, this is largely an artifact of the normalization of the results (centerline values of c are not predicted very well) and the nearness of these locations to prescribed boundary conditions at the burner exit and the flame tip. In contrast, predictions at intermediate locations are not in good quantitative agreement with the measurements and exhibit variations with ϕ that are not observed.

Turbulent Burning Velocities

In an effort to quantify diffusive-thermal effects on the properties of the turbulent flames, effective turbulent burning velocities were computed. This involved defining an effective conical flame surface having a base diameter equal to the burner exit diameter and a height equal to l. The effective turbulent burning velocity, $S_{T,e}$, was then defined as the mean velocity normal to this surface, assuming that the mean streamwise velocity was the same as at the burner exit. This assumption is justified because all flames for which $S_{T,e}$ was computed lie within the potential core of the jet, where the velocity does not vary in the axial direction, as shown later. This method of using the mean flame location to define an effective angle between the turbulent flame and the incoming reactant velocity has been commonly used to determine

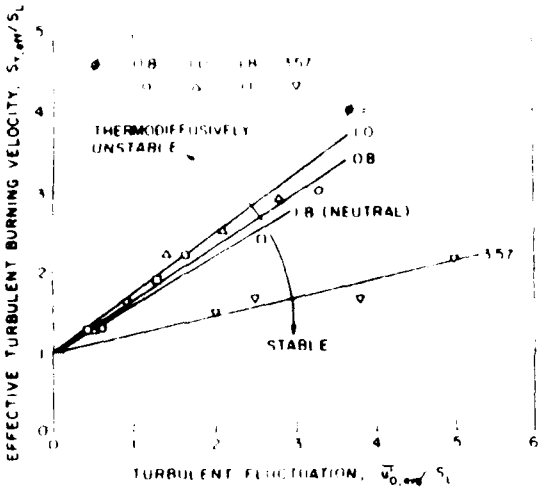

FIGURE 8. Effective turbulent burning velocity as a function of velocity fluctuations

turbulent burning velocity (Ballal, 1979; Grover *et al.*, 1989; Wohl *et al.*, 1953; Cheng and Ng, 1984; Damkeler and Gouldin, 1982; Driscoll and Gulati, 1988).

The resulting effective turbulent burning velocities are illustrated in Figure 8, which is a plot of $S_{T,eff}/S_L$ as a function of $u_{0,rms}/S_L$. The values of S_L used for these correlations were obtained from Andrews and Bradley (1973) and are summarized in Table II. Results plotted in Figure 8 include $\phi = 0.8$, 1.0, 1.8 and 3.57 for Re in the range 7000–40000. The measurements illustrated indicate that effective turbulent flame speeds fall on two branches: a neutral-unstable branch involving $\phi = 0.8$, 1.0 and 1.8, and a stable branch involving $\phi = 3.57$. The stable branch has substantially less response to increased turbulence levels (i.e., smaller slope) than the neutral-unstable branch. Furthermore, even within the neutral-unstable branch, unstable conditions are somewhat more responsive to increased turbulence levels than the neutral condition. These trends clearly imply that diffusive-thermal phenomena retard turbulent distortion of the flame surface for stable conditions (thus yielding lower values of $S_{T,eff}$), and, to a lesser degree, enhance distortion for unstable conditions (yielding higher values of $S_{T,eff}$).

Other measurements in the literature yield similar behavior. For example, Abdel-Gayed *et al.* (1976, 1984) measured turbulent burning velocities of hydrogen/air mixtures at various ϕ using a fan-stirred bomb. When these measurements are correlated in the same manner as Figure 8, two branches are also observed: results for $\phi = 0.42$–1.58 yielding an unstable branch, and results for $\phi = 3.57$ yielding a stable branch having a smaller response to increased turbulence levels. Abdel-Gayed *et al.* (1976) attribute the reduced response for $\phi = 3.57$ to quenching, however, since S_L for this condition actually exceeds values for some of the conditions in the unstable branch, diffusive-thermal phenomena must play an important role in this behavior. Liu and Lenze (1988) measured turbulent burning velocities of CH_4–H_2/air mixtures stabilized at a stagnation point. They also find that rich flames have reduced response

to increased turbulence levels in comparison to lean flames but do not propose a reason for this behavior. Based on present results, this effect probably involves diffusive-thermal phenomena.

Taken together, these results suggest that diffusive-thermal phenomena influence the rate of propagation of turbulent flames at all but *neutral conditions for high* Reynolds numbers as well as low Reynolds numbers. Stable conditions tend to reduce distortion of the flame surface by the turbulence and, to a lesser degree, unstable conditions tend to enhance distortion of the flame surface by turbulence. These effects may explain past difficulties in obtaining correlations of turbulent flame speeds along the lines of Figure 8, as well as reliable models of turbulent combustion for premixed flames. Finding a rational way to incorporate diffusive-thermal effects into methods of estimating turbulent flame speeds has important implications, *e.g.*, most practical premixed turbulent flames, like those of spark-ignition automotive engines, involve reactant systems having widely varying mass diffusivities and operate at stable conditions where diffusive-thermal effects are likely to significantly retard distortion of the flame surface by turbulence.

Velocities

Measured and predicted mean and r.m.s. fluctuating streamwise velocities along the axis of the jet flames are illustrated in Figures 9 and 10. Results are illustrated for $\phi = 0.3$, 1.0, 1.8 and 3.57 at $Re = 7000$ and 40000. Measured characteristic flame lengths, L_f, with their uncertainties denoted by brackets, are also marked on the plots. Except for some jumps in the region of the flame for $Re = 7000$, which will be taken up later, the measurements in Figures 9 and 10 indicate little change from burner exit velocities until $x/d = 10$. This is a rather extended potential core for fully developed turbulent pipe flow at the burner exit; *e.g.*, Chuech *et al.* (1989) find potential core lengths of ca. $x/d = 4$ for constant density gas jets with fully developed pipe flow at the jet exit. The reason for this behavior is that the flow of reactants along the axis is surrounded by hot combustion products from its own flame as well as the hot gas flow from the outer burner. Thus, the low density of the surroundings reduces the entrainment rates of the jet which extends the length of the potential core.

Except for $\phi = 1.8$, 1.0 and 3.57 (to a lesser degree) at $Re = 7000$, mean and r.m.s. fluctuating velocities in Figures 9 and 10 are not particularly influenced by the presence of the flames. This behavior can be explained by changes in the average angle of the flames with respect to the mean flow direction, along the lines of Bray *et al.* (1985). The conditions where streamwise velocities, particularly streamwise r.m.s. velocity fluctuations, increase in the vicinity of the flame, all involve the shortest flames that have the largest average angles with respect to the flame axis. Then, velocity increases normal to the flames, due to the density ratio of the flames, have the largest component in the streamwise direction, yielding the highest streamwise r.m.s. velocity fluctuations due to flame intermittency at the measuring location, similar to past velocity measurements for oblique flames (Gulati and Driscoll, 1986). Thus, the results illustrated in Figure 10 suggest that effects of streamwise transport are generally small, justifying the use of boundary-layer approximations for present predictions, with the possible exception of $Re = 7000$ and $\phi = 1.0$ and 1.8, as discussed earlier. Recognizing the extended length of the potential core, and the small changes of the streamwise velocity (particularly for high Reynolds numbers), use of burner exit conditions to characterize the turbulence properties of the unburned gas appears to be justified for present test conditions.

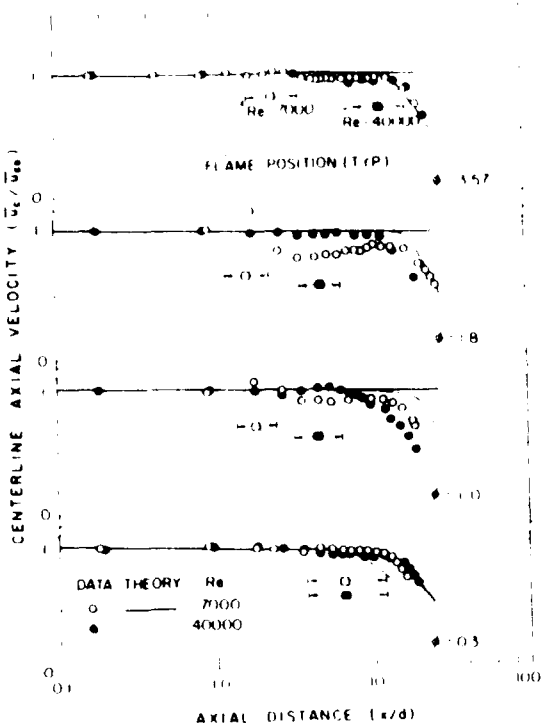

FIGURE 9. Streamwise mean velocities along the axis.

CONCLUSIONS

The major conclusions of the study can be summarized as follows:

1. In quiescent environments, hydrogen/air flames exhibit diffusive-thermal (preferential-diffusion) instabilities for fuel equivalence ratios less than the maximum laminar flame velocity ($\phi = 1.8$), as determined from Schlieren photographs.
2. Diffusive-thermal effects, similar to those described by Clavin (1985) for weakly-turbulent flames, persisted for the present high Reynolds number hydrogen/air turbulent jet flames. In particular, the turbulent distortion of the flame surface, and the response of profiles of unreactiveness and effective turbulent burning velocities to increased turbulence levels, were all damped for stable conditions, to a lesser degree, these properties were all enhanced for unstable conditions.
3. Diffusive-thermal damping effects at stable conditions are of particular importance: the effect was stronger than enhancement at unstable conditions for present test conditions, and many practical premixed flames involve high molecular weight fuels and operate lean, which places them in the diffusive-thermal stable regime. Thus, the tendency of some previous studies to assume that stable conditions are not affected by diffusive-thermal effects can be erroneous. Correlations, and notions of modeling turbulent premixed flames, should be reexamined to consider diffusive-thermal effects.
4. Estimates of flame properties based on a contemporary turbulence model due to Cant and Bray (1988), which allows for effects of flame stretch, yielded only fair agreement with measurements; extensions to improve estimates of the effect of burner exit Reynolds numbers (or u'_{rms} and u'_{rms}/S_L) and to allow for diffusive-thermal phenomena are needed to treat hydrogen/air turbulent jet flames—even at high Reynolds numbers within the mixing limited thin-flamelet regime.
5. Mean and r.m.s. fluctuating streamwise velocities along the axis generally did not vary significantly within the flame brush at high Reynolds numbers since the flames were oriented at a relatively small angle with respect to the flame axis at these conditions.
6. Present flames were not influenced by shear layer generated turbulence because they were within the potential core; thus, the flames only saw a turbulent field dominated by flow properties at the jet exit (fully developed pipe flow).

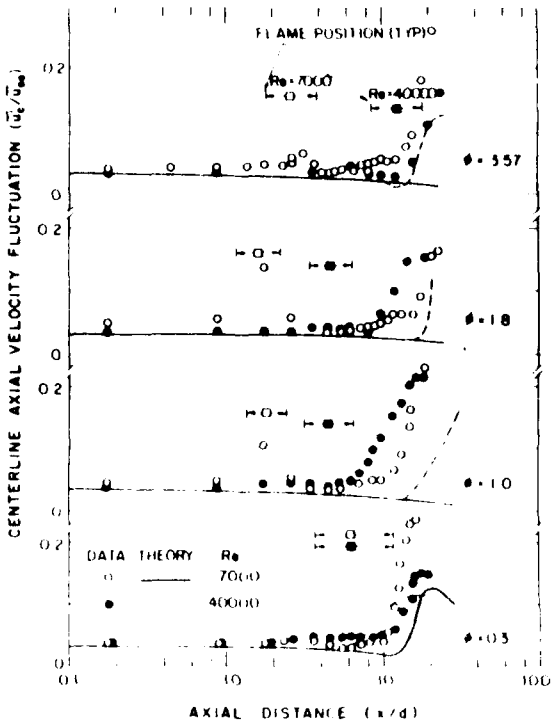

FIGURE 10. Streamwise r.m.s. velocity fluctuations along the axis.

ACKNOWLEDGEMENTS

This research was supported by the Office of Naval Research, Contract No. N00014-85-K-0698, with S. Ramberg serving as Scientific Program Officer. The authors also wish to thank E. G. Groff for many useful discussions and General Motors Research Laboratories for the loan of the fan stirred bomb.

REFERENCES

Abdel-Gayed, R. G. and Bradley, D. (1976). Dependence of turbulent burning velocity on turbulent Reynolds number and ratio of laminar burning velocity to r.m.s. turbulent velocity. *Sixteenth Symposium (International) on Combustion*, The Combustion Institute, Pittsburgh, pp. 1725–1735.
Abdel-Gayed, R. G., Bradley, D., Hamid, M. N. and Lawes, M. (1984). Lewis number effects on turbulent burning velocity. *Twentieth Symposium (International) on Combustion*, The Combustion Institute, Pittsburgh, pp. 505–512.
Andrews, G. E. and Bradley, D. (1973). Determination of burning velocity by double ignition in a closed vessel. *Combust. Flame* **20**, 77.
Ballal, D. R. (1979). The structure of a premixed turbulent flame. *Proc. R. Soc. London* A **367**, 353.
Boyer, L., Clavin, P. and Sabathier, F. (1980). Dynamic behavior of a premixed turbulent flame front. *Eighteenth Symposium (International) on Combustion*, The Combustion Institute, Pittsburgh, pp. 1041–1409.
Bray, K. N. C. (1980). Turbulent flows with premixed reactants. In P. A. Libby and F. A. Williams (Eds.) *Turbulent Reacting Flows*, Springer, Berlin, pp. 115–183.
Bray, K. N. C., Libby, P. A. and Moss, J. B. (1985). Unified modeling approach for premixed turbulent combustion, part I: general formulation. *Combust. Flame* **61**, 87.
Cant, R. S. and Bray, K. N. C. (1988). Strained laminar flamelet calculations of premixed turbulent combustion in a closed vessel. *Twenty-Second Symposium (International) on Combustion*, The Combustion Institute, Pittsburgh, pp. 791–799.
Cheng, R. K. and Ng, T. T. (1984). On defining the turbulent burning velocity in premixed V-shaped turbulent flames. *Combust. Flame* **57**, 155.
Church, S. G., Lu, M. C. and Faeth, G. M. (1989). Structure of turbulent sonic underexpanded free jets. *AIAA J.* **27**, 549.
Clavin, P. (1985). Dynamic behavior of premixed flame fronts in laminar and turbulent flows. *Prog. Energy Combust. Sci.* **11**, 1.
Clavin, P. and Williams, F. A. (1979). Theory of premixed flame propagation in large scale turbulence. *J. Fluid Mech.* **90**, 589.
Clavin, P. and Williams, F. A. (1982). Effects of molecular diffusion and of thermal expansion on the structure and dynamics of premixed flames in turbulent flows of large scale and low intensity. *J. Fluid Mech.* **116**, 251.
Dandekar, K. V. and Gouldin, F. C. (1982). Temperature and velocity [illegible] of premixed turbulent flames. *AIAA J.* **20**, 652.
Driscoll, J. F. and Gulati, A. (1988). Measurement of [illegible] in the turbulent kinetic energy balance within a flame and comparison with theory. *Combust. Flame* **72**, 131.
Fansler, T. D. (1989). Turbulence characteristics of a [illegible]. *Combust. Flame*, in press.
Gordon, S. and McBride, B. J. (1971). Computer program for calculation of complex chemical equilibrium compositions, rocket performance, incident and reflected shocks, and Chapman-Jouguet detonations. NASA Report SP-273, Washington.
Groff, E. G. (1982). The cellular nature of confined spherical propane-air flames. *Combust. Flame* **48**, 51.
Groff, E. G. (1987). An experimental evaluation of an entrainment flame-propagation model. *Combust. Flame* **67**, 153.
Grover, J. H., Fales, E. and Scurlock, A. C. (1959). Turbulent flame studies in a two-dimensional open burner. *ARS J.* **26**, 775.
Gulati, A. and Driscoll, J. F. (1986). Velocity-density correlations and Favre averages measured in a premixed turbulent flame. *Combust. Sci. and Tech.* **48**, 285.
Halstead, M. P., Pye, D. B. and Quinn, C. P. (1974). Laminar burning velocities and weak flammability limits under engine-like conditions. *Combust. Flame* **22**, 89.
Jeng, S. M. and Faeth, G. M. (1984). Species concentrations and turbulence properties in buoyant methane diffusion flames. *J. Heat Trans.* **106**, 721.
Jones, W. P. and Whitelaw, J. H. (1982). Calculation methods for reacting turbulent flows: a review. *Combust. Flame* **48**, 1.
Laufer, J. (1954). Cited in Hinze, J. O. (1975). *Turbulence*, McGraw-Hill, New York, 2nd edition, pp. 720–724.

Lee, T. W., Gore, J. P., Faeth, G. M. and Birk, A. (1988). Analysis of combusting high pressure monopropellant sprays. *Combust. Sci. and Tech.* **57**, 95.
Lewis, B. and von Elbe, G. (1961). *Combustion, Flames and Explosions of Gases*, 2nd edition, Academic Press, New York, pp. 381–384.
Libby, P. A., Sivasegaram, S. and Whitelaw, J. H. (1986). Premixed combustion. *Prog. Energy Combust. Sci.* **12**, 393.
Liu, Y. and Lenze, B. (1988). The influence of turbulence on the burning velocity of premixed CH_4-H_2 flames with different laminar burning velocities. *Twenty-Second Symposium (International) on Combustion*, The Combustion Institute, Pittsburgh, pp. 747–754.
Lockwood, F. C. and Naguib, A. S. (1975). The prediction of the fluctuations in the properties of free, round jet, turbulent diffusion flames. *Combust. Flame* **24**, 109.
Manton, J., von Elbe, G. and Lewis, B. (1952). Nonisotropic propagation of combustion waves in explosive gas mixtures and the development of cellular flames. *J. Chem. Phys.* **20**, 153.
Markstein, G. H. (1951). Experimental and theoretical studies of flame front stability. *J. Aero. Sci.* **18**, 199.
Nikuradse, J. (1932). Cited in Hinze, J. O. (1975). *Turbulence*, McGraw-Hill, New York, 2nd edition, pp. 725–727.
Searby, G. and Clavin, P. (1986). Weakly turbulent, wrinkled flames in premixed gases. *Combust. Sci. and Tech.* **46**, 167.
Semenov, E. S. (1965). Measurement of turbulence characteristics in a closed volume with artificial turbulence. *Combustion, Explosion and Shock Waves* **1**, 57.
Spalding, D. B. (1978). *GENMIX: A General Computer Program for Two-Dimensional Parabolic Phenomena*, Pergamon Press, Oxford.
Williams, F. A. (1985). *Combustion Theory*, 2nd edition, Benjamin Cummings, Menlo Park, CA, pp. 341–372, 411–445.
Wohl, K., Shore, L., Rosenberg, H. and Weil, C. W. (1953). Burning velocity of turbulent flames. *Fourth Symposium (International) on Combustion*, The Combustion Institute, Pittsburgh, pp. 620–644.

APPENDIX B: WU ET AL. (1991a)

Preferential Diffusion Effects on the Surface Structure of Turbulent Premixed Hydrogen/Air Flames

by

M. S. Wu, S. Kwon, J. F. Driscoll and G. M. Faeth
Department of Aerospace Engineering
The University of Michigan
Ann Arbor, Michigan 48109-2140

Abstract — An experimental study of the surface structure of high Reynolds number turbulent premixed hydrogen/air jet flames is reported. Test conditions involved various values of turbulence intensities relative to the laminar flame speed, and stable/neutral/unstable conditions for preferential diffusion, within the wrinkled and mixing-limited thin flamelet regimes. Measurements included laser light sheet imaging to characterize flame surface properties and conditional laser velocimetry to characterize the turbulence properties of the unburned gas. It was found that flame surface area (and thus the local turbulent burning velocity), flame brush thickness and the fractal dimension of the flame surface progressively increased with distance from the flameholder, with maximum values eventually limited by approach to the flame tip. Additionally, the rate of development of these properties with distance from the flameholder increased as turbulence intensities relative to the laminar flame speed increased. Finally, preferential diffusion reduced/increased the rate of increase of these properties for stable/unstable conditions. Taken together, these observations imply that models and correlations of turbulent premixed flame properties for turbulent jet flames must account for effects of flame development, e.g., distance from the flameholder or the point of ignition, and preferential diffusion, in order to adequately characterize flame properties.

Introduction

Turbulent premixed flames have numerous practical applications, e.g., spark-gnition engines, air-breathing propulsion systems, flames and furnaces used in nanufacturing and materials processing, and uncontrolled explosions. This has motivated nany earlier studies of turbulent premixed flames; however, current understanding is not ery complete due to the difficulties of dealing with turbulence/chemistry interactions. hus, existing correlations of flame properties are characterized by inconsistencies and arge scatter even for relatively limited ranges of flame conditions (Abdel-Gayed et al. 976, 1984; Liu and Lenze, 1988; Mantzaras et al., 1989; North and Santavicca, 1990; Villiams, 1985). Models of the process also are not highly developed and have had limited xperimental evaluation with only marginal success (Bray, 1980; Cant and Bray, 1988; Jouldin, 1987; Libby et al., 1988; Pope, 1990; Wu et al., 1990). Recent work in this aboratory suggests that effects of preferential-diffusion instability may be a factor in the ifficulties because this phenomenon can influence flame properties for both stable and nstable conditions — even at the high Reynolds number conditions representative of most ractical applications (Wu et al., 1990). The objective of the present investigation was to xtend this work to provide information on flame surface properties for stable, neutral and nstable preferential diffusion conditions. Similar to the earlier work, the investigation was imited to premixed turbulent hydrogen/air jet flames operating within the thin flamelet egime defined by Bray (1980).

Within the thin-flamelet regime, preferential diffusion involves the interaction etween diffusion of a faster-diffusing reactant and the variation of laminar burning elocity with fuel-equivalence ratio (Manton et al., 1952; Williams, 1985; Joulin and Mitani, 1981). Reactants are consumed within a thin reaction zone; therefore, the faster-iffusing species accumulates near bulges in the flame surface extending toward the eactants and is depleted from bulges extending toward the products. When the laminar urning velocity increases/decreases with increasing concentration of the fast diffusing

reactant, the bulges grow/decay and the flame is unstable/stable. Hydrogen is the faste diffusing reactant in hydrogen/air flames, and the ratio of the binary diffusivities o hydrogen to oxygen (both with respect to air at room temperature) is roughly 2.: (Incropera and DeWitt, 1981), while the maximum laminar burning velocity is reached at ϕ = 1.8 (Andrews and Bradley, 1973). Thus, these flames are unstable/stable for fue equivalence ratios below/above ϕ = 1.8.

Clavin and coworkers have studied effects of thermo-diffusive instability, which is closely related to preferential-diffusion instability, using theory and measurements for turbulent flows having large scale and low intensity (Boyer et al., 1980, Clavin and Williams, 1979, 1982; Searby and Clavin, 1986). As noted earlier, Wu et al. (1990) also observed preferential-diffusion phenomena in turbulent hydrogen/air jet flames at high Reynolds numbers. In both cases, turbulent distortion of the flame surface was enhanced for unstable conditions and retarded for stable conditions, influencing local turbulent burning velocities accordingly. The latter effect is particularly significant because many practical applications involve heavy hydrocarbons burning in air at fuel-lean conditions which is in the stable preferential-diffusion regime.

The conditions considered by Clavin and coworkers involved only weak turbulence which is not very representative of practical applications. Wu et al. (1990) consider jet flames having more representative turbulence properties; however, only schlieren imaging which averages properties over a path and is not very quantitative, and point measurements were undertaken. The objective of the present investigation was to complete a more detailed evaluation of effects of preferential diffusion on flame surface properties. This involved analysis of laser light sheet images of the flame surface at various distances from the burner exit, for stable/neutral/unstable preferential-diffusion conditions, and at various values of the relative turbulence intensity, $\bar{u}'/S_L$ — the last being a measure of the dominance of turbulent mixing on the combustion process. These results were characterized by the flame brush thickness, r'_f, the ratio of perimeters and areas of the

distorted and mean flame surfaces, P_T/P_L and A_T/A_L, the fractal dimension of the flame surface, D_2, and measures of the mean wavelength of flame wrinkles. Additionally, the turbulence characteristics of the unreacted gas were thoroughly characterized using conditional laser velocimetry. Thus, an attempt has been made, in conjunction with the findings of Wu et al. (1990), to provide measurements that can be used to help develop models of the turbulent flames subject to preferential diffusion effects, in addition to the direct experimental observations of flame properties under these conditions.

The paper begins with descriptions of experimental methods. Results are then considered treating unburned gas turbulence properties, visualization of the flame surface and flame surface properties in turn. The paper concludes with a discussion of the implications of the measurements for correlations and models of flame properties.

Experimental Methods

Apparatus

Only a brief description of the premixed burner apparatus will be provided because the arrangement was identical to Wu et al. (1990). A coaxial round jet burner was used, with an inner burner having a diameter of 11 mm and a tube length-to-diameter ratio of 50 to yield nearly fully-developed turbulent pipe flow at the burner exit. The outer burner had a diameter of 58 mm with the outer flame stabilized much like a flat-flame burner above a bed of beads and screens. The burners operated at atmospheric pressure with the combustion products removed through a hood. Instruments were mounted rigidly, therefore, the flame structure was measured by traversing the burner assembly with radial and vertical positioning accuracies of 10 μm and 1 mm, respectively.

All measurements were limited to the jet flame of the inner burner, the outer burner flame only served to provide a hot environment for the jet flame. No attempt was made to match flow properties of the inner and outer burners; rather, the outer burner operated fuel lean (ϕ=0.3) with a burner exit velocity of 1 m/s while the inner burner operated at various

test conditions. Thus, a mixing layer was present between the combustion product flows at the inner and outer burners. Nevertheless, the mixing layer was observed on schlieren photographs to be well outside the position of the inner jet flame and had negligible influence on its properties (Wu et al., 1990).

Hydrogen (99.95% purity) was supplied from commercial cylinders while dry air (dewpoint less than 240 K) was obtained from laboratory supplies. All gas flow rates were measured with rotameters which were sized to yield maximum uncertainties (95% confidence) of fuel-equivalence ratios less than 5%. The gases were mixed in a manifold and then flowed through lines having length-to-diameter ratios of 400 to achieve uniform mixtures at the burner inlets. Flame arrestor screens were installed in the reactant lines of both burners to control flashback.

Instrumentation

Flame Tomography. Measurements were limited to flame surface properties using flame tomography and unburned gas properties using laser velocimetry. Flame tomography involved seeding the unreacted gas with oil drops having a nominal diameter of 1 μm using a TSI 9306 atomizer. Oil drops of this diameter disappear at the flame surface (Boyer et al., 1980). The drops were illuminated by a 200 μm thick laser light sheet created using a Candela pulsed dye laser and two cylindrical lenses. The laser provided 600 mJ of light at 514.5 nm with a 1 μs pulse duration. The scattered laser light was collected using an 85 mm focal length, f1.2 lens and a 35 mm camera back that had its flash synchronization output wired to trigger the laser pulse. Effects of flame radiation were controlled using a 10 nm interference filter in front of the camera lens and a camera shutter duration of 16 ms. Vertical and horizontal light sheet images were obtained by orienting the arrangement accordingly.

The light sheet photographs were enlarged to a 100 × 150 mm format prior to analysis. The enlarged photographs were then digitized using an MTI 65 Vidicon camera

and processed using a Gould FD 5000 Image Display and IBM-AT/clone computer. Video camera resolution was the equivalent of 512 × 512 pixels yielding a potential spatial resolution of 140 and 30 μm per pixel for vertical and horizontal light sheet images. Thus, the 200 μm thickness of the light sheet actually controlled the spatial resolution. Experimental uncertainties of various flame surface properties will be taken up as they are discussed.

Laser Velocity (LV). Unburned gas properties were measured using laser velocimetry. The laser velocimetry system was modified somewhat from Wu et al. (1990) in order to provide conditional measurements of unburned gas properties, better spatial resolution, control of directional bias and ambiguity, and additional information concerning turbulence spectra and scales.

A dual-beam laser velocimetry system was used, based on the 488 nm line of a 1 W argon-ion laser. The arrangement had a relatively long focal length (600 mm) transmitting lens because of the relatively large mean velocities (up to 88 m/s). Reasonably good spatial resolution (250 μm long measuring volume) was achieved by observing the probe volume at right angles from the optical axis with 5/4 magnification and a 200 μm aperture in front of the detector. Flame luminousity was controlled using a laser line filter (10 nm bandwidth) in the detector optical path. Frequency shifting was not required for measurements of streamwise velocities because turbulence intensities were less than 15%; however, crosstream (radial) velocities were measured using 40 MHz frequency shifting which was downshifted to convenient frequency ranges for processing.

The seeding particles were oil droplets having a nominal diameter of 1 μm. These particles disappeared at the flame front; therefore, all velocity measurements are conditioned and only represent the properties of the reactants. Data sampling rates always exceeded 100 kHz, which allowed temporal power spectra to be determined up to 50 kHz. Velocity bias was eliminated by sampling the analog output of a commercial burst counter at 100

kHz, using a LeCroy a/d converter (12 bit). Power spectra were found from 64k samples at each location using an FFT algorithm and an IBM-AT/clone computer. Experimental uncertainties (95% confidence) were dominated by finite sampling times and are estimated to be less than 5% for mean and fluctuating velocities in the streamwise direction and fluctuating velocities in the radial direction.

Test Conditions

Test conditions were within the range considered by Wu et al. (1990). Table 1 is a summary of the properties of the test flames: two values of $\bar{u}'_{o,avg}/S_L$ (0.9 and 2.5) and three fuel-equivalence ratios (0.8, 1.8 and 3.6) were considered. All test conditions are in the thin-flamelet regime defined by Bray (1980), with the lower and higher values of $\bar{u}'_{o,avg}/S_L$ placing the flames in the wrinkled and mixing-limited thin flamelet regimes *respectively. In particular, flames with* $\bar{u}'_{o,avg}/S_L = 2.5$ *are more likely to have local* islands of reactants than those having $\bar{u}'_{o,avg}/S_L = 0.9$, although both have wrinkled continuous flame sheets (Bray, 1980). The three values of ϕ vary flame conditions with respect to preferential-diffusion instability: $\phi = 0.8$, 1.8 and 3.6 being in the unstable neutral and stable regimes, respectively. In addition, $\phi = 0.8$ and 3.6 have nearly the same laminar flame speeds (Andrews and Bradley, 1973) and burner exit conditions so that observed differences in flame surface properties between these two flames can be attributed to effects of preferential diffusion for each $\bar{u}'_{o,avg}/S_L$.

The values of $\bar{u}_{o,avg}$, $\bar{u}'_{o,avg}$ and $\ell_{u,o}$ in Table 1 were determined from the LV measurements, the last involving use of Taylor's hypothesis (Hinze, 1975). Burner exit and turbulence Reynolds numbers were in the range 7000-40000 and 200-1100, which includes the same range as Wu et al. (1990). Flame lengths, L_c, are taken as the condition where time-averaged unreactedness along the axis was 0.5, from the Rayleigh-scattering measurements of Wu et al. (1990). Flame lengths are in the range $L_c/d = 2.6$-7.7 which implies that the unreacted gas is largely within the potential core of the jet. The

Kolmogorov scales, ℓ_k, were estimated as $\ell_{u,o}/(\bar{u}'_{o,avg}\ell_{u,o}/\nu_o)^{3/4}$ from Tennekes and Lumley (1972): they are generally comparable or larger than the flame thickness which is representative of the thin flamelet regime.

Results and Discussion

Unburned Gas Properties

Mean and Fluctuating Velocities. The turbulent flow field properties of the unreacted gas were quantified in detail. Figure 1 is an illustration of conditional mean and fluctuating velocities along the axis for $\bar{u}'_{o,avg}/S_L = 0.9$ and $\phi = 1.8$. Findings for other conditions were similar, see Wu et al. (1990) for some typical examples of unconditioned velocities along the axis. The limits of flame position along the axis, which define the region of the flame brush, are also shown on the plot for reference purposes. Typical of flows within a potential core region, the unreacted gas exhibits only modest variations of mean and fluctuating velocities. Additionally, Wu et al. (1990) point out that the potential core is unusually long for present flows, extending up to x/d = 10 (for a decay of mean velocities less than 10%) because the immediate surroundings are the low-density gaseous combustion products of the outer burner flame which reduces entrainment rates.

Radial variations of mean and fluctuating velocities, for the same conditions as Figure 1, are illustrated in Figure 2 for x/d in the range 0.36-3; however, findings for x/d = 0.18, which was the position closest to the burner exit that could be accessed by laser velocimetry, can be found in Wu et al. (1990). Properties near the burner exit, x/d = 0.18 and 0.36, approximate the mean and fluctuating velocities of fully-turbulent pipe flow from Nikuradse (1932) and Laufer (1954). With increasing distance from the burner, however, the wake-like flow due to the pressure of the burner passage walls decays and flow properties become more uniform. In general, the flow is anisotropic with $\bar{u}'/\bar{v}'$ in the range 1.2-3.0, except for the region very near the passage walls where the degree of anisotropy is even larger.

Normalized probability density functions (PDF's) of streamwise and crosstream velocity functions for various points within the unreacted gas are plotted in Figure 3. These results are for the same flame as Figures 1 and 2, however, they are typical of other conditions. In spite of the anisotropy, the velocity fluctuations are seen to approximate Gaussian functions, which is characteristic of most turbulent shear flows (Hinze, 1975). A possible exception is a slight positive skewness of the streamwise velocity fluctuations but this is not felt to be significant in comparison to experimental uncertainties.

Spectra and Integral Scales. Conditional temporal power spectra of streamwise and crosstream velocity fluctuations for various streamwise and radial positions are plotted in Figures 4 and 5. These results also correspond to the flame considered in Figures 1 to 3. The present integral time scales, τ_u or τ_v, are defined by Hinze (1975) as the ordinate intercepts of the power spectra, $E_u(0)$ or $E_v(0)$, divided by 4 $\bar{u}'^2$ or 4 $\bar{v}'^2$. Thus, after normalization, the spectra of Figures 4 and 5 have an ordinate intercept of 4.0. Also shown on the plots are the power spectra when the autocorrelations are decaying exponential functions, i.e., when the power spectra are $4/(1 + (2\pi f\tau_{u \text{ or } v})^2)$. Except for the highest frequencies, where Kolmogorov scales are approached, the normalized streamwise power spectra illustrated in Figure 4 approximate the behavior of the exponential autocorrelation functions. Most of the normalized crosstream power spectra illustrated in Figure 5 also approximate the behavior of exponential autocorrelation functions as well. However, spectra near the axis and near the burner exit display a local maximum that is not observed elsewhere. Laufer (1954) measured similar spectra for transverse velocity fluctuations in turbulent pipe flows so that the effect is due to the origin of the flow. The reason for this behavior is that conservation of mass requires that spectra of transverse velocity fluctuations have a portion that becomes negative, resembling a Frenkiel function rather than an exponential function, with a corresponding peak in the temporal spectrum (Tennekes and Lumley, 1972). This feature decays rapidly, however

so that exponential autocorrelations, which simplify stochastic simulations of the flow field (Box and Jenkins, 1976), would be a reasonable approximation for most of the flow.

The temporal integral scales, τ_u and τ_v, are plotted in Figure 6 for positions corresponding to the spectra of Figure 5. The streamwise integral length scale, ℓ_u, is also shown on the plots. The length scales were found from the measured integral time scales and local mean velocities using Taylor's hypothesis, e.g., $\ell_u = \bar{u}\tau_u$. It was found that ℓ_u was 4 ± 1 mm at all 16 axial and radial locations where measurements were made. This value is consistent with Laufer's (1954) measurements which indicate $\ell_u \approx 0.4d$ or roughly 4 mm for present measurements. The integral time scale, τ_u, exhibits a greater variation than ℓ_u within the unreacted gas, largely through the variation of mean velocities seen in Figure 2 as reflected by Taylor's hypothesis. The integral time scale, τ_v, is generally less than τ_u because the autocorrelation function for v' has a negative portion whereas the autocorrelation for u' approximates an exponential function (Tennekes and Lumley, 1972).

Flame Surface Properties

Light Sheet Images. Typical light sheet images for vertical planes through the axis appear in Figures 7 and 8 for $\bar{u}'_{o,avg}/S_L = 0.9$ and 2.5. Note that the quality of these tomographs is much poorer than those that were analyzed because a large field of view was used to cover the entire flame height in a few images. Each figure includes results for unstable, neutral and stable fuel equivalence ratios, along with $\ell_{u,o}$ as a measure of turbulent length scales. The results show that the flame structure varies with height above the burner, $\bar{u}'_{o,avg}/S_L$ and preferential diffusion regime. First of all, the extent of wrinkling and lateral deflection of the flame surfaces increases progressively with height above the burner. This follows because time, or equivalently distance, is required for the random motion of the turbulent field to deflect the flame laterally from the points of attachment at its base. This behavior is analogous to the progressively increasing lateral

spread of fluid particles with distance from their source due to turbulent dispersion (Hinze, 1975).

Increasing the relative turbulence intensity, $\bar{u}'_{o,avg}/S_L$, causes both the flame length and degree of distortion of the flame surface to increase, compare Figures 7 and 8. The increased flame length follows from the nature of the present experiments where increased $\bar{u}'_{o,avg}/S_L$ is accompanied by increased $\bar{u}_{o,avg}/S_L$ because the turbulence intensity at the burner exit, $\bar{u}'_{o,avg}/\bar{u}_{o,avg}$, is nearly constant over the test range. Then low values of relative turbulence intensities imply only small increases of the effective turbulent burning velocity from the laminar burning velocity so that the angle of the flames to the mean flow direction must decrease with increasing mean velocities -- increasing the flame length. This behavior continues until $\bar{u}'_{o,avg}/S_L$ becomes large, ca. 10, where mixing-limited combustion is achieved and the flame length is relatively independent of the mean burner exit velocity (Bray, 1980; Wu et al., 1990).

Comparing Figures 7 and 8 shows that a much finer grained flame surface structure is created as $\bar{u}'_{o,avg}/S_L$ is increased. Peters (1986) discusses this behavior in terms of the Gibson scale, ℓ_G, which is the scale of vortices that have circumferential velocities comparable to the laminar burning velocity. Because both circumferential velocities and times of propagation across vortex elements decrease with decreasing vortex size, the Gibson scale is a measure of the smallest vortices that can appreciably deflect the flame surface. Peters (1986) suggests that $\ell_G = \ell_{u,o}\,(S_L/u'_{o,avg})^3$ for $u'_{o,avg}/S_L > 1$, assuming that burner exit conditions are representative of the flame as a whole, yielding $\ell_G = 200$ μm for $\bar{u}'_{o,avg}/S_L = 2.5$. Similar considerations suggest that ℓ_G is of the same order of magnitude as spatial integral scales, 3-4 mm, for $\bar{u}'_{o,avg}/S_L = 0.9$. Based on these ideas, the finer grained flame structure for $\bar{u}'_{o,avg}/S_L = 2.5$ than 0.9 is not surprising.

The third main effect seen in Figures 7 and 8 relates to preferential diffusion. In particular, differences between the flames at $\phi = 0.8$ and 3.6 for each value of relative turbulence intensity can be attributed to preferential diffusion because these flames are

otherwise nearly identical, i.e., they have nearly the same values of $\bar{u}_{o,avg}$, $\bar{u}'_{o,avg}$ and S_L (see Table I). The effect of preferential diffusion is clearly quite pronounced even at the relatively high Reynolds numbers of the present tests: the unstable ($\phi = 0.8$) flames are significantly shorter and have higher levels of surface distortion at a given distance from the burner exit than the stable ($\phi = 3.6$) flames. This provides direct evidence that the mechanism of preferential diffusion is acting to either enhance or retard turbulent distortion of the flame surface for unstable or stable conditions. Naturally, effects of increasing distortion with increasing distance from the burner exit still act, thus, while the stable flames have less distortion than the unstable flames at a given height above the burner exit, the stable flames still exhibit significant degrees of distortion near their tips which are much farther from the burner exit than those of the unstable flames. The neutral ($\phi = 1.8$) flames have behavior somewhat intermediate between the unstable and stable flames with respect to flame length and surface distortion for present test conditions. This comes about due to complex interactions between the initial conditions and S_L, the presence or absence of preferential diffusion effects, and the distance from the burner because $\bar{u}_{o,avg}$, $\bar{u}'_{o,avg}$ and S_L are roughly 50% larger for $\phi = 1.8$ than for $\phi = 0.8$ or 3.6.

Some typical light sheet images for horizontal planes at various heights above the burner appear in Figures 9 and 10. Values of relative turbulence intensity and ϕ for these figures are the same as Figures 7 and 8. The region considered is toward the base of the longest flames, $x/d \leq 4$, so that results for all three values of ϕ can be compared. The general features of these results are similar to the vertical light sheet photographs of Figures 7 and 8: the degree of surface distortion increases with increasing height above the burner, the degree of fine-grained roughness of the flame surface increases with increasing $\bar{u}'_{o,avg}/S_L$, and the distortion of the flame surface at a particular x/d is greater for unstable ($\phi = 0.8$) than for stable ($\phi = 3.6$) preferential diffusion conditions even through other properties of these flames are the same.

Flame Position. Mean flame positions, $\bar{r}_f$ and the r.m.s. fluctuation of flame position or flame brush thickness, $\bar{r}'_f$, are plotted as a function of height above the burner in Figures 11 and 12 for $\bar{u}_{o,avg}/S_L$ = 0.9 and 2.5. These results were obtained by ensemble-averaging 12-20 digitized light sheet images in the vertical plane at each spatial location. Experimental uncertainties (95% confidence) of these measurements are less than 5% for $\bar{r}_f$, and 15% for $\bar{r}'_f$.

Mean flame positions in Figures 11 and 12 monotonically decay toward the flame axis from the burner exit. Thus, the flame zone was generally well inside the position of the mixing layer between the inner and outer burner flows which was located at r/d > 0.5 — aside from the region near the point of flame attachment. The development of flame distortion with distance from the burner exit can be seen from the rapid increase of $\bar{r}'_f/d$ near the burner exit. However, the boundary conditions also require that the flames have a finite length so that after reaching a maximum value $\bar{r}'_f/d$ begins to decline again toward the flame up — this is particularly evident for $\bar{u}'_{o,avg}/S_L$ = 0.9 and ϕ = 1.8.

Effects of preferential diffusion also can be seen in Figures 11 and 12. As discussed earlier, unstable (ϕ = 0.8) and stable (ϕ = 3.6) conditions increase and decrease turbulent distortion of the flame surface. This is reflected by an increased rate of reduction of mean flame radius and larger maximum values of the flame brush thickness near the burner exit for unstable than for stable conditions. However, the progressive increase of flame surface distortion with distance from the burner exit counteracts effects of preferential diffusion somewhat for the longer flames at stable conditions, i.e., at larger x/d, $\bar{r}'_f/d$ is actually largest for the stable flame. Differences between stable and unstable conditions, however, tend to become smaller as $\bar{u}'_{o,avg}/S_L$ increases — particularly in the region near the burner exit. As noted earlier, properties of the neutral flames tend to be intermediate of the unstable and stable flames but this is somewhat fortuitous because the operating conditions for the neutral flame differ appreciably from the other two at each value of $\bar{u}'_{o,avg}/S_L$.

Flame Perimeter and Area. A measure of the distortion of the flame surface was found by measuring the perimeters of the flame surfaces on the vertical and horizontal light sheet images. For the vertical light sheet images, the flame length was divided into segments having a length of 0.7d and the perimeter of the wrinkled surface, $P_{T,V}$, and the ensemble-averaged perimeter of the mean flame position, $P_{L,V}$, were found for each segment. For the horizontal light sheet images, the perimeter of the wrinkled surface, $P_{T,H}$, can be found directly while $P_{L,H}$ was taken to be the perimeter of a circle having the same area as the flame image. Flame surface distortions as small as the Gibson scale for $u'_{o,avg}/S_L$ = 2.5 could be resolved (roughly 200 μm). In view of this, and findings to be discussed in connection with fractal properties, effects of filtering of fine scale features by limited resolution were not very significant. Accounting for potential filtering, experimental uncertainties (95% confidence) of $P_{T,V}/P_{L,V}$ and $P_{T,H}/P_{L,H}$ were estimated to be less than 10 and 20% for $u'_{o,avg}/S_L$ = 0.9 and 2.5.

The variations of $P_{T,V}/P_{L,V}$ and $P_{T,H}/P_{L,H}$ are plotted as a function of distance from the burner in Figure 13. Unlike the flame brush thickness, the perimeter ratios increase monotonically with increasing distance from the flameholder. Effects of preferential diffusion can also be seen, with the perimeter ratios for unstable (ϕ = 0.8) conditions being consistently larger than those of stable (ϕ = 3.6) conditions at a given distance from the burner exit, even though turbulence properties and laminar flame speeds are nearly identical. However, effects of preferential diffusion are clearly smaller for the larger value of relative turbulence intensity. This is reasonable because effects of passive turbulent distortion are more dominant than active preferential diffusion flame propagation relative to the velocity field when relative turbulence intensities are large. Another interesting feature of these results is that perimeter ratios in the vertical and horizontal directions are nearly the same for unstable (ϕ = 0.8) conditions but the vertical are larger than the horizontal perimeter ratios for stable (ϕ = 3.6) conditions. This suggests that the enhanced distortion at unstable conditions tends to be more isotropic because much of it is generated by the

flame itself, while reduced levels of distortion for stable conditions tend to reflect the underlying anisotropy of the turbulent field of the unburned gas to a greater degree.

The average surface area of the wrinkled interface, A_T, was determined from the perimeters of the horizontal and vertical light sheet images using the exact definitions of perimeter and surface area:

$$P_{TV} = \int_{x_1}^{x_2} (1 + (\partial r_f/\partial x)^2)^{1/2} dx \tag{1}$$

$$P_{TH} = \int_{0}^{2\pi \bar{r}_f} (1 + (\partial r_f/\partial y)^2)^{1/2} dy \tag{2}$$

$$A_T = \int_{x_1}^{x_2} \int_{0}^{2\pi \bar{r}_f} (1 + (\partial r_f/\partial x)^2 + (\partial r_f/\partial y)^2)^{1/2} dy\, dx \tag{3}$$

where r_f is the radial location of the flame surface, x is the streamwise coordinate and y is the azimuthal coordinate, $r_f d\theta$, in this cylindrical coordinate system. A simple closed form expression relating A_T, P_{TV} and P_{TH} can be derived if the derivatives $\partial r_f/\partial x$ and $\partial r_f/\partial y$ are sufficiently small; then the kernals of the integrals in Eqs. (1) and (2) become $(1 + (\partial r_f/\partial x)^2/2)$ and $(1 + (\partial r_f/\partial y)^2/2)$ so that Eq. (3) can be approximated as

$$A_T/A_L = (P_{TV}/P_{LV}) + (P_{TH}/P_{LH}) - 1 \tag{4}$$

Equation (4) is not exact for large amplitude wrinkles; however, the uncertainty of the approximation can be estimated by evaluating both sides for a wavy sinusoidal surface $z = z_o \sin(2\pi x_1/\lambda_1) \sin(2\pi x_2/\lambda_2)$. For wrinkles having amplitude-to-wavelength ratios (z_o/λ) less than 5, the approximation is correct within 10%. All wrinkles that were observed met this criterion so that Eq. (4) was used to evaluate A_T/A_L for the present flames. Then in view of the uncertainties of the perimeter ratios, the experimental uncertainties (95% confidence) of A_T/A_L are estimated to be less than 20 and 30% for $u'_{o,avg}/S_L = 0.9$ and 2.5.

The flame surface area ratios, A_T/A_L, are plotted as a function of height above the burner in Figure 14. Similar to the perimeter ratios, A_T/A_L increases with increasing height above the burner. To the extent that A_T/A_L is a measure of the local turbulent burning velocity, which is most appropriate for neutral conditions for preferential diffusion and modest stretch rates (Gouldin, 1987), this means that the use of effective turbulent burning velocities for jet flames, based on an average taken over the flame surface (Ballal, 1979; Dandekar and Gouldin, 1982; Grover et al., 1959; Wu et al., 1990), provides a measure of effects of turbulence on flame speeds but tends to obscure important effects of distance from the point of flame attachment.

Similar to the perimeter ratios, the area ratios illustrated in Figure 14 exhibit effects of preferential diffusion by comparing results for unstable ($\phi = 0.8$) and stable ($\phi = 3.6$) conditions. The unstable flame generally has a larger value of A_T/A_L at a given distance from the burner exit; however, differences between unstable and stable conditions decrease as the relative turbulence intensity increases for the reasons discussed earlier. The effect of the growth of the flame surface distortions with distance plays a role as well, for example, the stable flames extend farther than the rest due to lower levels of distortion near the burner, but eventually at large distances from the burner exit actually exhibit higher values of A_T/A_L than the other flame conditions.

Assuming that S_T/S_L is primarily controlled by the distortion of the flame surface as represented by A_T/A_L, the results illustrated in Figure 14 can be related to other observations of effects of preferential diffusion. In particular, Wu et al. (1990) find two branches for S_T/S_L averaged over the entire length of turbulent jet flames when plotted as a function of $u'_{o,avg}/S_L$: a stable branch and a neutral/unstable branch, the latter exhibiting a faster rate of increase with $u'_{o,avg}/S_L$. Similarly, observations of Abdel Gayed et al. (1976, 1984) for turbulent hydrogen/air flames and Liu and Lenze (1988) for turbulent

hydrogen/methane/air flames exhibited faster growth rates of S_T/S_L with increasing $u'_{o,avg}/S_L$ for neutral/unstable conditions than for stable conditions. The results illustrated in Figure 14 generally agree with these trends, but also suggest effects of distance from the burner exit on S_T/S_L at various $u'_{o,avg}/S_L$ as well as greater differences between results for neutral and unstable conditions.

Fractal Properties. A popular measure of the degree of wrinkledness of flame surfaces is the fractal dimension, D_2 (Gouldin, 1987; Gouldin et al., 1988; Mantzaras et al. 1989; Murayama and Takeno, 1988; North and Santavicca, 1990; Santavicca et al., 1990; Videto and Santavicca, 1990). D_2 was found for the present flames by measuring values of the flame perimeter using rulers of different size, ε, as discussed by Mandelbrot (1982). Beginning with one location on the interface, a computer routine was used to find the locus of points on an arc of radius ε about that location. The point where the arc intersects the interface determines the next location where the arc is to be centered, etc., until the extent of the surface has been reached. If the arc intersects the interface at more than one location, the next center is taken to be the nearest intersection along the interface. The flame perimeter associated with a given value of ε is the number of arcs drawn, multiplied by the radius (ε) of each.

A typical plot of normalized perimeter as a function of normalized ruler size is illustrated in Figure 15. These measurements are for horizontal light sheet images at x/d = 6.9, $u'_{o,avg}/S_L$ = 2.5 and ϕ = 3.6, ensemble-averaging results for each ruler size over 12 images in order to smooth the plot. The plot approaches two limits: at small ε where the complete perimeter is resolved, and at large ε where ruler sizes approach the maximum dimension of the flame perimeter so that round off of the procedure causes the perimeter to vary in an irregular manner. Between these limits, the curve exhibits a relatively smooth slope that is suggestive of fractal-like behavior. The slope of the best fit linear curve for this intermediate region is $1-D_2$, assuming that the flame surface is fractal (Mandelbrot, 1982). Estimated experimental uncertainties (95% confidence) are less than 20% for D_2.

In order to compare present results with other work, where the assumption of isotropic surface properties is generally invoked (Gouldin, 1987; Lovejoy, 1982; Mantzaras et al., 1989; North and Santavicca, 1990; Sreenivasan and Meneveau, 1986), it will be assumed that $D_3 = 1 + D_2$ (Mandelbrot, 1982), in the following.

In Figure 15, the intersections between the linear fit and the small and large scale limits define inner and outer cut-offs that are representative of the small and large scale irregularities of the flame surface (Gouldin, 1987). Present outer scales were simply comparable to the largest dimensions of the flame perimeter while inner scales were marginally resolvable at $u'_{o,avg}/S_L$ = 2.5; therefore, cut offs are not reported in the following. However, behavior near the inner cut off provides insight concerning the resolution of flame surface perimeters. In particular, results of Figure 15 are for $u'_{o,avg}/S_L$ = 2.5 with a very irregular surface that yielded a large fractal dimension. Even at this condition, however, the variation of P_1/P_0 is gradual near the inner cut off ($\varepsilon/\varepsilon_1$ = 1). Applying fractal relationships for the variation of P_1 with ε (Gouldin, 1987), between the inner cut-off and the Gibson scale, yields potential underestimation of P_1 less than 10% (at least to the extent that the Gibson scale represents the smallest surface distortions). This is representative of results at $u'_{o,avg}/S_L$ = 2.5, while similar considerations suggest negligible resolution errors for results at $u'_{o,avg}/S_L$ = 0.9.

Values of D_2 as a function of height above the burner are plotted for all six flames tested in Figure 16. These results were obtained using horizontal light sheet images in order to provide results at well-defined distances from the burner exit; the range x/d = 1 up to the region of the flame tip was considered. Values of D_2 are seen to be influenced by height above the burner, $u'_{o,avg}/S_L$ and effects of preferential diffusion instability, similar to the normalized flame area. For all conditions, D_2 progressively increases with increasing distance from the burner. Murayama and Takeno (1988) report similar behavior for D_2 found from horizontal light sheet photographs for lean methane/air turbulent jet flames. Near the burner exit, D_2 approaches unity, which is the value representative of a

smooth geometrical surface (Mandelbrot, 1982). This follows since the point of attachmer of the flame is fixed along the periphery of the burner passage exit and the turbulence doe not have sufficient distance (time) to distort the flame surface from this boundary condition With increasing distance from the burner exit, the degree of distortion of the flame surfac increases, somewhat analogous to the larger lateral distances reached by fluid particles wit increasing distance from a fixed source in a uniform turbulent flow due to turbulen dispersion as noted earlier. This results in increased values of D_2 with height above th burner, analogous to the increases of $\bar{r}'_f$, P_T/P_L and A_T/A_L seen in Figures 11-14, at leas until the region of the flame tip is approached. The finite extent of the unburned ga imposes another boundary condition which limits the growth of D_2 so that the larges values of D_2 seen in Figure 16 are generally associated with the longest flames. Unlike $\bar{r}'_f$, however, which tends to decrease as the flame tip boundary condition is approached D_2 behaves more like P_T/P_L and A_T/A_L which simply exhibit reduced rates of growth neai the flame tip (see Figures 11-14). A second factor that limits the estimate growth of D_2 involves the maximum levels of distortion of surfaces within turbulent flow fields. Measurements of passive surfaces associated with turbulence, like the turbulent/nonturbulent interface in free shear layers and cloud surfaces, yield values of D_3 in the range 2.3-2.4 (Sreenivasan and Meneveau, 1986; Lovejoy, 1982). Gouldin (1987) suggests that similar maximum values of D_3 are appropriate for premixed turbulent flames when u'/S_L is large; in fact, values in the range 2.3-2.4 have been observed at large u'/S_L by Mantzaras et al. (1989) and North and Santavicca (1990). Notably, results for the longest flame in Figure 16 appear to be approaching similar values if the isotropic approximation $D_3 = 1 + D_2$ is applied, even though this flame is stable and $u'_{o,avg}/S_L$ is only 2.5.

The main effect of $u'_{o,avg}/S_L$ on D_2 seen in Figure 16 is that small values of this parameter result in shorter flame lengths for present test conditions which limits the

maximum values that D_2 can achieve. Other trends with respect to $u'_{o,avg}/S_L$ alone tend to be obscured by limited experimental accuracy and effects of preferential diffusion.

Effects of preferential diffusion are quite evident from the results plotted in Figure 16. The effect is most readily seen for $u'_{o,avg}/S_L = 0.9$ where the initial rate of growth of D_2 is much more rapid for $\phi = 0.8$ (unstable) than for $\phi = 3.6$ (stable). Nevertheless, effects of distance from the burner exit also play a role and values of D_2 near the flame tip are actually larger for the longer stable flame than for the unstable flame. Differences between initial growth rates for $\phi = 0.8$ and 3.6 are smaller for $u'_{o,avg}/S_L = 2.5$ than 0.9 but the unstable flame still exhibits higher initial growth rates. Nevertheless, as noted earlier, the long stable flame eventually exhibits the highest values of D_2 observed during present measurements -- reaching values expected for passive surfaces in turbulent flows.

Surface Length Scales Measures of flame surface distortion like P_T/P_L, A_T/A_L and D_2 are of interest but it is difficult to relate these quantities to the characteristic scales of the turbulence that are the major factors causing the distortion. As noted earlier, present measurements did not yield useful inner and outer fractal scales: the outer scales were largely fixed by the burner size in the region that could be measured while the inner scales were comparable to present limits of spatial resolution. As an alternative, a flame surface scale or wrinkled wavelength, λ_P, was defined as the wavelength of a square wave that has the same perimeter and r.m.s. fluctuation as the measured flame surface. By calculating the perimeter of a rectangular wave, it is easily shown that

$$\lambda_P = 4\bar{r}'_f/(P_T/P_L - 1) \qquad (5)$$

Then using the values of $\bar{r}'_f$ and P_T/P_L plotted in Figures 11-13, the values of λ_P were found. The resulting values of λ_P/ℓ_{uo} are plotted as a function of x/d in Figure 17 for all six flames tested.

In general, wrinkle wavelengths illustrated in Figure 17 are comparable to the integral scale of the turbulence within the unburned gas. Wrinkle wavelengths also decrease with increasing $u'_{o,avg}/S_L$, indicating a finer degree of wrinkling of the flame

surface as effects of turbulence begin to dominate the combustion process. Effects of flame position are more complex due to the boundary conditions, with λ_P/ℓ_{uo} increasing near the burner exit and then tending to decrease again as the flame tip is approached. The initial growth is due to development of flame surface distortion, since some distance is required to complete large scale deflections. The final reduction near the flame tip is caused by the reduced size of the region containing unburned gas which limits the scale of the largest distortions. Effects of preferential diffusion can be seen at $u'_{o,avg}/S_L = 0.9$, where λ_P/ℓ_{uo} is generally smaller for the unstable than the stable flame, reflecting the growth/damping of small-scale disturbances for unstable/stable conditions. However, these trends are not apparent at $\bar{u}'_{o,avg}/S_L=2.5$ where effects of preferential diffusion are smaller and are obscured by experimental uncertainties.

Discussion

The conditions of present observations of flame surface properties involved relatively uniform turbulence properties of the unburned gas. Thus, flame sheet properties were largely the result of distortion of the flame surface by a nearly uniform turbulence field. Additionally, present test conditions are far from extinction conditions with relatively high laminar flame speeds and laminar flame thicknesses that are comparable or somewhat smaller than Kolmogorov scales based on reactant gas properties. Thus, effects of local flame stretch (or curvature) mostly influence preferential diffusion (which is absent for neutral conditions) rather than cause local quenching.

The main features of the present observations involve effects of evolution of the distortion of the flame surface with distance from the burner exit, $u'_{o,avg}/S_L$, preferential diffusion, and the implications of these phenomena on models of premixed turbulent flames. Effects of flame surface evolution are best considered for neutral conditions where S_T/S_L is proportional to A_T/A_L (Gouldin, 1987). Present results show that A_T/A_L is strongly affected by the geometry of the flame through the boundary conditions. A_T/A_L

increases with increasing distance from the burner exit with maximum values largely governed by the length of the flame. The relative turbulence intensity, $u'_{o,avg}/S_L$ primarily affects the initial rate of growth of A_T/A_L. Thus, general correlations between S_T/S_L and $\bar{u}'/S_L$ cannot be expected for turbulent jet flames because the simple expedient of increasing the burner diameter would increase the flame length and accordingly the maximum values of A_T/A_L and S_T/S_L. This behavior is quite plausible at the limit of large $\bar{u}'/S_L$ where the flame surface is similar to an isoproperty surface within a turbulent field (Gouldin, 1987). In these circumstances, turbulent dispersion is well known to increase the lateral spread of tagged fluid particles with increasing distance from the source, leading to a corresponding increase of A_T/A_L. Similarly, flames ignited from a source in a turbulent field undergo progressive development of distortion as they propagate. Thus, while $\bar{u}'/S_L$ influences the rate of increase of A_T/A_L, all flames have large degrees of surface distortion at large distances from the source. As a result, correlations of S_T/S_L solely as a function of $\bar{u}'/S_L$ are only successful to the extent that the rate of growth of A_T/A_L is affected by $\bar{u}'/S_L$ and the fact that they generally involve a limited range of flame sizes. Much of the scatter seen in plots of this type can probably be attributed to effects of the distance from the point of attachment or ignition to the point where the measurements were made. Notably, recent measurements of Trautwein et al. (1990), where the correlation specifically highlights information on distance from the flame source, illustrates this point quite well. In particular, S_T/S_L exhibits a progressive increase with increasing flame size at the time of measurement, analogous to effects of distance from the burner exit observed here. This implies that models of turbulent premixed flames based solely on local conditions, ignoring effects of boundary conditions and distance or time of propagation, are intrinsically incomplete. Thus, premixed turbulent flames are invariably geometry specific, similar to nonpremixed flames which have always been treated as geometry specific.

The same properties of flow development carry over to other parameters of the flame surface like D_2, Γ_1, and λ_P, therefore, present findings concerning these properties

are only pertinent for similar flame conditions. Again limiting considerations to neutral conditions, a finite relative velocity of a fluid point with respect to the flow, like S_L, influences the rate of development of flame surface distortion but eventually the degree of distortion must become large just like distances between fluid particles during turbulent dispersion. This implies that the fractal dimension, D_2, must eventually approach values characteristic of isoproperty surfaces in turbulent fields. Indeed, the longest flame studied here eventually approached $D_2 = 1.35$ which is within the range expected, 1.3-1.4, based on past measurements for passive conditions (Lovejoy, 1982; Sreenevasan and Meneveau, 1986). Thus, correlations of D_2 solely as a function of $\bar{u}'/S_L$, like those reported by Mantzaras et al. (1989) and North and Santavicca (1990), are only appropriate for a particular time from ignition or distance from a stabilization point. The scatter seen in correlations of this type is probably partly due to effects of flame development, except as the limiting range of D_2 is approached. Certainly, present measurements of D_2 over the six flames would measurably add to the scatter of the plots due to a somewhat different range of flame sizes and the progressive increase of D_2 from values near unity at the burner exit, see Figure 16. Thus, in the absence of a successful method for computing the evolution of D_2, application of fractals to estimate turbulent flame speeds is most appropriate for conditions where D_2 is in the limiting range 1.3-1.4, as originally proposed by Gouldin (1987). Similarly, the largest scales of flame distortion are not fundamentally comparable to integral scales, as has been suggested in previous theories (Shchelkin, 1943), any more than the largest separation distances between fluid particles undergoing turbulent dispersion are limited to integral scales (Hinze, 1975).

Effects of preferential diffusion add another level of complexity to the behavior of premixed turbulent flames. Present results, and the companion study of Wu et al. (1990), demonstrate unequivocally that preferential diffusion is a factor that influences turbulent flame speeds and the rate of development of turbulent distortion of the flame surface at Reynolds numbers of interest for practical applications. The effect is to reduce/increase the

rate of increase of flame distortion for stable/unstable conditions, similar to the predictions of Clavin and Williams (1979, 1982) for premixed flames in weak turbulence. When preferential diffusion effects are present, direct proportionality between S_T/S_L and A_T/A_L is questionable (Gouldin, 1987); nevertheless, existing observations suggest that this correspondence is at least roughly correct. Recognizing this and the fact that correlations of S_T/S_L as a function of u'/S_L for particular test conditions largely reflect the rate of growth of flame distortion, several other studies support present findings. For example, Abdel-Gayed et al. (1976, 1984) and Wu et al. (1990) observe higher values of S_T/S_L at particular values of u'/S_L for lean (unstable) than rich (stable) hydrogen/air flames. Liu and Lenze (1988) report similar findings for flames involving CH_4 H_2 mixtures and air. Finally, Abdel-Gayed et al. (1984) find higher values of S_T/S_L at a given u'/S_L for rich (unstable) than lean (stable) propane/air and iso octane/air flames. The last observations are of particular interest because many practical premixed turbulent flames, like those in spark-ignition engines, involve heavy hydrocarbons burning in air at lean (stable) conditions where effects of preferential diffusion can significantly retard the rate of growth of distortion of the flame surface.

Taken together, effects of the development of flame surface distortion and preferential diffusion preclude the effective use of premixed turbulent combustion models that are based solely on local conditions and only involve passive propagation of the flame at a fixed laminar flame speed with respect to the unburned gas. A possible exception involves mixing controlled neutral stability conditions where D_2 is in the range appropriate for isoproperty surfaces in turbulent fields and u'/S_L is small (Bray, 1980; Gouldin, 1987; Wu et al., 1990). Thus, because practical applications meeting the criteria of the exceptions are limited, while existing models and correlations of premixed turbulent flame phenomena are generally incomplete with respect to flame development and preferential diffusion, past ideas concerning models and correlations of turbulent premixed flame processes should be re examined.

Conclusions

The major conclusions of the study can be summarized as follows:

1. Spatial variations of flame surface properties were quantified. As the distance from the flameholder increased, even though unburned gas turbulence properties were relatively constant, the following properties increased in value: flame surface area (and thus the local turbulent burning velocity), flame brush thickness and the fractal dimension of the flame surface. Approach to the flame tip limits the maximum value of these properties. Thus, effects of the attachment and flame tip boundary conditions imply that turbulent premixed flames are geometry specific while the spatial variations imply that models or correlations of turbulent flame properties based on local properties alone, and don't specifically account for distance from the flameholder, are intrinsically incomplete.

2. Increasing values of u'/S_L tend to increase the rate of turbulent distortion of the flame surface with distance from the flameholder and also increase levels of fine-grained roughness of the flame surface. Thus correlations of S_T/S_L solely as a function of $\bar{u}'/S_L$ can be found because they reflect this rate of increase over limited ranges of flame dimensions. Nevertheless, such correlations are incomplete unless they account for development of flame surface properties with distance from the flameholder (or point of ignition).

3. Effects of preferential diffusion were significant even at the high Reynolds numbers of present experiments, acting to reduce/increase the rate of flame distortion (and correspondingly the local turbulent burning velocity) for stable/unstable conditions. Review of earlier work in the literature revealed that this behavior is not limited to the present hydrogen/air flames due to the unusually large mass diffusivity of hydrogen, e.g., similar behavior has been observed for methane, propane and iso-octane/air flames (Abdel-Gayed et al., 1976, 1984; Liu and Lenze, 1988). In particular, spark ignition engines use mixtures of heavy hydrocarbons and air and

operate fuel lean; this places them in stable preferential diffusion conditions which should retard the rate of development of flame surface distortion. Few practical applications involve neutral preferential diffusion conditions; therefore, models and correlations of premixed flame properties should be re-examined to consider effects of preferential diffusion that are important for both stable and unstable conditions. Exceptions may be found at large u'/S_L and distances from the flameholder where effects of preferential diffusion tend to decrease, however, additional study is needed to confirm this trend.

4. Measurements showed that the turbulence properties of the unburned gas were relatively uniform and did not change appreciably as the flame surface was approached. Present measurements include findings for stable, neutral and unstable preferential diffusion conditions (with nearly identical burner exit conditions and laminar flame speeds for stable and unstable conditions), various values of $\bar{u}'_{o,avg}/S_L$, and a reasonably complete characterization of unburned gas properties. Coupled with current understanding of the structure of laminar hydrogen/air flames, it is hoped that this information will prove to be useful for developing more complete models and correlations of the properties of premixed turbulent combustion processes than now exist.

Acknowledgements

This research was supported by the Office of Naval Research, Contract No. N00014-87-K-0698, with S. Ramberg serving as Scientific Program Officer.

References

Abdel-Gayed, R. G., and Bradley, D. (1976). Dependence of turbulent burning velocity on turbulent Reynolds number and ratio of laminar burning velocity to r.m.s. turbulent velocity. *Sixteenth Symposium (International) on Combustion*, The Combustion Institute, Pittsburgh, pp. 1725-1735.

Abdel-Gayed, R. G., Bradley, D., Hamid, M. M., and Lawes, M. (1984). Lewis number effects on turbulent burning velocity. *Twentieth Symposium (International) on Combustion*, The Combustion Institute, Pittsburgh, pp. 505-512.

Andrews, G. E., and Bradley, D. (1973). Determination of burning velocity by double ignition in a closed vessel. *Combust. Flame* 20, 77.

Ballal, D. R. (1979). The structure of a premixed turbulent flame. *Proc. R. Soc. London* A367, 353.

Box, G. P., and Jenkins, G. M. (1976). *Time Series Analysis*, Holden-Day, San Francisco, CA, pp. 47-66.

Boyer, L., Clavin, P., and Sabathier, F. (1980). Dynamic behavior of a premixed turbulent flame front. *Eighteenth Symposium (International) on Combustion*, The Combustion Institute, Pittsburgh, pp. 1041-1049.

Bray, K.N.C. (1980). Turbulent flows with premixed reactants. In P. A. Libby and F. A. Williams (Eds.), *Turbulent Reacting Flows*, Springer, Berlin, pp. 115-183.

Cant, R. S., and Bray, K.N.C. (1988). Strained laminar flamelet calculations of premixed turbulent combustion in a closed vessel. *Twenty-Second Symposium (International) on Combustion*, The Combustion Institute, Pittsburgh, pp. 791-799.

Clavin, P. (1985). Dynamic behavior of premixed flame fronts in laminar and turbulent flows. *Prog. Energy Combust. Sci.* 11, 1.

Clavin, P., and Williams, F. A. (1979). Theory of premixed-flame propagation in large-scale turbulence. *J. Fluid Mech.* 90, 589.

Clavin, P., and Williams, F. A. (1982). Effects of molecular diffusion and of thermal expansion in the structure and dynamics of premixed flames in turbulent flows of large scale and low intensity. *J. Fluid Mech.* 116, 251.

Gouldin, F. C. (1987). An application of fractals to modeling premixed turbulent flames. *Combust. Flame* 68, 249.

Gouldin, F. C., Hilton, S. M., and Lamb, T. (1988). Experimental evaluation of the fractal geometry of flamelets. *Twenty-Second Symposium (International) on Combustion*, The Combustion Institute, Pittsburgh, pp. 541-550.

Grover, J. H., Fales, E., and Scurlock, A. C. (1959). Turbulent flame studies in a two-dimensional open burner. *ARS J.* 26, 275.

Hinze, J. O. (1975). *Turbulence*, McGraw-Hill, New York, 2nd edition, Chapt. 4.

Incropera, F. P., and DeWitt, D. P. (1981). *Fundamentals of Heat Transfer*, John Wiley & Sons, New York, p. 785.

Joulin, G., and Mitani, T. (1981). Linear stability analysis of two-reactant flames. *Combust. Flame* 40, 235.

Laufer, J. (1954). Cited in Hinze, J. O. (1975), *Turbulence*, McGraw-Hill, New York, 2nd edition, pp. 720-724.

Libby, P. A., Sivasegaram, S., and Whitelaw, J. H. (1986). Premixed combustion. *Prog. Energy Combust. Sci.*, 12, 353.

Liu, Y., and Lenze, B. (1988). The influence of turbulence on the burning velocity of premixed CH_4-H_2 flames with different laminar burning velocities. *Twenty-Second Symposium (International) on Combustion*, The Combustion Institute, Pittsburgh, pp. 747-754.

Lovejoy, S. (1982). Area-perimeter relation for rain and cloud-areas. *Science* 216, 185.

Mandelbrot, B. B. (1982). *The Fractal Geometry of Nature*, W. H. Freeman, San Francisco.

Manton, J., von Elbe, G., and Lewis, B. (1952). Nonisotropic propagation combustion waves in explosive gas mixtures and development of cellular flan *J. Chem. Phys.* 20, 153.

Mantzaras, J., Felton, P. G., and Bracco, F. V. (1989). Fractals and turbulent premi engine flames. *Combust. Flame* 77, 295.

Murayama, M., and Takeno, T. (1988). Fractal-like character of flamelets in turbul combustion. *Twenty-Second Symposium (International) on Combustion*, T Combustion Institute, Pittsburgh, pp. 551-559.

Nikuradse, J. (1932). Cited in Hinze, J. O. (1975), McGraw-Hill, New York, 2 edition, pp. 725-727.

North, G. L., and Santavicca, D. A. (1990). The fractal nature of premixed turbul flames. *Combust. Sci. and Tech.*, in press.

Peters, N. (1986). Laminar flamelet concepts in turbulent combustion. *Twenty-Fi Symposium (International) on Combustion*, The Combustion Institute, Pittsburg pp. 1231-1250.

Pope, S. B. (1990). Computations of turbulent combustion: progress and challenge *Twenty-Third Symposium (International) on Combustion*, The Combusti Institute, Pittsburgh, in press.

Santavicca, D. A., Liou, D., and North, G. L. (1990). A fractal model of turbulent flan kernal growth. SAE Paper No. 900024.

Searby, G., and Clavin, P. (1986). Weakly turbulent, wrinkled flames in premixed gase *Combust. Sci. and Tech.*, 46, 167.

Shchelkin, K. I. (1943). Cited in Lewis, B., and von Elbe, G. (1961). *Combustion Flames and Explosions in Gases*, Academic Press, New York, 2nd edition, Sectio 6.3.

Sreenivasan, K. R., and Meneveau, C. (1986). The fractal facets of turbulence. *J. Flui Mech.* 173, 357.

Tennekes, H., and Lumley J. L. (1972). *Turbulence*, M.I.T. Press, Cambridge, MA, pp. 67.

Trautwein, S. E., Grudno, A., and Adomeit, G. (1990). The influence of turbulence intensity and laminar flame speed on turbulent flame propagation under engine like conditions. *Twenty-Third Symposium (International) on Combustion*, The Combustion Institute, Pittsburgh, in press.

Videto, B. D., and Santavicca, D. A. (1990). Flame turbulence interactions in a freely-propagating, premixed flame. *Combust. Sci. and Tech.*, in press.

Williams, F. A. (1985). *Combustion Theory*, Benjamin/Cummings, Menlo Park, CA, 2nd edition, pp. 341-372, 411-445.

Wu, M.-S., Kwon, S., Driscoll, J. F., and Faeth, G. M. (1990). Turbulent premixed hydrogen/air flames at high Reynolds numbers. *Combust. Sci. and Tech.* 73, 327.

Nomenclature

A_L/A_T	average surface area of time-averaged flame surface, of wrinkled interface
d	burner exit diameter
D_2	fractal dimension of a contour line
$E_k(f)$	temporal power spectral density of velocity component i
f	frequency
ℓ_i	integral length scale based on velocity component i
ℓ_G	Gibson scale
ℓ_k	Kolmogorov scale
L_c	flame length based on a time-averaged reactedness of 0.5
P_L, P_T	perimeter of time-averaged flame surface, of wrinkled interface
r	radial distance
r_f	radial distance to flame surface
Re_d	Reynolds number based on burner exit conditions, $\bar{u}_{o,avg}d/\nu_o$
Re_t	turbulence Reynolds number $\bar{u}'_{o,avg}\ell_{uo}/\nu_o$
S_L, S_T	laminar and turbulent burning velocity
u	streamwise velocity
v	crosstream velocity
x	streamwise distance
y	azimuthal distance, $rd\theta$

Greek Letters

α	thermal diffusivity
δ_L	laminar flame thickness
ϵ	ruler length for fractal property measurement
θ	azimuthal angle
λ_P	wavelength of flame wrinkles
ν	kinematic viscosity
ρ	density
τ_i	integral time scale based on velocity component i
ϕ	fuel-equivalence ratio

Subscripts

1,2	particular positions
avg	mean burner exit value
c	centerline value
H,V	horizontal and vertical light sheet image
o	burner exit condition

Superscripts

$(\bar{\ }),(\bar{\ })'$	time-averaged mean and r.m.s. fluctuating property

Table I Summary of Test Conditions[a]

$\bar{u}'_{o,avg}/S_L$	0.9			2.5		
ϕ	0.8	1.8	3.6	0.8	1.8	3.6
Preferential Diffusion Regime	Unstable	Neutral	Stable	Unstable	Neutral	Stable
$\bar{u}_{o,avg}$ (m/s)	20.4	31.1	20.4	55.0	88.0	58.3
$\bar{u}'_{o,avg}$ (m/s)	2.0	3.1	2.0	5.5	8.8	5.8
S_L (m/s)[b]	2.2	3.5	2.3	2.2	3.5	2.3
ν_o($m^2/s \times 10^6$)	19.8	24.7	32.0	19.8	24.7	32.0
α_o($m^2/s \times 10^6$)	42.1	60.0	80.9	42.1	60.0	80.9
$Re_d=\bar{u}_{o,avg}\, d/\nu_o$	11300	13900	7000	30600	39200	20000
$Re_t=\bar{u}'_{o,avg}\, \ell_{uo}/\nu_o$	313	389	194	861	1104	562
L_o/d[c]	2.6	2.6	2.8	4.0	5.3	7.7
ℓ_k (μm)[d]	42	35	60	20	16	27
$\delta_L=\alpha_o/S_L$ (μm)	19	17	35	19	17	35
Flame Regime[e]	Wrinkled, Thin Flamelets			Mixing-Limited, Thin Flamelets		

[a]Round jet burner (d=11 mm) directed vertically upward with ℓ_{uo} = 3.1 mm. Outer burner flame: ϕ = 0.3, Re_d = 3400 and $\bar{u}_{o,avg}$ = 1 m/s.

[b]Laminar flame speeds from Andrews and Bradley (1973).

[c]Normalized flame length, based on Rayleigh-scattering measurements of Wu et al. (1990).

[d]Kolmogorov scale, $\ell_k = \ell_{u,o}/(\bar{u}'_{o,avg}\, \ell_{u,o}/\nu_o)^{3/4}$, from Tennekes and Lumley (1972).

[e]Based on definitions from Bray (1980).

List of Figures

Figure 12 Mean and fluctuating radial flame position as a function of height above burner: $\bar{u}'_{o,avg}/S_L = 2.5$.

Figure 13 P_T/P_L as a function of height above the burner for vertical (V) horizontal (H) planes.

Figure 14 A_T/A_L as a function of height above the burner.

Figure 15 Sample determination of D_2 for a horizontal plane: $\bar{u}'_{o,avg}/S_L = 2.5$, 3.6 and x/d = 6.9.

Figure 16 Fractal dimension, D_2, for horizontal planes as a function of height ab the burner.

Figure 17 Wavelength of flame wrinkles as a function of height above the burner.

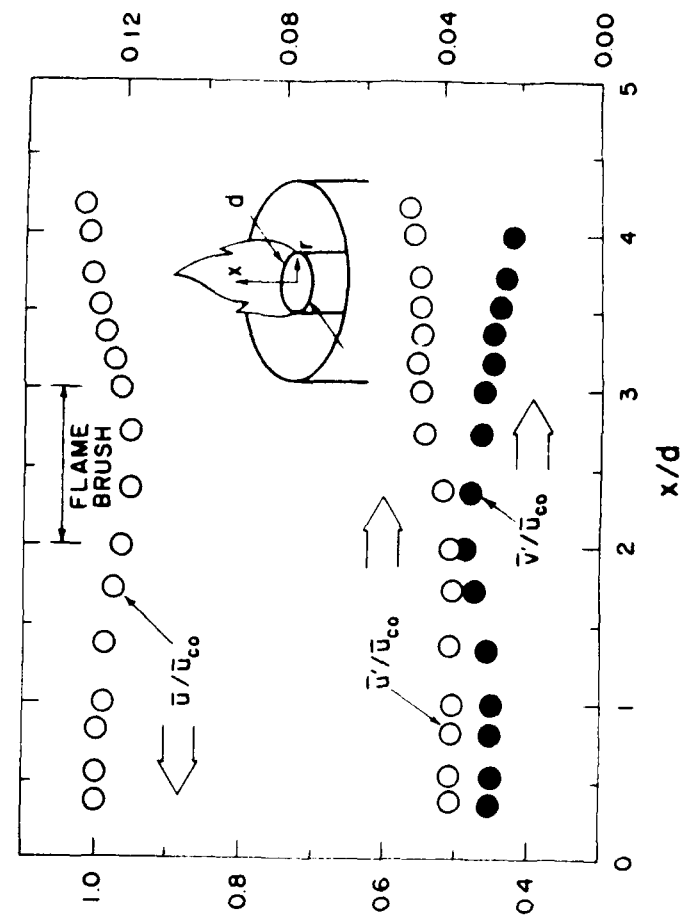

FIG 1

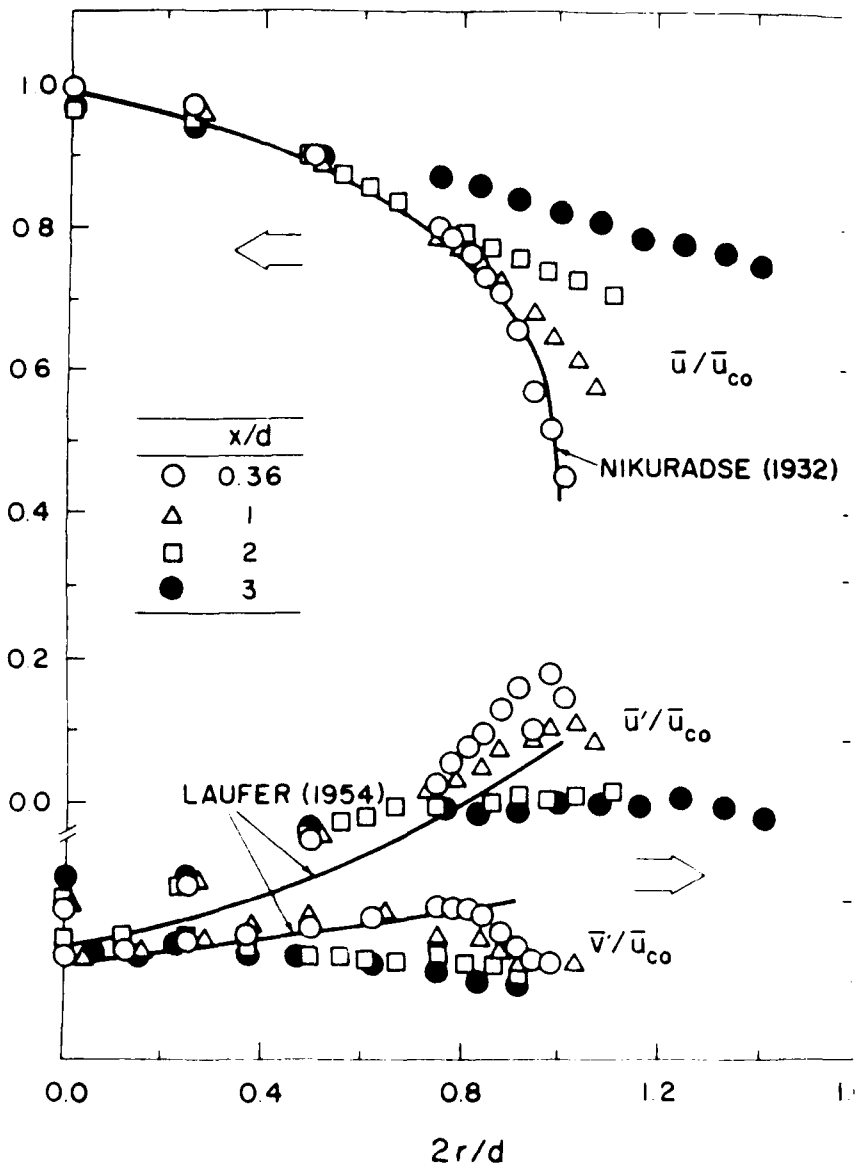
1.0
0.8
0.6
0.4
0.2
0.0
x/d
0.36
1
2
3
$\bar{u}/\bar{u}_{co}$
NIKURADSE (1932)
$\bar{u}'/\bar{u}_{co}$
LAUFER (1954)
$\bar{v}'/\bar{u}_{co}$
0.0
0.4
0.8
1.2
2r/d

FIG. 2

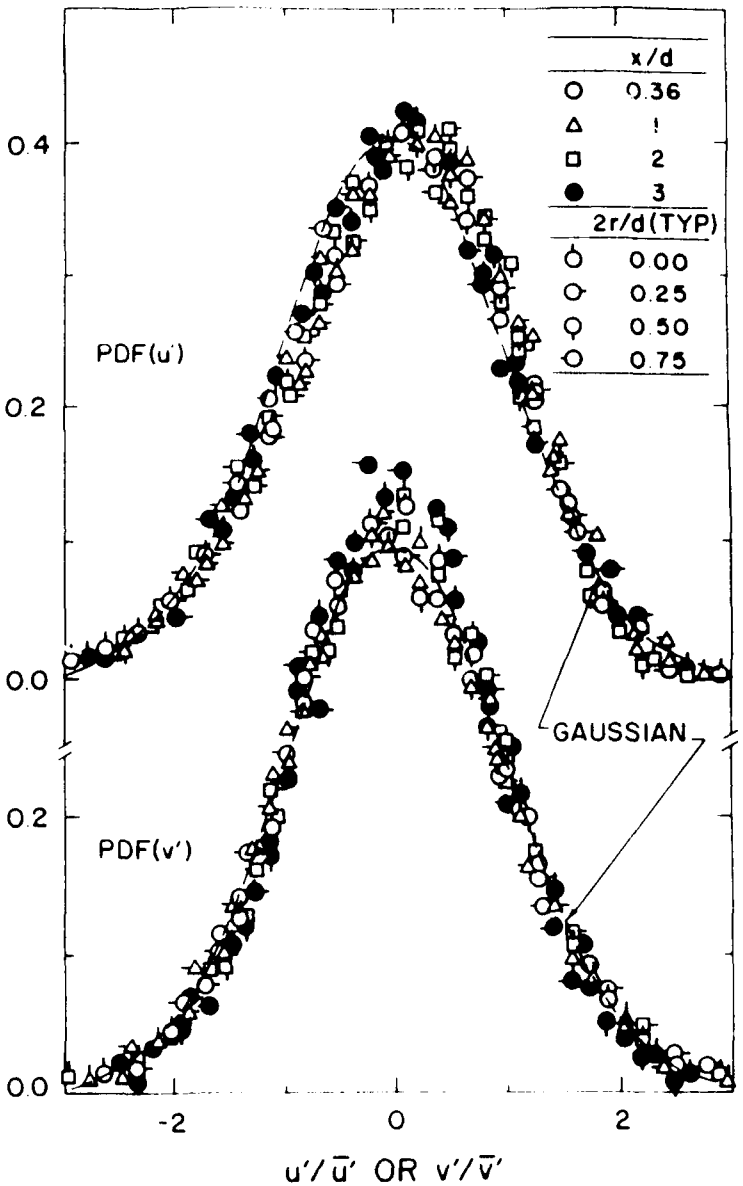
x/d
0.36
1
2
3
2r/d(TYP)
0.00
0.25
0.50
0.75
PDF(u')
PDF(v')
GAUSSIAN
0.4
0.2
0.0
0.2
0.0
-2
0
2
u'/ū' OR v'/v̄'

FIG. 3

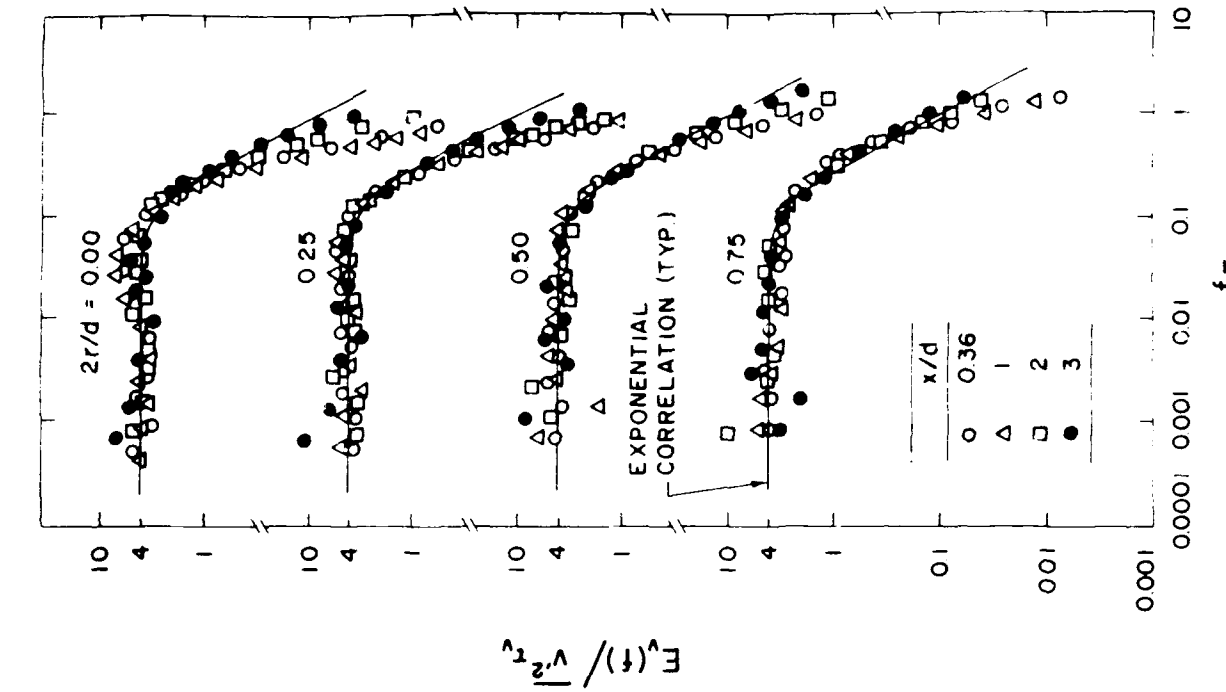
2r/d = 0.00
0.25
0.50
0.75
EXPONENTIAL CORRELATION (TYP.)
x/d
0.36
1
2
3
$E_v(f)/\overline{v'^2}\tau_v$
$f\tau_v$

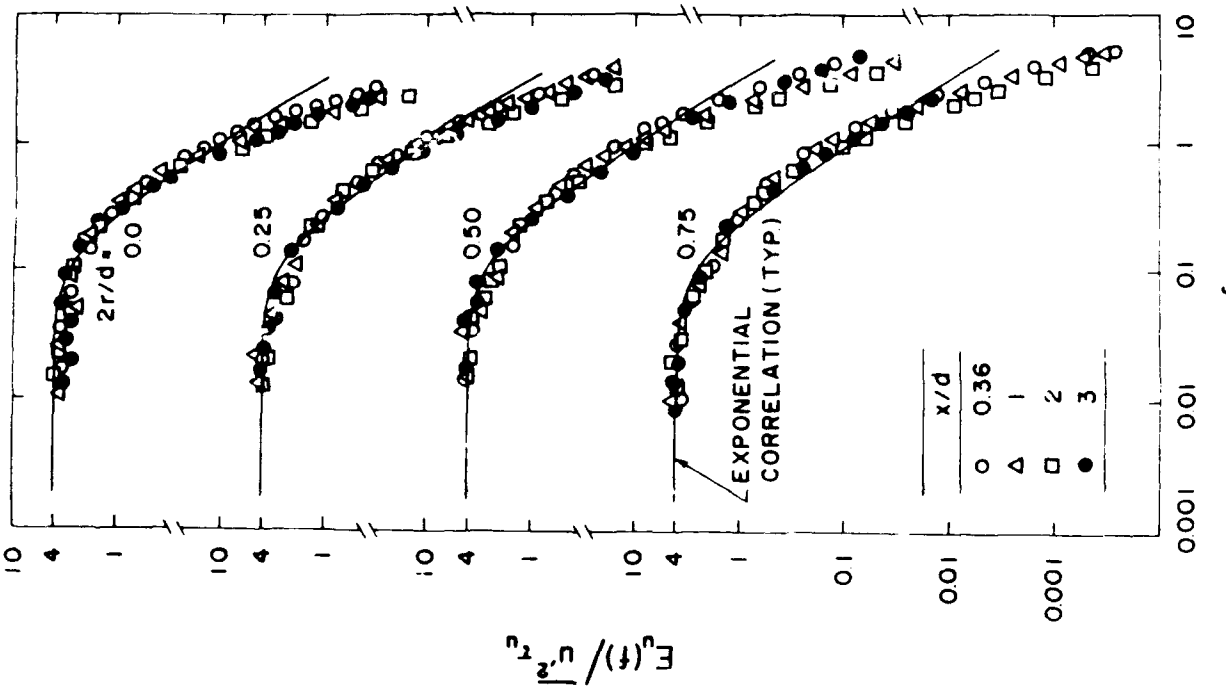
2r/d = 0.0
0.25
0.50
0.75
EXPONENTIAL CORRELATION (TYP.)
x/d
0.36
1
2
3
$E_u(f)/\overline{u'^2}\tau_u$
$f\tau_u$

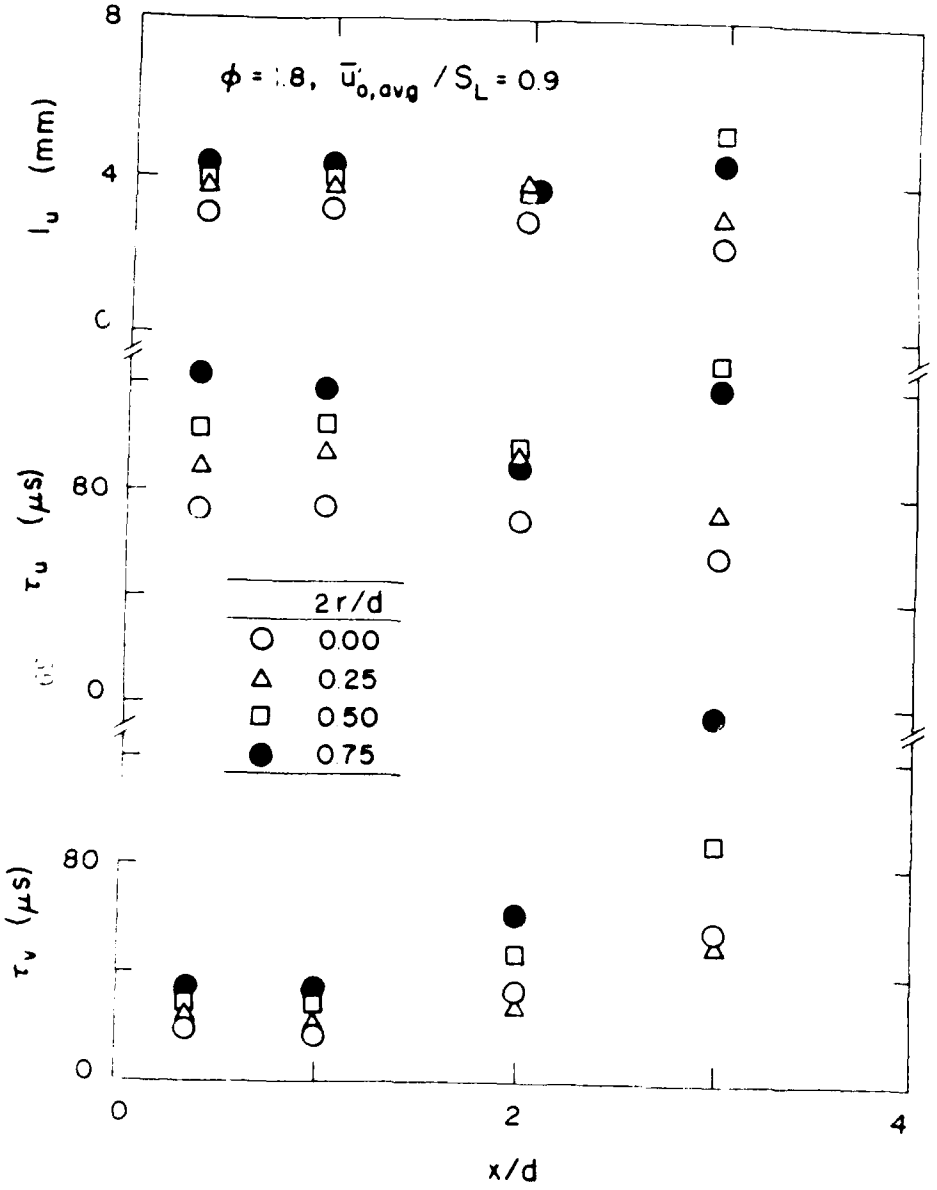
ϕ = 1.8, $\bar{u}'_{o,avg} / S_L$ = 0.9
l_u (mm)
τ_u (μs)
τ_v (μs)
2r/d
0.00
0.25
0.50
0.75
x/d

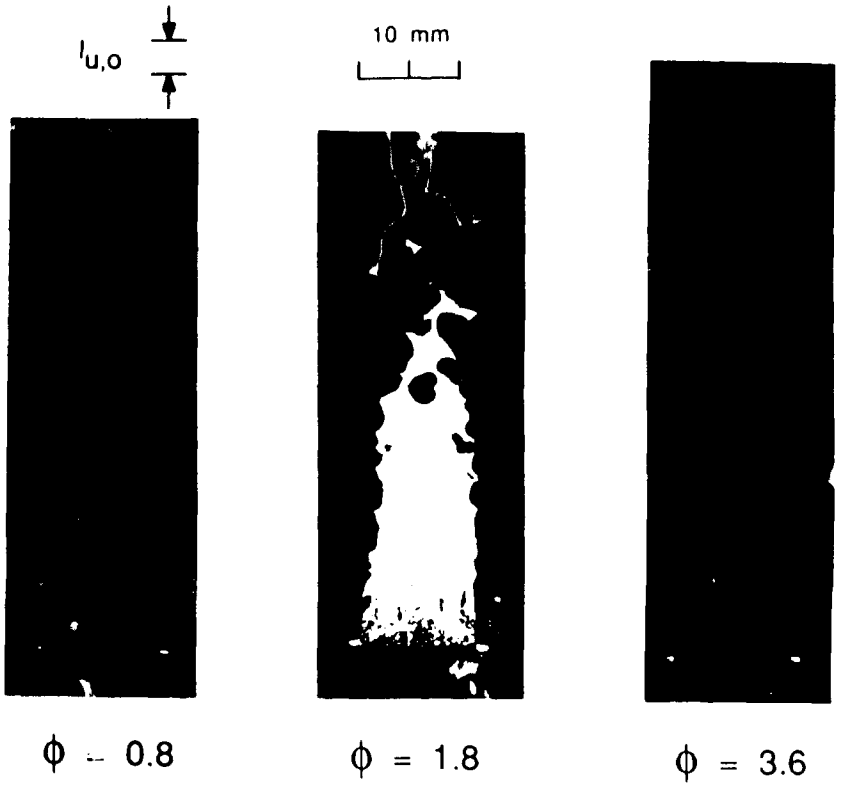
$l_{u,o}$
10 mm
ϕ = 0.8
ϕ = 1.8
ϕ = 3.6

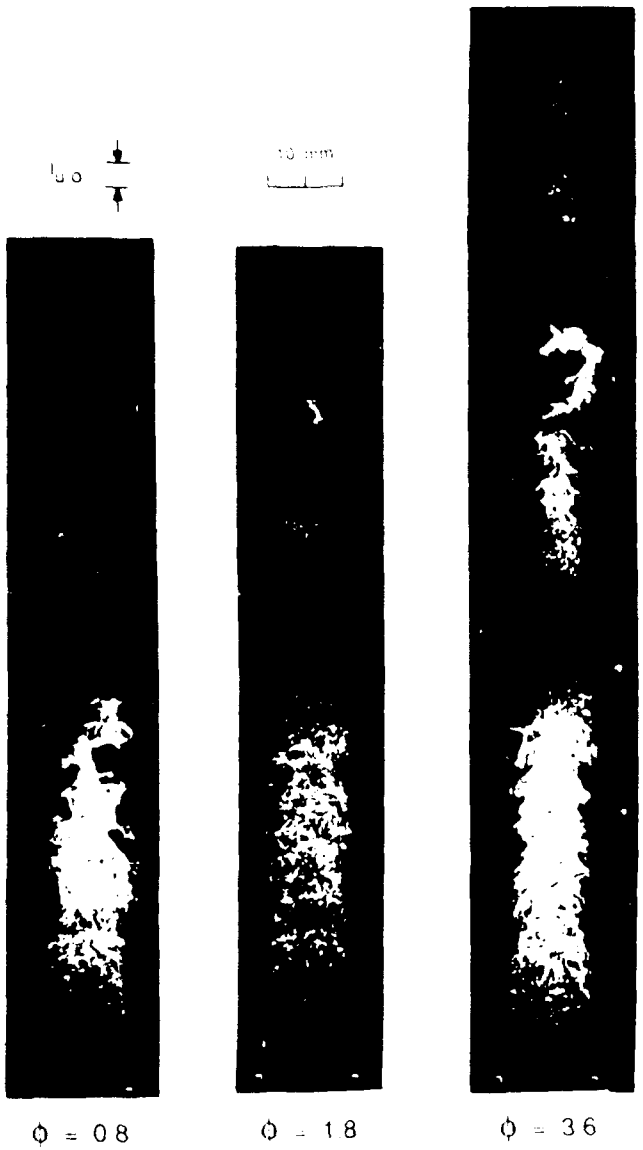

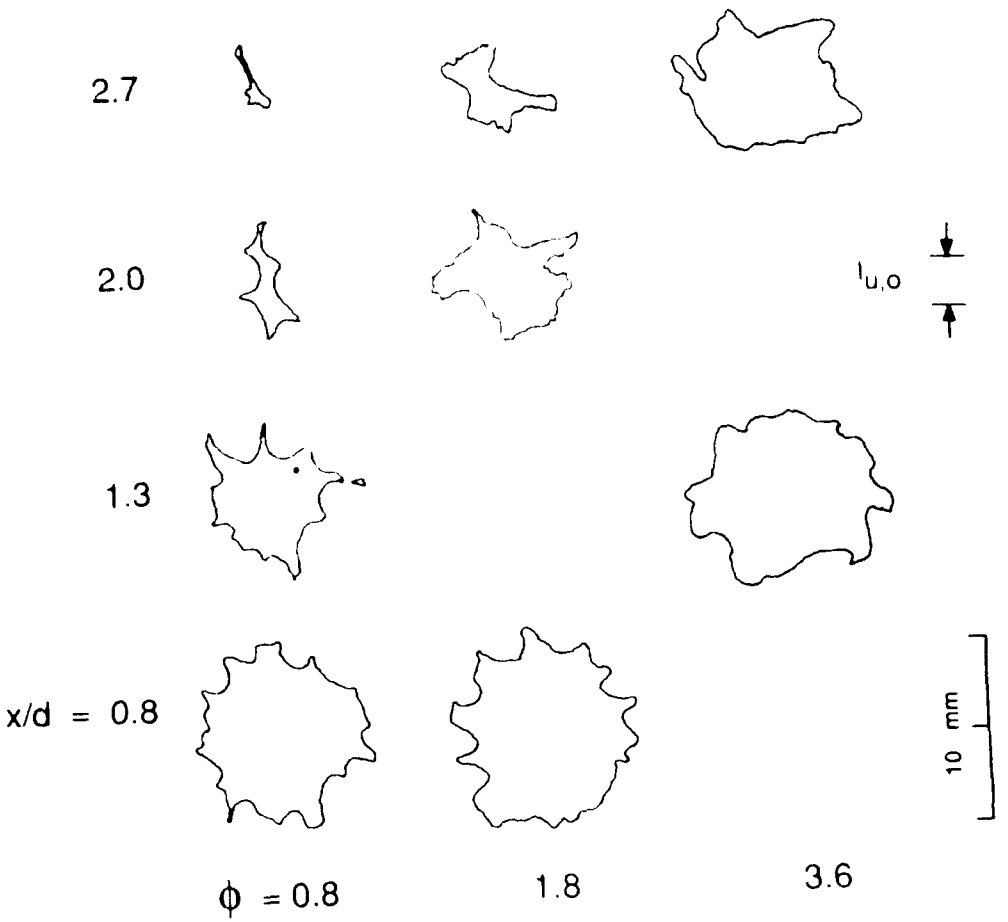

FIG. 3

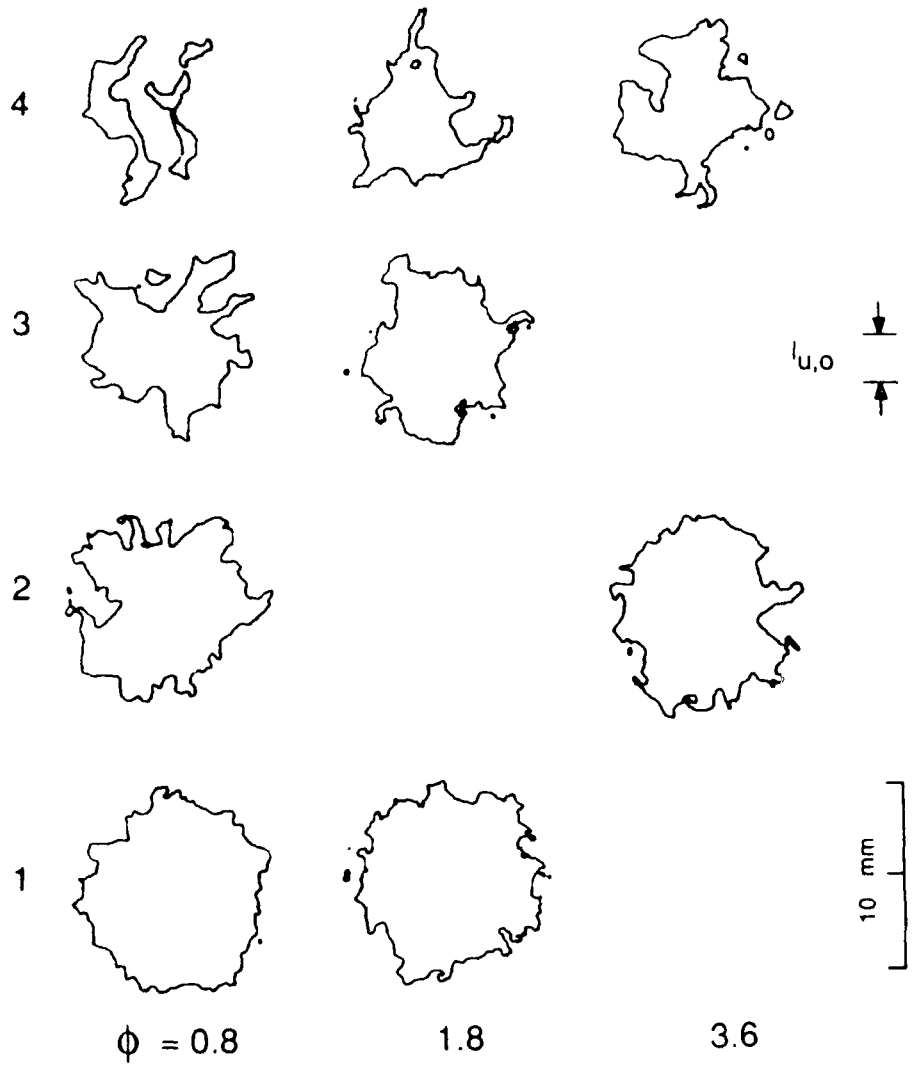
4
3
2
1
$I_{u,o}$
10 mm
ϕ = 0.8
1.8
3.6

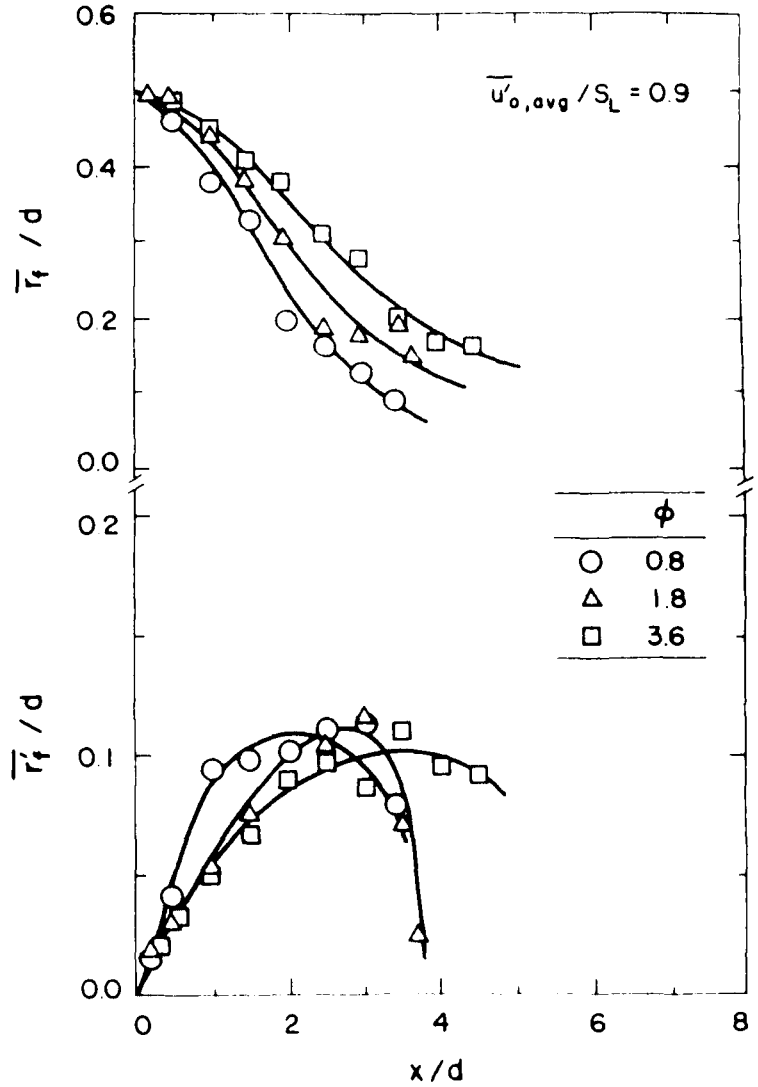
$\overline{u'_{o,avg}} / S_L$ = 0.9
$\overline{r_f} / d$
$\overline{r'_f} / d$
0.6
0.4
0.2
0.0
0.2
0.1
0.0
0
2
4
6
8
x/d
ϕ
0.8
1.8
3.6

FIG.

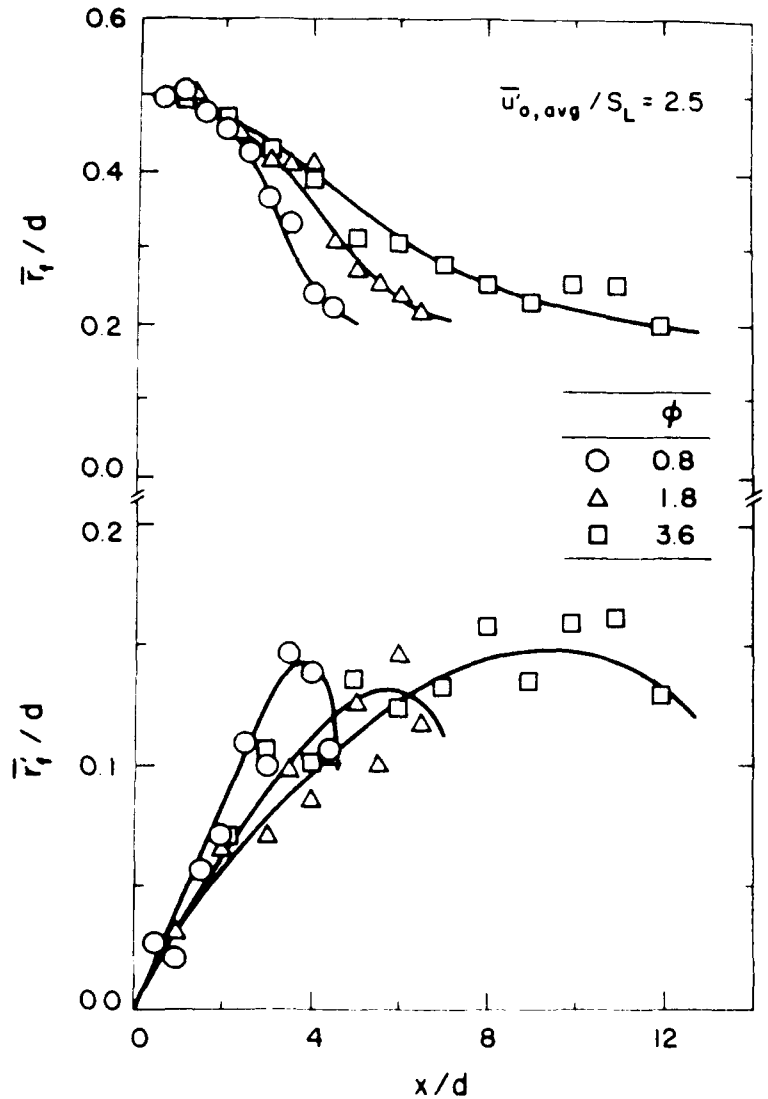
0.6
0.4
0.2
0.0
$\overline{u'}_{o,avg}/S_L = 2.5$
$\overline{r_f}/d$
ϕ
0.8
1.8
3.6
0.2
0.1
0.0
$\overline{r_f'}/d$
0
4
8
12
x/d

FIG. 12

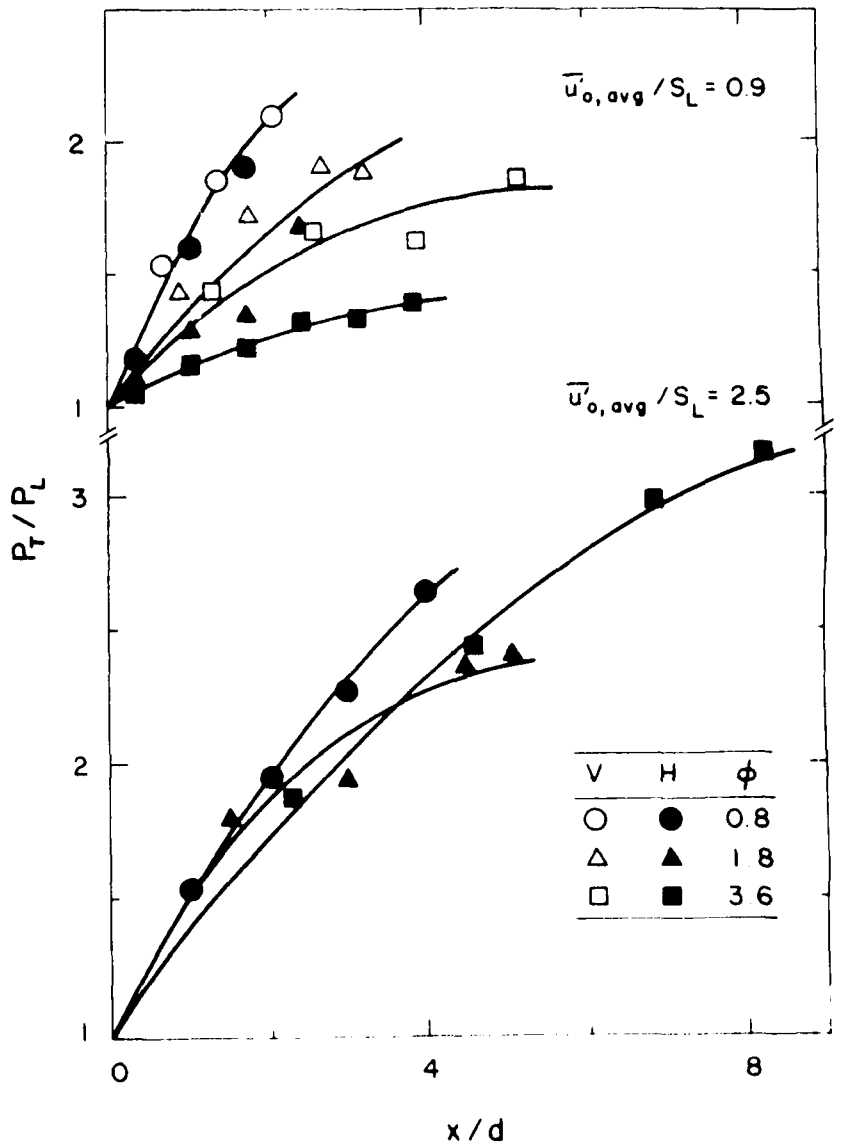
$\overline{u'}_{o,avg}/S_L = 0.9$
$\overline{u'}_{o,avg}/S_L = 2.5$
2
1
3
2
1
P_T/P_L
V
H
ϕ
0.8
1.8
3.6
0
4
8
x/d

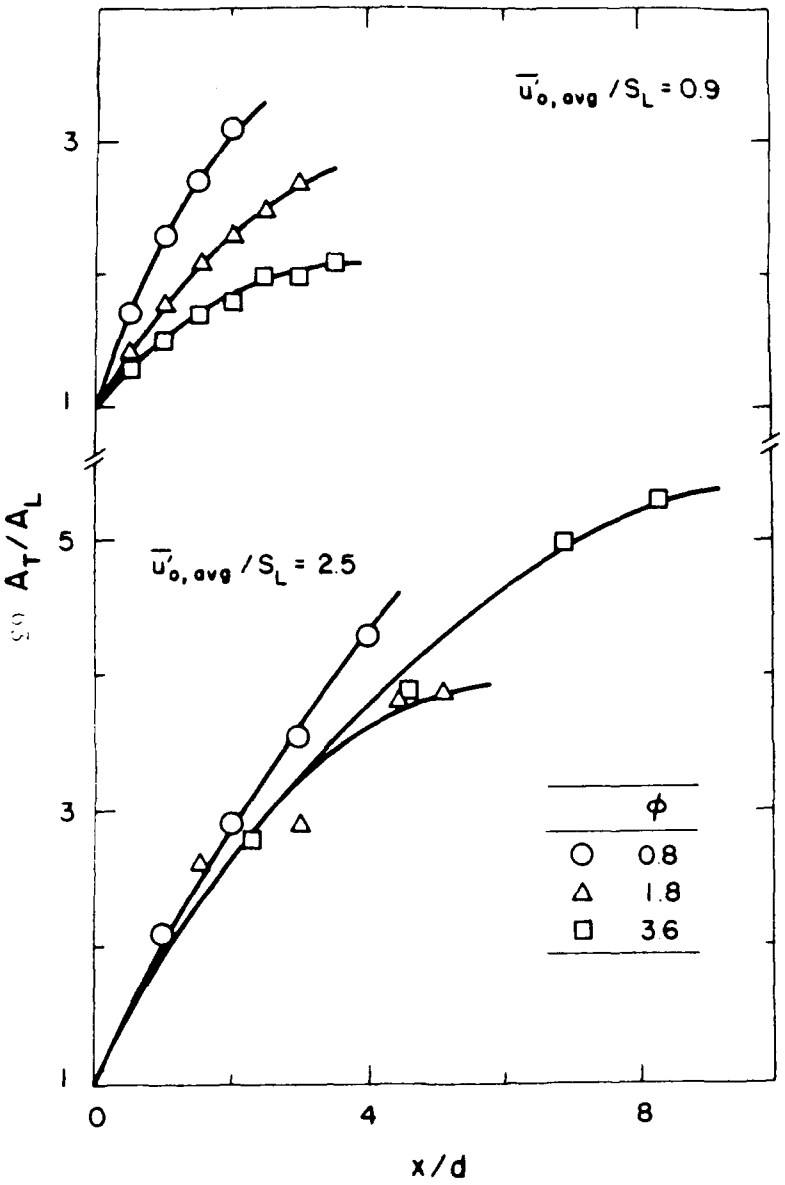
$\overline{u'_{o,avg}}/S_L = 0.9$
$\overline{u'_{o,avg}}/S_L = 2.5$
A_T/A_L
x/d
φ
0.8
1.8
3.6

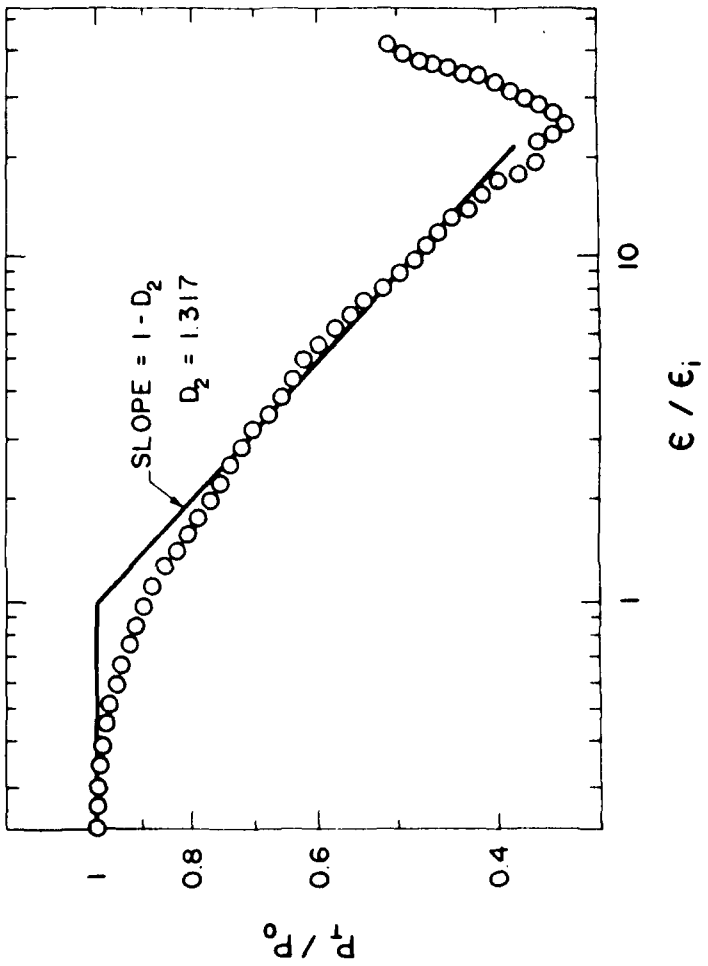
SLOPE = 1 - D_2
D_2 = 1.317
P_T/P_o
ε / $ε_i$

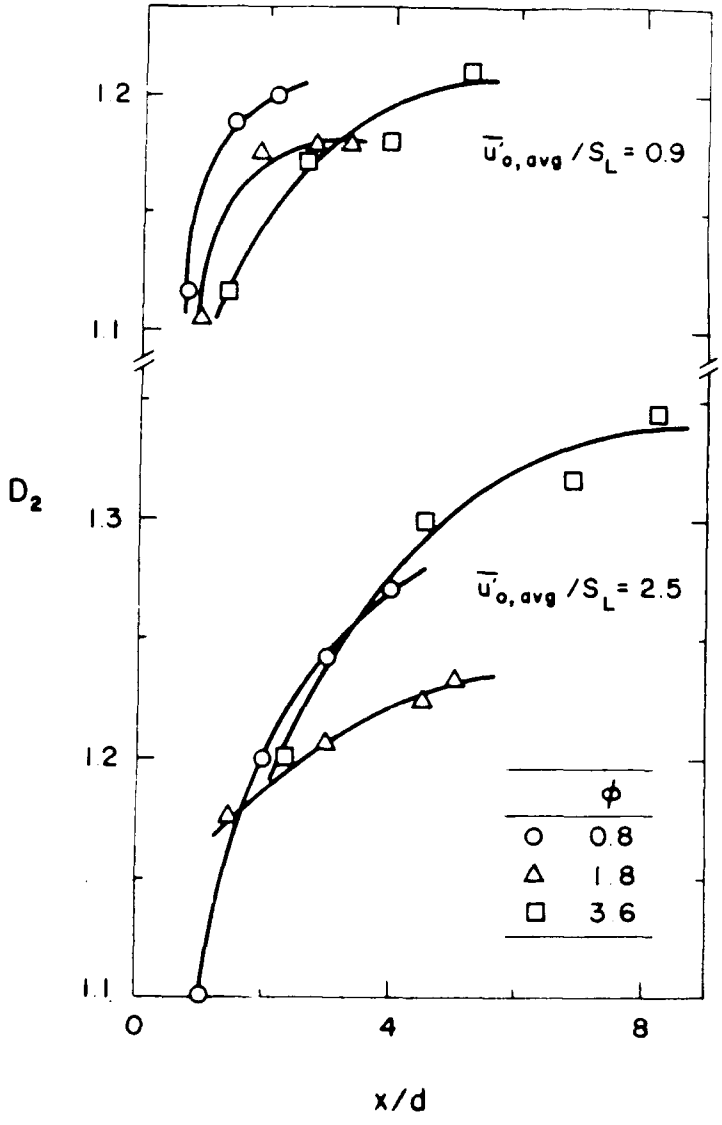
1.2
1.1
1.3
1.2
1.1
D_2
$\overline{u'}_{o,avg}/S_L = 0.9$
$\overline{u'}_{o,avg}/S_L = 2.5$
ϕ
○ 0.8
△ 1.8
□ 3.6
0
4
8
x/d

FIG. .

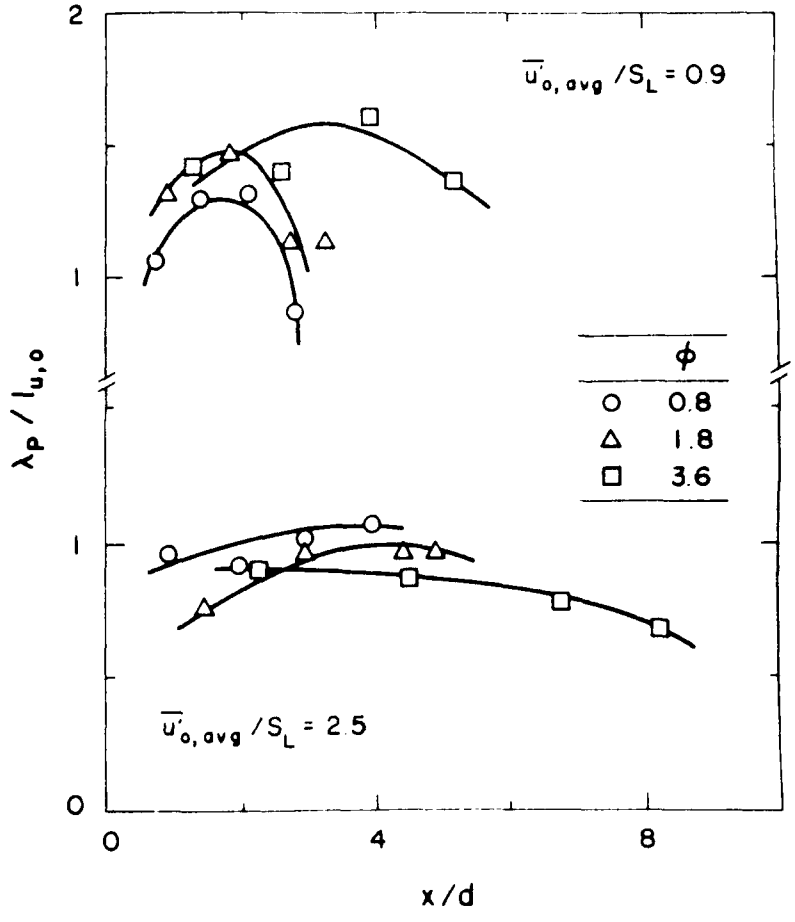
2
1
1
0
$\lambda_p / l_{u,o}$
$\overline{u'}_{o,avg}/S_L = 0.9$
$\overline{u'}_{o,avg}/S_L = 2.5$
ϕ
○ 0.8
△ 1.8
□ 3.6
0
4
8
x/d

FIG. .

APPENDIX C: KWON ET AL. (1991)

Flame Surface Properties of Premixed Flames in Isotropic Turbulence: Measurements and Numerical Simulations

by

S. Kwon, M.-S. Wu, J.F. Driscoll and G.M. Faeth

Department of Aerospace Engineering

The University of Michigan

Ann Arbor, Michigan 48109-2140

Abstract

An experimental and theoretical investigation of free turbulent premixed flames propagating in isotropic turbulence at neutrally-stable preferential diffusion conditions is described. Experiments were limited to the wrinkled thin laminar flamelet regime and involved mixtures of hydrogen, air and nitrogen ignited within a fan-stirred combustion chamber. Measurements included flame tomography for flame surface statistics and two-point laser velocimetry for unburned gas turbulence properties. Flame surface properties were numerically simulated using a two-dimensional flame propagation algorithm combined with statistical time series simulation of unburned gas velocities along the flame surface. Measurements showed progressively increasing flame radius fluctuations, flame surface fractal dimensions and turbulent/laminar flame perimeters with increasing mean flame radius. The rate of increase of these properties all increased with increasing turbulence intensities relative to the laminar flame speed. Simulated flame properties duplicated these trends but underestimated the effects of turbulence due to the limitations of a two-dimensional simulation. Extension of the method to a three-dimensional simulation, to remove this deficiency, appears to be computationally feasible.

Nomenclature

A_L, A_T	average surface area of mean and wrinkled flame surfaces
D_3	fractal dimension of flame surface
D_2	fractal dimension of intersection of flame surface with a plane
$E_i(f)$	temporal power spectral density of velocity component i
f	frequency
$f(\Delta x)$	longitudinal spatial correlation coefficient
F	value of $f(\Delta x) = f(\Delta y)$
$g(\Delta x)$	transverse spatial correlation coefficient

G	value of $g(\Delta x) = g(\Delta y)$
ℓ_K	Kolmogorov length scale
L	average flame surface perimeter for ruler of length ϵ
N	fan speed
$O_2/(N_2+O_2)$	volumetric fraction of O_2 in nonfuel gas
P_L,P_T	average perimeter of mean and wrinkled flame surfaces
r	radial distance
r_f	flame radius
Re_T	Reynolds number of turbulence, $u'\Lambda/\nu$
s_{uo}, s_{vo}	uncorrelated Gaussian random shock for u and v velocity components at point 0
S_L, S_T	laminar and turbulent burning velocity
t	time
T	value of temporal correlation coefficient at Δt
u,v	vertical (radial) and horizontal velocities
U_{oi}, V_{oi}	weighting factors in autoregressive process
x,y	orthogonal coordinate directions

Greek Symbols

α	thermal diffusivity
δ_L	laminar flame thickness
Δt	time increment
Δx,Δy	orthogonal distance increments
Λ,Λ_f	longitudinal integral length scale
Λ_g	transverse integral length scale for exponential approximation
ν	kinematic viscosity
ρ	density
τ	integral time scale
ϕ	fuel-equivalence ratio

Subscripts

b	burned gas
u	unburned gas

Superscripts

$\bar{(\ )}$, $(\ )'$	time-averaged mean and r.m.s. fluctuating property

Introduction

An experimental and theoretical investigation of free turbulent premixed flame propagating in isotropic turbulence at neutrally-stable preferential diffusion conditions i. described. This problem is of interest because the constraints of flame holding and th complications of effects of preferential diffusion are absent, while the flame is subjected t the simplest hydrodynamic state of turbulence. The experiments involved mixtures o hydrogen, air and nitrogen ignited within a fan-stirred combustion chamber Measurements included flame tomography to find flame surface statistics and two-poin laser velocimetry to find the turbulence properties of the unburned gas, similar to recen work on turbulent premixed jet flames in this laboratory [1]. Test conditions yielde turbulent Reynolds numbers of 0-4195 and turbulence intensities relative to the laminar flame speed in the range 0-1.6, with ℓ_K/δ_L on the order of 10. Thus, the experiments were in the wrinkled thin laminar flamelet regime with turbulence levels typical of practical applications [2,3]. Flame surface properties were numerically simulated using a flame propagation algorithm coupled with statistical time series simulation [4] of unburned gas velocities along the flame surface. This approach was examined because it offers a computationally tractable treatment of flame surface distortion by turbulence.

Within the thin flamelet regime, preferential diffusion involves the interaction between a faster-diffusing reactant and the variation of laminar burning velocity such that increasing or decreasing laminar burning velocity with increasing concentration of the faster-diffusing reactant yields unstable or stable flames [5]. Hydrogen is the faster diffusing reactant in hydrogen/air/nitrogen mixtures which have a maximum laminar flame speed at a fuel-equivalence ratio of 1.8 [6,7]; therefore, these flames are unstable or stable for fuel-equivalence ratios below or above this fuel-equivalence ratio. Recent work in this laboratory showed that effects of preferential diffusion instability are important for turbulent premixed hydrogen air flames with turbulent distortion of the flame surface enhanced for unstable conditions and retarded for stable conditions [1,8]. Thus, present experiments were carried out at $\phi = 1.8$ where preferential diffusion effects are suppressed

Earlier measurements of free turbulent premixed flames in isotropic turbulence are reported by Abdel-Gayed et al. [9,10], Groff [11], Mantzaras et al. [12], Santavicca and coworkers [13-15], Trautwein et al. [16], Cheng et al. [17] and references cited therein. The main distinction between the present measurements and these studies is a greater emphasis on the evolution of measured flame surface statistical properties during propagation from the point of ignition and the absence of preferential diffusion effects. Additionally, it is hoped that the small rates of flame stretch in comparison to extinction conditions, the simple and well characterized turbulence field, and the information on

flame surface development, will be useful for developing and evaluating models of the process.

Past attempts to develop models or simulations of premixed turbulent flames in the thin laminar flamelet regime have been recently reviewed by Peters [18] and Pope [19]. Present methods are most closely related to direct numerical simulations (DNS) of turbulent premixed flames, see Ghoniem et al. [20,21] and Ashurst and Barr [22] for early examples of this methodology. The advantage of DNS is that they provide a complete description of the process with potential to treat complications such as preferential diffusion in a fundamental way. However, DNS of both the flow field and flame propagation are computationally intensive so that treating practical flames in this manner is unlikely for some time to come [19]. Thus, the present investigation sought an approximate method that is more computationally tractable, involving a flame propagation algorithm coupled with statistical time series methods to numerically simulate velocities of the unburned gas along the flame surface, analogous to methods recently developed to treat turbulent dispersion [23] and turbulence/radiation interactions [24]. The approximate simulations were evaluated using the new measurements.

The paper begins with descriptions of experimental methods and the turbulence properties of the unburned gas. Numerical simulation of the flames is then discussed. The paper concludes with discussion of measured flame surface statistics and their comparison with numerical simulation predictions. The following discussion is brief, more details and a complete tabulation of data can be found in Kwon [25].

Experimental Methods

Apparatus

The fan-stirred combustion chamber was developed by Groff [11] based on an original concept of Semenov [26]. A similar arrangement has been used by Abdel-Gayed et al. [9,10]. The chamber is quasi-spherical with a volume of 10600cc and a 260 mm crossectional diameter at the center. Optical access is provided by two 92 mm diameter quartz windows in the end walls and two 10 mm diameter windows in the side walls, with each pair of windows mounted opposite one another. The isotropic turbulent field was generated by four fans located at 90° intervals along the periphery of the chamber. The fans had 8 blades with a 30° pitch, outer and inner diameters of 135 and 20 mm, and a streamwise length of 23 mm. The fans directed their flow toward the walls of the chamber and were driven by variable-speed synchronous motors. Fansler and Groff [27] show that this arrangement provides an isotropic flow field in the central region of the chamber.

Hydrogen and nitrogen (99.95% purity) were supplied from commercial cylinders while dry air (dew point less than 240 K) was obtained from laboratory supplies. The proper partial pressures of hydrogen, nitrogen and air were mixed together with the fans prior to a test. The mixture was spark ignited at the center of the chamber using electrodes extending from the top and bottom. The spark gap was roughly 3 mm while the sparks had a duration of 0.5 ms and stored energies of 0.3 mJ. After a test, the chamber was purged with warm dry air to remove condensed water.

Instrumentation

Laser Velocimetry. Measurements involved laser velocimetry (LV) to characterize the flow properties of the unburned gas, and flame tomography (FT) for flame surface statistics. Small (< 1 μm diameter) kerosene drops were added to the gas for both techniques using a TSI 9306 atomizer. Based on observations of laminar premixed flames, the oil drops disappeared at the flame surface, similar to earlier findings of Boyer et al. [28].

Single and two-point LV arrangements were used. The LV's used the 514.5 nm line of a 2W argon-ion laser with dual-beam arrangements: 50 mm initial spacing × 250 mm focal length for single-point measurements and 9 mm initial spacing and 1000 mm focal length for two-point measurements. The single-point measurements involved directing the laser beams through one of the large windows, and observing the probe volume in the forward-scattering direction through the other large window, yielding a measuring volume having a diameter of 250 μm and a length of 1.5 mm. The two-point measurements involved directing the beams through one of the small windows with the small beam angle creating a probe volume that was 70 mm long. This probe volume was observed normal to the optical axis through the large windows with two traversable detectors, yielding measuring volumes having diameters of 200 μm and lengths of 1 mm. In both cases, rotating the beams provided velocity data in the vertical and horizontal directions. The laser beams were frequency shifted to eliminate directional bias and ambiguity, because turbulence intensities were generally greater than 500%. Length scales were large and seeding was heavy for present test conditions so that the burst counter analog output was low-pass filtered and digitally sampled at equal time intervals to yield unbiased time-averaged results. Experimental uncertainties (95% confidence) were largely limited by finite sampling times and are estimated to be less than 10% for rms velocity fluctuations and 15% for spatial correlation coefficients and temporal spectra. All measurements were repeatable within these limits over the period of testing.

Flame Tomography. A pulsed dye laser, providing 0.6 J of light per pulse at 514.5 nm with a 2 μs pulse duration, was used for the FT measurements. The laser beam was focussed with spherical and cylindrical lenses and directed through one of the small windows to produce a 200 μm thick laser light sheet across the mid-plane of the combustion chamber. Light scattered from the particles in the unburned gas was recorded by a 35 mm SLR camera (Kodak Tri-X film) viewing the light sheet normal to the optical axis through one of the large windows. A 10 nm bandwidth laser line filter between the window and the camera reduced background radiation from the flame. The development of the flames was observed using various delays between the time of ignition and the time of the laser pulse.

The flame surface was found by tracing the edge of the region scattering light using a Gould FD 5000 Image Display. Analysis of 8 realizations, for each delay time and reactant mixture ratio, yielded the mean flame radius and perimeter based on the centroid of the flame image, the r.m.s. fluctuation from the mean, the fractal dimension (D_3) defined according to Mandelbrot [29], and the perimeter of the actual flame surface. Gouldin [30] defines outer and inner scales based on flame surface fractal properties; unfortunately, outer scales were comparable to $\bar{r}_f$ and were not very informative while inner scales could not be resolved due to the spatial resolution limits of the laser sheet (200 μm).

Test Conditions

The laminar flame properties of the reactant mixtures are summarized in Table 1 as a function of the volumetric fraction of oxygen in the nonfuel gas. All tests were carried out at ϕ=1.8, which places them at the maximum laminar flame speed condition [6,7]. The initial pressure was 3 atm.: pressure measurements using a piezoelectric transducer showed that combustion chamber pressure essentially remained at this value for the period where measurements were made. The density ratio, ρ_u/ρ_b, was found assuming thermodynamic equilibrium in the burned gas using the Gordon and McBride [31] algorithm. The unburned gas kinematic viscosity and thermal conductivity were found using the methods of Brokaw, and Mason and Saxena [32], with pure gas properties drawn from Keenan et al. [33]. Laminar burning velocities were measured from schlieren motion pictures of the flame ball under quiescent conditions [1]: present measurements at 3 atm. agreed with results summarized by Lewis and von Elbe [8] at 1 atm. within experimental uncertainties (10%). Characteristic laminar flame thicknesses, $\delta_L = \alpha / S_L$,

are small, 1.8 - 3.3 μm, because of the relatively high laminar flame speeds and pressure of the tests.

Test conditions for the turbulent flame experiments are summarized in Table 2 Measurements of turbulence properties appearing in the table will be discussed subsequently. A range of mixtures and rotational speeds were considered to provide $\bar{u}'/S_L$ in the range 0-1.6 and turbulence Reynolds numbers in the range 0-4195. Kolmogorov length scales were estimated as $\ell_K = \Lambda/Re_T^{3/4}$ from Tennekes and Lumley [34]: they are generally an order of magnitude larger than the flame thickness, which is representative of the thin laminar flamelet regime. Mean velocities were variable over the region within 30 mm of the center of the chamber, however, $\bar{u} / \bar{u}'$ was generally less than 20%.

Unburned Gas Properties

Turbulence Properties

Velocity statistics of the unburned gas were measured to provide parameters needed to numerically simulate the velocity field. Fansler and Groff [27] also measured turbulence properties in this combustion chamber and their results will be compared with present findings wherever possible.

Velocity fluctuations in the vertical and horizontal directions, $\bar{u}'$ and $\bar{v}'$, are plotted as a function of fan speed in Fig. 1. Results were obtained at the center as well as ± 30 mm from the center of the chamber at pressures of 1 and 3 atm. A correlation for $\bar{u}'$ at the center of the chamber for pressures of 1,3 and 5 atm, reported by Fansler and Groff [27], is also shown on the plot. The two sets of measurements are in good agreement, yielding a nearly linear increase of $\bar{u}'$ with fan speed and relatively small effects of pressure. The value of $\bar{u}'$ varied less than 10% over the region ± 30 mm from the center of the chamber which also agrees with [27]. Finally, $\bar{v}'/\bar{u}'$ was generally within 10% of unity over the same region, indicating reasonably isotropic turbulence. Probability density functions of $\bar{u}'$ and $\bar{v}'$ also satisfied Gaussian probability density functions within experimental uncertainties [25,27].

Temporal power spectral densities of vertical velocity fluctuations are plotted as a function of frequency in Fig. 2. Results for various positions, fan-speeds, pressures and velocity components are essentially the same [25]. The present integral time scales are defined by Hinze [35] as the ordinate intercepts of the power spectra divided by 4 $\bar{u}'^2$; therefore, the normalized spectra have an ordinate intercept of 4.0. Due to the high Re_T, the spectra exhibit an extended inertial range where they decay proportional to the -5/3 power of frequency. The LV measuring volume was generally an order of magnitude larger than

the Kolmogorov scales so that the higher rate of decay as these scales are approached could not be observed.

Present measurements of temporal integral scales are plotted as a function of fan speed in Fig. 3. Finding τ using the Hinze [35] procedure introduces uncertainties from scatter of the spectra at low frequencies, see Fig. 2; nevertheless, experimental uncertainties (95% confidence) of τ are less than 20%. A correlation of present measurements and an earlier correlation of Fansler and Groff [27] are also shown on the plot. Effects of pressure and position on τ are not large in comparison to experimental uncertainties. The correlations follow from the assumption of nearly constant spatial integral scales, velocity fluctuations proportional to fan speeds, and Taylor's hypothesis ($\tau \sim \Lambda / \bar{u}'$). This yields τ (s) = 12 / N (rpm) for the present measurements. Values of τ from [27] are roughly twice as large as present measurements, which is surprising because the same apparatus was used. The factor of two difference may have resulted from errors introduced due to the presence of mean velocities when recurrence rate correlations, used in [27], are corrected for directional bias. In any event, present values of τ represent conventional evaluations of τ from an experimental time series of velocity fluctuations and are consistent with measurements of integral length scales to be discussed next. Thus the present values of τ were adopted for the numerical simulations.

Measurements of the transverse spatial correlation coefficients are plotted as a function of distance between the points, Δ x, in Fig. (4). Let the x coordinate axis pass through the two points, with u' and v' being velocity fluctuations along and normal to the x axis. Then, the transverse correlation coefficient is defined as $g(\Delta x) = \overline{v'(x)v'(x+\Delta x)} / \overline{v'^2}$. This correlation is relatively independent of fan speed and position within the central region of the chamber. Conservation of mass in isentropic turbulence requires a region where $g(\Delta x) < 0$, yielding a shape somewhat like a Frankiel function [35].

The longitudinal spatial correlation, $f(\Delta x) = \overline{u'(x)u'(x+\Delta x)} / \overline{u'^2}$ also is required for numerical simulation of the velocity field. It was not possible to measure $f(\Delta x)$ using the present LV configuration; therefore, it was computed from the fit of the present measurements of $g(\Delta x)$ through the differential equation relating the two for isotropic turbulence [35]:

$$d/d\Delta x(\Delta x^2 f(\Delta x)) = 2\Delta x g(\Delta x) \qquad (1)$$

where $f(0) = 1$ by definition. The resulting plot of $f(\Delta x)$ is also illustrated in Fig. 4. Due to the small values of the Kolmogorov length scales, the curvature of $f(\Delta x)$ could not be resolved at small Δx, yielding roughly an exponential shape over the range of the present measurements. Integrating $f(\Delta x)$ yielded the spatial integral scale, Λ = 12.5 mm. As noted

earlier, this length scale is consistent with present measurements of integral time scale through Taylor's hypothesis but the value is roughly half the value found by Fansler and Groff [27] from their recurrence-rate temporal correlation measurements.

Mean Velocities

Mean radial velocities in the unburned gas were measured as the flames propagated from the center of the chamber. These measurements employed the single-channel LV with the measuring volume located 30 mm from the center of the chamber. The velocities for various values of $\bar{r}_f$ were ensemble averaged over 8 tests to yield an experimental uncertainty (95% confidence) less than 15% for mean velocities greater than 10% of the maximum mean velocity.

Measured values of $\bar{u}$ at a fixed radial location during flame propagation were compared with predictions assuming that the flame surface represents a volumetric source in the mean, due to the density change at the surface, and inviscid spherically symmetric constant density mean flow of the reactant gas. This yields

$$\bar{u} / (S_T(\rho_u/\rho_b - 1)) = (\bar{r}_f/r)^2 \qquad (2)$$

Measured values of $\bar{u}$ are plotted as suggested by Eq. (2) in Fig. 5. The density ratios used in the normalization appear in Table 1 while S_T and $\bar{r}_f$ were found from the FT measurements to be discussed later. Except for conditions far from the flames, where low velocities limit measuring accuracy, Eq. (2) provides an excellent correlation of the data. This implies that the chamber walls did not exert a significant effect on flow properties in the region where measurements were made. Equation (2) also provides a simple description of mean velocities in the unburned gas for the numerical simulation.

Theoretical Methods

General description

Turbulent flame propagation was numerically simulated using the flame propagation algorithm of Chorin [36] coupled with statistical time series simulation [4] of the velocity field in the unburned gas along the flame surface. The flame propagation algorithm was adapted from MIMOC [37] and only can provide a two-dimensional time-dependent simulation. This is a major limitation but it was desired to evaluate the simplified simulation before extending it to treat three-dimensional effects.

Other major assumptions of the numerical simulation are as follows: constant pressure turbulent deflagration wave; infinitely-thin flame sheet with constant unburned and burned gas properties, stationary homogeneous isotropic turbulence in the unburned gas,

unaffected by the presence of the flame; neutrally-stable flame with negligible effects of quenching, i.e., relative to the gas, the flame propagates normal to its surface at the laminar burning velocity ; and mean velocity field in unburned gas found assuming that the flame acts like a spherically-symmetric volumetric source (Eq.(2)).

The constant pressure and thin flamelet assumptions are conditions of the experiments: the chamber pressure rise was negligible in the region where measurements were made while characteristic flame thicknesses (see Table 1) were 10-100 times smaller than Kolmogorov length scales and available spatial resolution. The assumption that turbulence properties of the unburned gas are not affected by the flame is an open issue for the present test flames. However, Videto and Santavicca [13] do not observe significant changes of unburned gas turbulence properties for free premixed turbulent flames. This implies that the volumetric expansion of the flame passively convects the unburned gas turbulence field away from the ignition source. Neutral stability is a condition of the experiments while effects of quenching are not large because present flames were well away from extinction conditions and had modest values of u'/S_L. Finally, the volumetric source approximation is justified by the measurements illustrated in Fig. 5.

Statistical simulations of the velocity field can be designed to satisfy any number of the statistical properties of turbulence: mean velocities, the PDF of velocity fluctuations, temporal and spatial correlations, cross correlations, instantaneous conservation of mass, higher-order correlations, etc. Priorities must be set, however, because computation and memory requirements increase as the number of properties to be simulated increase. Thus, present calculations were limited to simulating mean velocities, Gaussian PDFs of velocity fluctuations and temporal and spatial correlations. Cross autocorrelations were ignored because they are zero for isotropic turbulence. Satisfying conservation of mass has not been important for other statistical simulations of turbulence [23,24] and is partly accounted for by the properties of the longitudinal and transverse spatial correlations discussed in connection with Eq. (1). Considering higher-order correlations is not very attractive because this information is rarely available.

A final approximation was to represent the spatial and temporal correlations as exponential functions, because this yields a Markov-like simulation that substantially simplifies the computations [4,23,24]. Exponential fits are reasonably good for temporal and longitudinal spatial correlations but do not represent the negative portion of the Frenkiel function shape of the transverse spatial correlation (see Fig. 4). Nevertheless, the approximation was adopted for the transverse spatial correlation as well, because the

significant portion of the correlation curve, where the values of the correlation are near unity, is reasonably represented by an exponential function.

Velocity Simulation

Mean velocities are known from Eq. (2), because the simulation provides a running estimate of $\bar{r}_f$ and S_T; therefore, only velocity fluctuations must be simulated. The flame mostly affects the calculations through the mean velocity; therefore, the turbulent velocity field of the unburned gas was found for the whole flow (to minimize bookkeeping problems) even though only the portion near the flame surface was needed for the flame propagation algorithm. This inefficient approach was acceptable because the velocity simulation consumed much less computer time than the flame propagation algorithm.

An autoregressive process was used for the simulation; therefore, the velocity fluctuation at the point to be computed was a weighted sum of velocity fluctuations computed earlier and a random shock [4]. Each component of velocity at a point can be found independently because they are statistically independent for isotropic turbulence. The process will be formulated to find the velocity fluctuations at a generic point x_o, y_o, t_o in the flow field, assuming that previous computations have found velocity fluctuations at n previous points, e.g., x_1, y_1, t_1;...; x_n, y_n, t_n. This numerical ordering of previous points can be arranged in any convenient manner, because only correlations among points must be considered explicitly, not their positions in space and time. With this arrangement, the unknown velocity fluctuations at 0 are found from the following autoregressive processes [4]

$$u_o' = \sum_{i=1}^{p} U_{oi}\, u_i' + s_{uo} \; ; \; v_o' = \sum_{i=1}^{p} V_{oi}\, v_i' + s_{vo} \qquad (3)$$

where $p \le n$ is selected to eliminate points having small correlation coefficients with respect to point 0. The U_{oi}, V_{oi} are weighting factors selected so that the simulated correlations between points can be satisfied. The s_{uo} and s_{vo} are uncorrelated random variables (random shocks) having Gaussian PDF's with mean values of zero and variances selected to match the PDF's of u_o' and v_o'.

The procedure to find the properties of the weighting factors and random shocks is identical to any other autoregressive process. Taking u_o' as an example, the U_{oi} can be found by solving the following system of linear algebraic equations, given the correlations between points [4,24]:

$$\overline{u_o' u_k'} = \sum_{i=1}^{p} U_{oi}\, \overline{u_i' u_k'} \; ; \qquad k=1,\ldots,p \qquad (4)$$

Once the U_{oi} are determined, the variance of s_{uo} can be found from:

$$\bar{s}_{uo}^2 / \bar{u}_o'^2 = 1 - \sum_{i=1}^{p} U_{oi}\, (\overline{u_i' u_o'} / \bar{u}_o'^2) \qquad (5)$$

This provides all properties needed to find u_o', and analogously v_o', from Eqs. (3) for any point 0. Finally, $u_o = \bar{u}_o + u_o'$, where u_o is found from Eq. (2) given $\bar{r}_f$ and S_T from the flame propagation algorithm.

As a practical matter, resolution of the flame surface in space and time requires relatively small spatial and temporal increments in comparison to the integral scales; therefore, the correlation coefficients of the important nearest neighbors of the point being computed are all near unity. Then it is reasonable to decompose general correlations into products of correlations along the individual coordinate axes as follows:

$$\overline{u'(x,y,t)u'(x-i\Delta x,y-j\Delta y,t-k\Delta t)} / \overline{u'^2} = F^{|i|} G^{|j|} T^{|k|} \qquad (6)$$

where

$$F = \exp(-\Delta x/\Lambda_f),\; G = \exp(-\Delta y/\Lambda_g),\; T = \exp(-\Delta t/\tau) \qquad (7)$$

are the correlation coefficients for single increments in each coordinate direction. Equation (6) is formally correct in each coordinate direction, e.g., i varying with j=k=0, due to the properties of exponential functions. However, it is only approximate for general variations of i,j and k. In particular, for $\Delta x = \Delta y$, $\overline{u'(x,y,t)u'(x-\Delta x,y-\Delta y,t)} / \overline{u'^2} = (F^{\sqrt{2}} + G^{\sqrt{2}})/2$ rather than FG, etc. [35]. Nevertheless, the difference between the two expressions is less than 10% for F and G ca. 0.9 so that the error is acceptable in view of the other approximations of the simulation. Finally, the mean motion of the gas affects the spatial and temporal correlations with respect to observations from a fixed Eulerian grid. This effect was considered, however, $\Delta\tau/\tau$ and $u\,\Delta\tau/\Lambda << 1$, etc., for present conditions so that the

correction was small. Thus, F, G and Γ, as well as $\bar{u}'$ and $\bar{v}'$, were essentially constant over the flow field for the present conditions.

Under the approximations of the previous paragraph, Kwon [25] shows that only the seven nearest neighbors of the point being computed have values of U_{oi} and V_{oi} that are not zero. This behavior is similar to pure time series simulations with exponential temporal correlations (Markov processes) where an autoregressive process including only the previous time step still satisfies the temporal correlation for all time [4].

The locations of the seven points of the approximate simulations, and the corresponding weighting factors and variances of the random shocks, are summarized in Table 3. Initial conditions at t=0, and boundary points at x=0 or y=0, require corrected procedures because all seven points are not available. In these cases, the unavailable points can simply be deleted while dropping the corresponding terms in the expressions for s_{uo}^2 and $\bar{s}_{vo}^2$ (note that the corresponding terms are simply U_{oi}^2 or V_{oi}^2). For example, u_o' at x=y=t=0 implies that no previous points are available so that $u_o'=s_{uo}$ and $\overline{s_{uo}^2} = \bar{u}'^2$.

The approximate simulation was tested for grid arrangements and values of F, G and T typical of actual simulations. Plots of typical simulated temporal and spatial correlations are illustrated in Fig. 6. This simulation involved F=T=0.95 for a 100 × 100 spatial grid and 4000 time steps. The temporal correlation is shown for a point near the center of the grid while spatial correlations in the vertical and horizontal directions provide two realizations of this property. The correlations are reproduced reasonably well in the region where they are large. Larger errors and irregular behavior of the spatial correlations at large separation distances are due to sampling limitations, and can be reduced by averaging over more realizations [25]. PDF's of velocity fluctuations were also reproduced quite well over the grid [25].

Flame Propagation Computations

Flame surface properties were found using the flame propagation portion of MIMOC [37]. This involves the simple line interface calculation (SLIC) of Noh and Woodward [38] to treat advection of the flame surface at $u = \bar{u} + u'$ and $v = \bar{v} + v'$, and the implementation of Huygens' principle by Chorin [36] to propagate the flame relative to these velocities at its laminar burning velocity and normal to its surface. The modification of the original algorithm [37] by Sethian [39], to remove bias of off-axis propagation caused by the order of x and y sweeps, was adopted for the present calculations.

Results reported here are based on a 100 × 100 grid with $\Delta x = \Delta y = 1$ mm and Δt = 0.03 - 0.08 ms. Numerical accuracy was evaluated by finding $\bar{r}_f$, $\bar{r}_f'$, D_3 and P_T/P_L for grid sizes 1/2, 1 and 2 times as large as the final computations. Extrapolation of the results

indicated that the numerical uncertainties of the results reported here are less that 4%, which is small in comparison to uncertainties introduced by the two-dimensional simulation.

Results and Discussion

Flame Visualization

Typical flame tomographs for the present neutrally-stable conditions at the highest values of $\bar{u}'/S_L$ used are illustrated in Fig. 7. The tomographs are for $\bar{r}_f$ = 15, 30 and 45 mm. The results show a progressive increase of flame surface distortion with increasing mean radius (i.e., time). This behavior is analogous to the progressively increasing distortions of the flame surface of premixed turbulent jet flames with increasing distance from the flameholder [1].

Simulated flame surfaces at $\bar{u}'/S_L$ = 1.6 (the experimental value) and 3.2 are also illustrated in Fig. 7. Both simulations represent the trend that flame surface distortion increases with mean flame radius (time). The main effect of increasing $\bar{u}'/S_L$ is to increase the degree of distortion of the surface at particular values of $\bar{r}_f$ so that the larger $\bar{u}'/S_L$ yields a more irregular surface with finer-grained distortion. Both simulations are qualitatively similar to the flame tomographs, however, the small-scale distortions are better represented by the results for $\bar{u}'/S_L$ = 3.2 (which is twice the experimental value). More quantitative assessment of the simulations will be undertaken in the following.

Flame Surface Statistics

Moments. The measured and simulated variations of $\bar{r}_f$ and $\bar{r}_f'$ as a function of time after ignition are illustrated in Figs. 8-10 for all conditions tested. In order to avoid disturbances from the spark ignition process, measurements begin at $\bar{r}_f$ = 10 mm which is reached roughly 1-2 ms after ignition. Trends of flame properties at earlier times are complex due to disturbances from the electrodes and the spark discharge. Thus, the measurements do not extrapolate linearly to $\bar{r}_f$ = 0 at t=0 while computational noise dominates simulation properties at small times due to limited spatial resolution. In order to eliminate these effects, measured and simulated times when $\bar{r}_f$ = 10 mm have been made coincident, although the times shown in Figs. 8-10 are times after the start of spark discharge.

Measured values of $\bar{r}_f$ increase linearly with time for laminar conditions, $\bar{u}'/S_L$ = 0, for the time period illustrated in Figs. 8-10. This is expected because the flames are neutral with respect to preferential diffusion instability and the flame surfaces do not self distort [8]. The linear increase of $\bar{r}_f$ with time is also preserved for small values of $\bar{u}'/S_L$ and time,

although $d\bar{r}_f/dt$ at a particular $\bar{r}_f$ progressively increases as $\bar{u}'/S_L$ increases due to increased levels of flame surface distortion by the turbulence. At larger times and $\bar{u}'/S_L$, however, $d\bar{r}_f/dt$ increases with increasing time as well, because effects of the progressive growth of flame surface distortion become large enough to be resolved.

Measured values of $\bar{r}_f'$ also increase with time for the results illustrated in Figs. 8-10. Finite, but small, values of $\bar{r}_f'$ are also observed for $\bar{u}'/S_L = 0$, even though the flame surface is smooth. This is caused by distortion of the overall flame shape by the presence of the electrodes and small flow disturbances in the chamber. For nonzero values of $\bar{u}'/S_L$, the kernel is initially smooth and nearly spherical. With increasing time, however, the flame surface becomes progressively more distorted by the turbulence. The rate of increase of $\bar{r}_f'$ with time increases as $\bar{u}'/S_L$ increases because larger velocity fluctuations imply larger deformations of the surface in a given time interval. Although $\bar{r}_f'$ increases significantly in the time period illustrated in Figs. 8-10, maximum values are generally less than 30% of the spatial integral scale (12.5 mm). The reason for this is that turbulent deformation of the flame surface does not have much time to develop due to the relatively large turbulent flame speed for present test conditions, e.g., maximum times of propagation are in the range 0.4-1.3 integral time scales.

Naturally, the simulated $\bar{r}_f$ at $\bar{u}'/S_L = 0$ agree with measurements in Figs. 8-10 because surface distortion and limitations of a two-dimensional simulation are absent for laminar conditions. Effects of $\bar{u}'/S_L$ on the variation of $\bar{r}_f$ with time are also predicted reasonably well by the simulations when these effects are small. There are greater deficiencies, however, in the region where $d\bar{r}_f/dt$ itself begins to noticeably increase with time (large $\bar{u}'/S_L$ and long times) where the simulations underestimate the rate of increase of $d\bar{r}_f/dt$. This is felt to be due primarily to the limitations of a two-dimensional simulation of a three-dimensional turbulent process.

Predictions of $\bar{r}_f'$ for $\bar{u}'/S_L = 0$ are illustrated in Figs. 8-10 in order to quantify numerical distortions introduced by the flame propagation algorithm. In particular, while $\bar{r}_f'$ should be zero for $\bar{u}'/S_L = 0$, finite values are predicted that fortuitously agree with the measurements. These variations are caused by the limited spatial resolution of the calculations, incomplete correction of off-axis bias within the advection algorithm [39], and the limited directional resolution of the Huygens' principle implemented to treat flame propagation [36]. The effect of these difficulties tends to decrease as $O_2 / (N_2 + O_2)$ decreases, but it is generally less than 1 mm for the time period considered, and generally less than 30% of predicted values of $\bar{r}_f'$ for finite values of $\bar{u}'/S_L$.

Simulated values of $\bar{r}_f'$ exhibit trends similar to the measurements in Figs. 8-10; namely, $\bar{r}_f'$ increases with time and the rate of increase tends to increase as $\bar{u}'/S_L$ becomes larger. However, the simulations generally underestimate $\bar{r}_f'$. This behavior is consistent with the corresponding underestimation of $d\bar{r}_f/dt$ by the simulation and is accordingly attributed to the limitations of a two dimensional simulation.

Fractal Dimensions. Recently, the fractal dimensions of turbulent premixed flame surfaces have received a great deal of attention as a means of quantifying the degree of wrinkledness [12-15, 30]. The main parameters are the fractal dimensions of the surface, D_3, and the fractal dimension of the intersection of the surface with a plane, D_2 [29]. The value of D_2 was found by measuring the flame perimeter, L, using rulers of different size, ϵ, similar to past work [1].

Typical plots of L as a function of ϵ for the simulations are illustrated in Fig. 11. These results are for $\bar{u}'/S_L = 1.6$ at various values of $\bar{r}_f$, ensemble-averaging results for each ruler size over 16 realizations in order to smooth the plot. Except for regions near small and large values of ϵ, where the ruler sizes approach available spatial resolution and the mean diameter of the flame, the curves exhibit a relatively smooth slope that is characteristic of fractal like behavior. The slope of the intermediate region is $1-D_2$, assuming that the flame surface is fractal, and $D_3 = D_2 + 1$, assuming that the flame surface is isotropic [29]. The value of D_3 in previous flame studies has varied between 2, for smooth geometrical surfaces like spheres, to 2.3 - 2.4, which is representative of maximum levels of of distortion of isochoric or premixed flame surfaces within turbulent flow fields [12, 14, 40, 41].

Measured values of fractal dimensions were found in the same manner as Fig. 11 from the flame tomographs. In this case, results for 8 realizations were averaged at each test condition and $\bar{r}_f$ to obtain relatively smooth plots of L as a function of ϵ. Experimental uncertainties of these measurements were limited by the finite number of samples and the available span of ϵ to find the slope. The resulting uncertainties (95% confidence) of $D_3 - 2$ are estimated to be less than 20%. Evaluation of D_3 from the simulations yielded similar uncertainties.

Measured and simulated values of D_3 are plotted as a function of $\bar{r}_f$ in Fig. 12. Measurements are illustrated for all test conditions, grouped according to $O_2/(N_2 + O_2)$. Simulations of D_3 are illustrated for parametric values of $\bar{u}'/S_L$. At small $\bar{r}_f$, D_3 is nearly 2.0, which is representative of the smooth spherical spark kernel. The subsequent increase is due to progressive deformation of the flame surface by turbulence, somewhat analogous to the behavior of D_3 for turbulent jet flames with increasing distance from the flame holder

[1]. Maximum values of D_3, however, are not large, generally less than 2.15. This is caused by the limited propagation time of present tests which is 0.4-1.3 times the integral time scale, as noted earlier. In terms of distance, these measurements only correspond to distances of propagation into the unreacted gas mixture on the order of one spatial integral scale (the larger displacements of r_f in Fig. 12 are caused by volumetric expansion of the flames due to their density ratio, see Table 1). Based on results observed at largest distances from the flame holder for premixed turbulent jet flames [1], it is expected that D_3 would eventually approach values in the range 2.3-2.4 that are characteristic of passive isoclinic surfaces in isotropic turbulent fields. However, measurements for larger values of r_f / Λ are needed to confirm this behavior.

Simulated values of D_3 in Fig. 12 also exhibit a progressive increase with increasing flame radius. However, use of the experimental value of u'/S_L yields simulated values of D_3 significantly below the measurements for each value of $\bar{r}_f$. Analogous to the individual realization illustrated in Fig. 7, however, doubling u'/S_L for the simulation yields a reasonably good estimate of the variation of D_3 with $\bar{r}_f$. A probable reason for this deficiency is that out of plane distortions of the flame surface, which should contribute to its irregularity, are suppressed by two-dimensional simulations.

Flame Perimeter Another measure of the distortion of the flame surfaces by turbulence was found by measuring the perimeters of flame surfaces. For present conditions flame wrinkles are not large and it is reasonable to assume that flame surface properties are isotropic so that the average surface area of the wrinkled surface can be related to the perimeter as follows [8].

$$A_T/A_L = 2(P_T/P_L) - 1 \qquad (8)$$

Additionally, for neutral preferential diffusion conditions and modest stretch rates, A_T/A_L is a measure of S_T/S_L [30].

Measured values of P_T/P_L for all the test conditions are plotted as a function of r_f in Fig. 13, grouped according to $O_2/(N_2 + O_2)$. Values of P_T/P_L from the simulations also are shown on the plots, for parametric values of u'/S_L that match the experiments, as well as twice the maximum experimental value, as before. Measured values of P_T/P_L were found from 8 realizations with uncertainties (95% confidence) of $P_T/P_L - 1$ estimated to be less than 25%. Results for the simulations involved averages over 16 realizations, yielding uncertainties of $P_T/P_L - 1$ of less than 15%.

Measured results in Fig. 13 show that P_T/P_L is near unity for small values of $\bar{r}_f$, which is representative of the nearly smooth spherical spark kernel in this region. Similar to D_3, however, P_T/P_L progressively increases with increasing $\bar{r}_f$ for present test conditions, with the rate of increase being more rapid as u'/S_L increases. No limiting behavior of P_T/P_L is observed for the present relatively short propagation times. However, since D_3 should approach a limit for isoclinic surfaces in turbulent environments, the considerations of Gouldin [30] suggest that A_T/A_L (and thus P_T/P_L through Eq. (18)) would eventually approach a limit for fixed unburned gas turbulence properties as well, as long as the outer scale was proportional to the spatial integral scale. Tests involving longer propagation times in comparison to integral time scales are needed to address this important property of turbulent flames. Associating P_T/P_L with S_T/S_L indicates that it increases with $\bar{r}_f$, with u'/S_L largely controlling the rate of increase. Thus, correlations of S_T/S_L solely as a function of $\bar{u}'/S_L$ are only appropriate for particular values of r_f, as recently shown by Trautwein et al. [16].

Because D_3 and P_T/P_L are closely related flame surface features, the comparison between measured and simulated values of P_T/P_L in Fig. 13 is similar to results for D_3 in Fig. 12. In general, the simulations yield the correct trends of P_T/P_L with increasing $\bar{r}_f$, and $\bar{u}'/S_L$ but quantitative agreement is only achieved when values of u'/S_L roughly twice the experimental value are used. As before, the limitations of a two-dimensional simulation are the most probable cause of this difficulty.

Conclusions

The major conclusions of the study can be summarized as follows:

1. Flame tomograph measurements showed that dr_f/dt, $\bar{r}_f'$, D_3 and P_T/P_L (and thus S_T/S_L) increase with time (distance) from the point of ignition. Observed times and distances of propagation, however, were on the order of integral scales in the unreacted gas so that these results represent a developing period of flame distortion by the turbulence. At larger times and distances, D_3 is expected to approach values found for isoclinic surfaces in isotropic turbulence and the variation of flame properties with time (distance) should change: measurements are needed to resolve behavior in this limiting region.
2. Measurements showed that increasing u'/S_L tends to increase the rate of turbulent distortion of the flame surface with time (distance) from the point of ignition. Thus, previous correlations of S_T/S_L and D_3 solely as a function of u'/S_L were found because

they reflect this rate of increase for limited ranges of flame dimensions. Nevertheless, such correlations are incomplete unless they account for the development of flame surface properties. Models or correlations of turbulent premixed flame properties that only consider local conditions, and do not account for effects of time (distance) from the point of ignition, are intrinsically incomplete. A possible exception is behavior at long times when D_3 may approach values for isochinic surfaces in turbulence but this still must be studied.

3. The present numerical simulation successfully predicted the trends of flame surface properties but underestimated their rate of increase with time (distance) from the point of ignition. Quantitatively accurate predictions could be obtained by the artifice of doubling $\bar{u}'/S_L$ in order to compensate for a two-dimensional simulation, however, the general effectiveness of this approach is unknown. Extension to three-dimensional simulations is computationally feasible, even for high Reynolds number flames, and should be undertaken to evaluate the methodology more thoroughly. Other aspects of the simulation that need to be assessed are as follows: are unburned gas turbulence properties significantly modified as the flame surface is approached; is simulation of moments, PDFs and spatial and temporal correlations in the unburned gas sufficient to treat flame surface distortion, what are the limitations of the approach as δ_L becomes comparable to ℓ_K, and characteristic flame development times approach turbulent time scales, and can effects of preferential diffusion and quenching be successfully simulated?

This research was supported by the Office of Naval Research, contract No. N00014-87-K-0698 with S. Ramberg serving as Scientific Program Officer. The authors also wish to thank General Motors Research Laboratories for donation of the combustion chamber and E.G. Groff and T. Fansler for useful discussions concerning the research.

References

1. Wu, M.S., Kwon, S., Driscoll, J.F. and Faeth, G.M., Combust. Sci. Tech., in press.
2. Bray, K.N.C., in Turbulent Reacting Flows (P.A. Libby and F.A. Williams, Eds.), Springer Verlag, Berlin, 1980, pp. 115-135.
3. Abraham, J., Williams, F.A. and Bracco, F.V., SAE Paper No. 850345, 1985.
4. Box, G.E.P. and Jenkins, G.M., Time Series Analysis, Holden Day, San Francisco, 1976, pp. 47-66.
5. Manton, J., von Elbe, G. and Lewis, B., J. Chem. Phys. 20:153-158 (1952).

6. Lewis, B. and von Elbe, G., Combustion, Flames and Explosions of Gases, Academic Press, New York, 1961, pp. 381-384.
7. Andrews, G.E. and Bradley, D., Combust. Flame 20: 77-89 (1973).
8. Wu, M.S., Kwon, S., Driscoll, J.F. and Faeth, G.M., Combust. Sci. Tech. 73: 327-350 (1990).
9. Abdel-Gayed, R.G. and Bradley, D., Sixteenth Symposium (International) on Combustion, The Combustion Institute, Pittsburgh, 1976, pp. 1725-1735.
10. Abdel-Gayed, R.G., Bradley, D., Hamid, M.N. and Laws, M., Twentieth Symposium (International) on Combustion, The Combustion Institute, Pittsburgh, 1984, pp. 505-512.
11. Groff, E.G., Combust. Flame 67:153-162 (1967).
12. Mantzaras, J., Felton, P.G. and Bracco, F.V., Combust. Flame 77:295-310 (1989).
13. Videto, B.D. and Santavicca, D.A., Combust. Sci. Tech. 70:47-73 (1990).
14. Santavicca, D.A., Liou, D. and North, G.L., SAE Paper No. 900024, 1990.
15. North, G.L. and Santavicca, D.A., Combust. Sci. Tech., in press.
16. Trautwein, S.E., Grudno, A. and Adomeit, G., Twenty-Third Symposium (International) on Combustion, The Combustion Institute, Pittsburgh, in press.
17. Cheng, W.K., Keck, J.C., Hamsworth, E., Lai, M.C., Ferreira, E., Hurlburt, E., Pope, S.B. and Girimaji, S.S., Turbulent Premixed Flame Study, Final Report, Contract DE-FG02-86ER 13553, MIT, Cambridge, MA, 1990.
18. Peters, N., Twenty-First Symposium (International) on Combustion, The Combustion Institute, Pittsburgh, 1988, pp. 1231-1250.
19. Pope, S.B., Twenty-Third Symposium (International) on Combustion, The Combustion Institute, Pittsburgh, in press.
20. Ghoniem, A.F., Chorin, A.J. and Oppenheim, A.K., Eighteenth Symposium (International) on Combustion, The Combustion Institute, Pittsburgh, 1980, pp. 1375-1383.
21. Ghoniem, A.F., Chorin, A.J. and Oppenheim, A.K., Trans. Roy. Soc. London A394:303-325 (1982).
22. Ashurst, W.T. and Barr, P.K., Comb. Sci. Tech. 34:227-256 (1983).
23. Parthasarathy, R.N. and Faeth, G.M., J. Fluid Mech. 220:515-537 (1990).
24. Kounalakis, M.E., Sivathanu, Y.R. and Faeth, G.M., J. Heat Trans., in press.
25. Kwon, S., Premixed Hydrogen/Air Flames in Isotropic Turbulence, Ph.D. Thesis, University of Michigan, Ann Arbor, 1990.
26. Semenov, E.S., Comb. Expl. Shock Waves 1:57-62 (1965).
27. Fansler, T.D. and Groff, E.G., Combust. Flame 80:350-354 (1990).

28. Boyer, L., Clavin, P. and Sabathier, F., Eighteenth Symposium (International) on Combustion, The Combustion Institute, Pittsburgh, 1980, pp. 1401-1409.
29. Mandelbrot, B.B., J. Fluid Mech. 72:401-416 (1975).
30. Gouldin, F.C., Combust. Flame 68:249-266 (1987).
31. Gordon, S. and McBride, G.J., Computer Program for Calculations of Complex Chemical Equilibrium Compositions, Rocket Performance, Incident and Reflected Shocks, and Chapman-Jouguet Detonations, NASA Report SP-273, Washington, 1971.
32. Reid, R.C., Prausnitz, J.M. and Sherwood, T.K., The Properties of Gases and Liquids, 3rd edition, McGraw-Hill, New York, 1977, pp. 391-516.
33. Keenan, J.H., Chao, J. and Kaye, J., Gas Tables, John Wiley & Sons, New York, 1980.
34. Tennekes, H. and Lumley, J.L., Turbulence, M.I.T. Press, Cambridge, 1972, pp. 67.
35. Hinze, J.O., Turbulence, McGraw-Hill, New York, 2nd ed., 1975, Chapt. 3.
36. Chorin, A.J., J. Comp. Phys. 35:1-11 (1980).
37. Ghoniem, A.F., Marek, C.J. and Oppenheim, A.K., Modeling Interface Motion of Combustion (MIMOC), NASA TP-2132, 1983.
38. Noh, W.T. and Woodward, P., Fifth International Conference on Numerical Methods in Fluid Dynamics (A.I. Vooren and P.J. Zandbergen, Eds.), Springer-Verlag, Berlin, 1976, pp. 330-339.
39. Sethian, J., J. Comp. Phys. 54:425-456 (1984).
40. Lovejoy, S., Science 216:185-187 (1982).
41. Sreenivasan, K.R. and Meneveau, C., J. Fluid Mech. 173:357-386 (1986).

Table 1 Summary of Laminar Flame Properties[a]

$O_2/(N_2 + O_2)$[b] (--)	ρ_u/ρ_b (--)	α (mm^2/s)	ν (mm^2/s)	S_L[c] (m/s)	δ_L (μm)
0.210	6.4	4.6	7.6	2.5	1.8
0.150	5.4	4.2	6.9	1.5	2.8
0.125	5.2	4.0	6.5	1.2	3.3

[a] Hydrogen, air and nitrogen mixtures with a fuel equivalence ratio of 1.8, initial pressure and temperature of 3 atm. and 298 ± 3K.

[b] Relative oxygen concentration by volume.

[c] From Lewis and von Elbe [8].

Table 2 Summary of Turbulent Flame Test Conditions[a]

$O_2/(N_2+O_2)$ (-)	N (rpn)	$\bar{u}'$ (m/s)	$\bar{u}'/S_L$ (-)	Re_T (-)	ℓ_K (μm)	ℓ_K/δ_L (-)
0.210	1000	1.2	0.48	1965	42	21
	2000	2.4	0.96	3930	25	12
0.150	1000	1.2	0.80	2095	40	13
	2000	2.4	1.60	4195	24	8
0.125	1000	1.2	1.00	2320	37	12

[a]Unreacted mixture properties from Table 1, integral length scale of turbulence of 12.5 mm $\bar{u}/\bar{u}'$ less than 10% for all conditions within ± 30 mm from the center of the chamber.

Table 3 Parameters of the Approximate Simulation[a]

i	Location	U_{oi}	V_{oi}
1	$x-\Delta x, y, t$	F	G
2	$x, y-\Delta y, t$	G	F
3	$x, y, t-\Delta t$	T	T
4	$x-\Delta x, y-\Delta y, t$	-FG	-FG
5	$x-\Delta x, y, t-\Delta t$	-FT	-GT
6	$x, y-\Delta y, t-\Delta t$	GT	-FT
7	$x-\Delta x, y-\Delta y, t-\Delta t$	FGT	FGT

$\bar{s}_{uo}^2/\bar{u}'^2=\bar{s}_{vo}^2/v'^2 = 1-F^2-G^2-T^2+(FG)^2+(FT)^2+(GT)^2-(FGT)^2$

$F = \exp(-\Delta x/\Lambda_f)$, $G = \exp(-\Delta x/\Lambda_g)$, $T = \exp(-\Delta t/\tau)$

[a]For a square grid, $\Delta x=\Delta y$, with correlations decomposable as products according to Eq. (6) and for stationary homogeneous and isotropic turbulence.

List of Figures

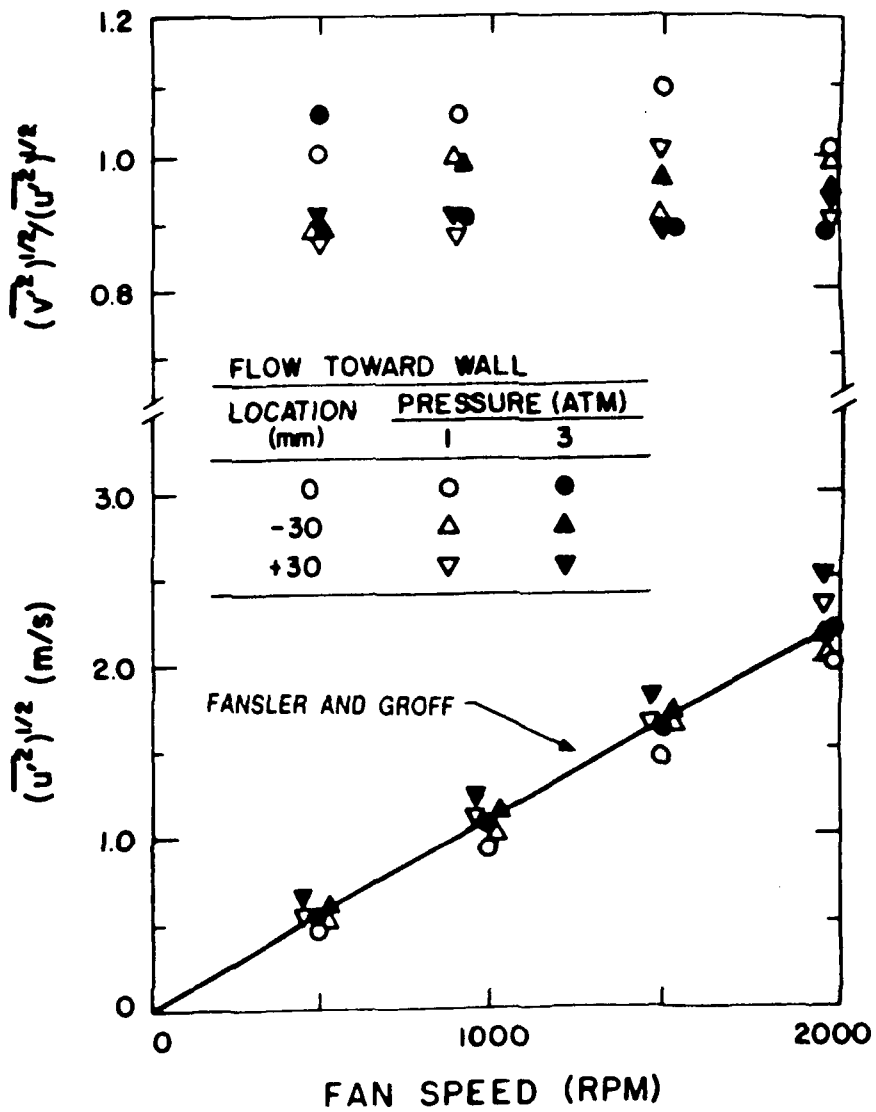

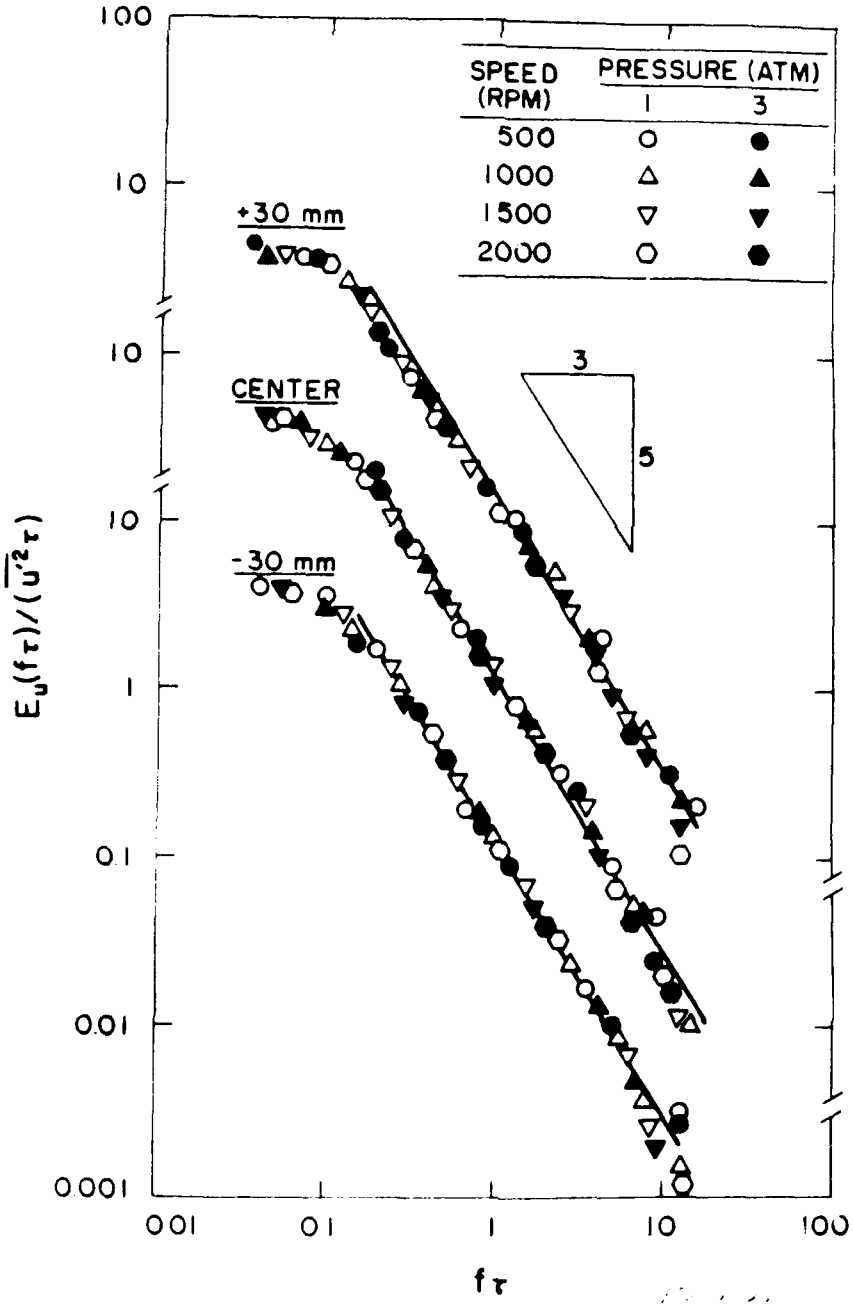
SPEED (RPM)
PRESSURE (ATM)
1
3
500
1000
1500
2000
+30 mm
CENTER
-30 mm
3
5
100
10
10
10
1
0.1
0.01
0.001
0.01
0.1
1
10
100
$E_u(f\tau)/(\overline{u'^2}\tau)$
$f\tau$

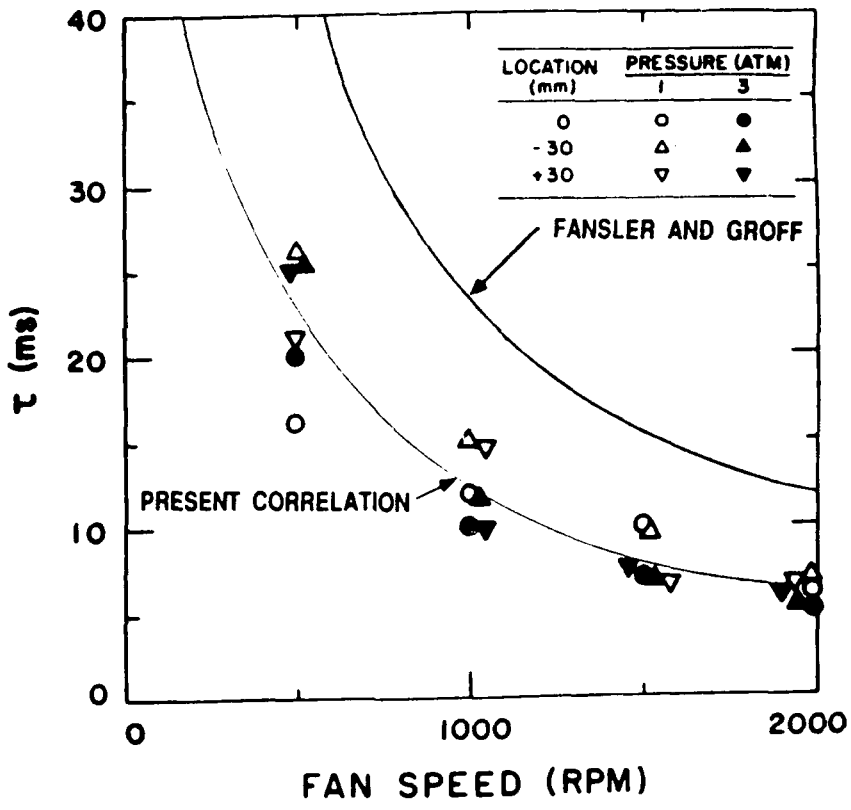
LOCATION (mm)
PRESSURE (ATM)
1
3
0
-30
+30
FANSLER AND GROFF
PRESENT CORRELATION
40
30
20
10
0
0
1000
2000
τ (ms)
FAN SPEED (RPM)

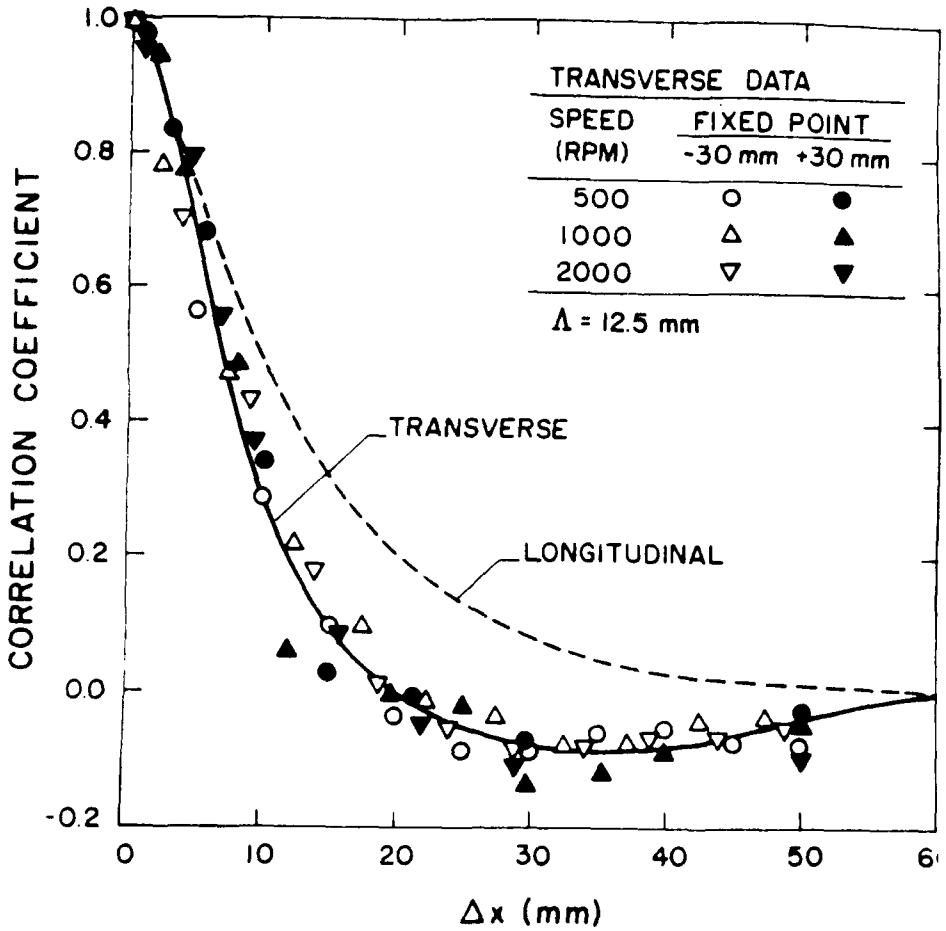
CORRELATION COEFFICIENT
1.0
0.8
0.6
0.4
0.2
0.0
-0.2
0
10
20
30
40
50
Δx (mm)
TRANSVERSE DATA
SPEED (RPM)
FIXED POINT
-30 mm
+30 mm
500
1000
2000
Λ = 12.5 mm
TRANSVERSE
LONGITUDINAL

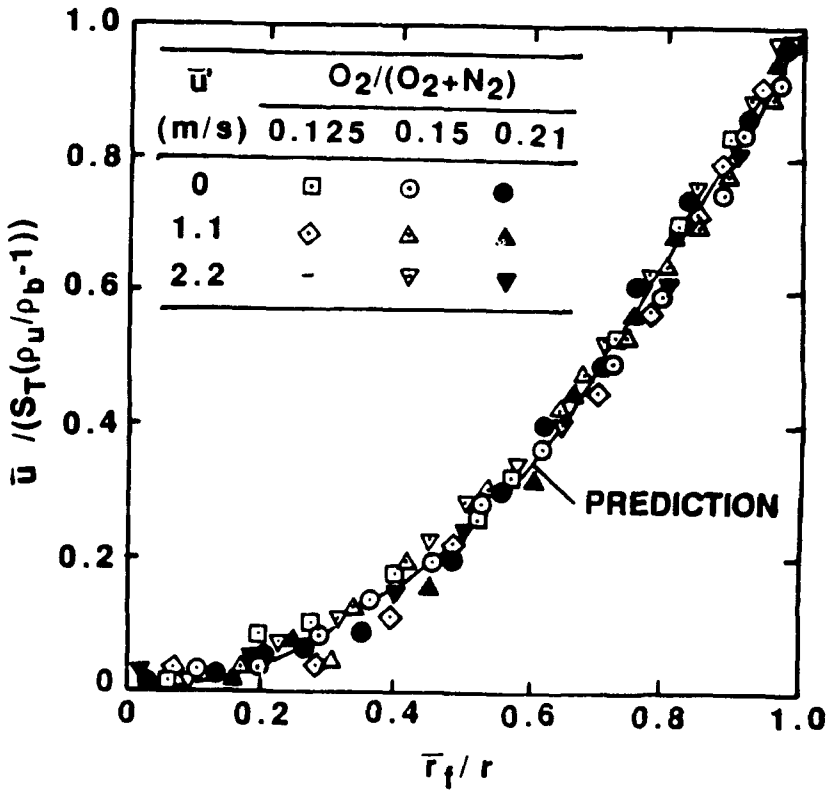
ū /(S_T(ρ_u/ρ_b-1))
1.0
0.8
0.6
0.4
0.2
0
0.2
0.4
0.6
0.8
1.0
r̄_f / r
ū' (m/s)
O2/(O2+N2)
0.125
0.15
0.21
0
1.1
2.2
PREDICTION

FIG. 5

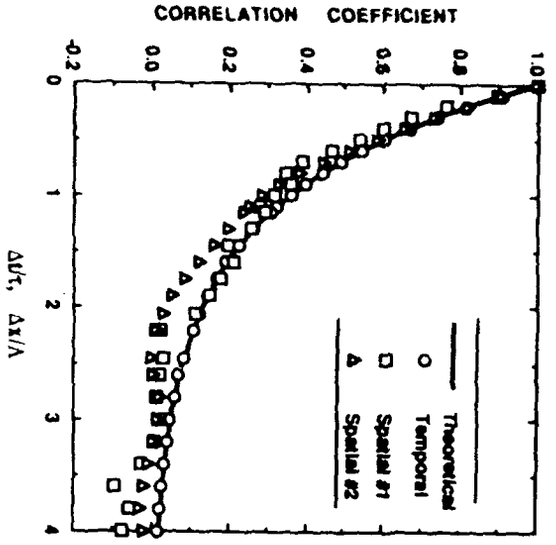

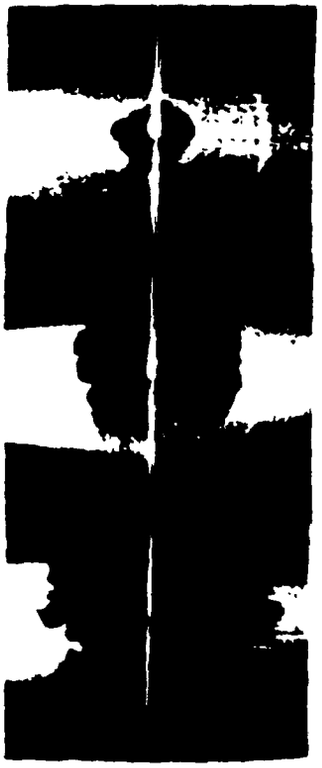

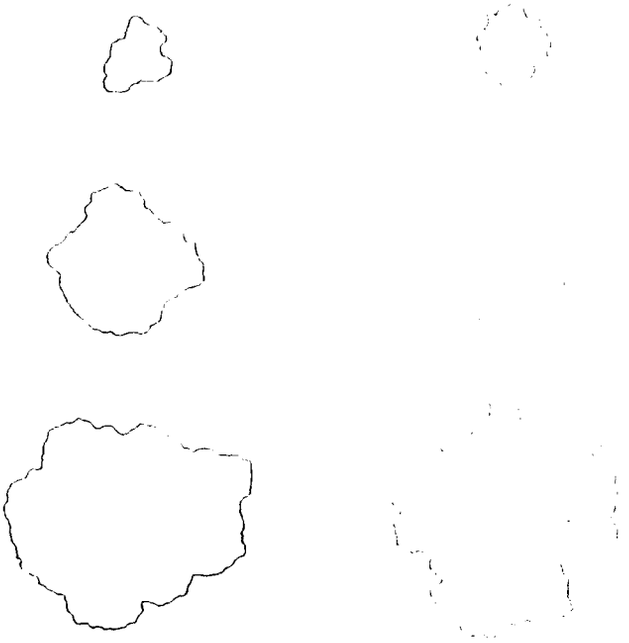

$\bar{u}'/S_L = 1.6$ $\bar{u}'/S_L = 1.6$ (SIM.) $\bar{u}'/S_L = 3.2$ (SIM.)

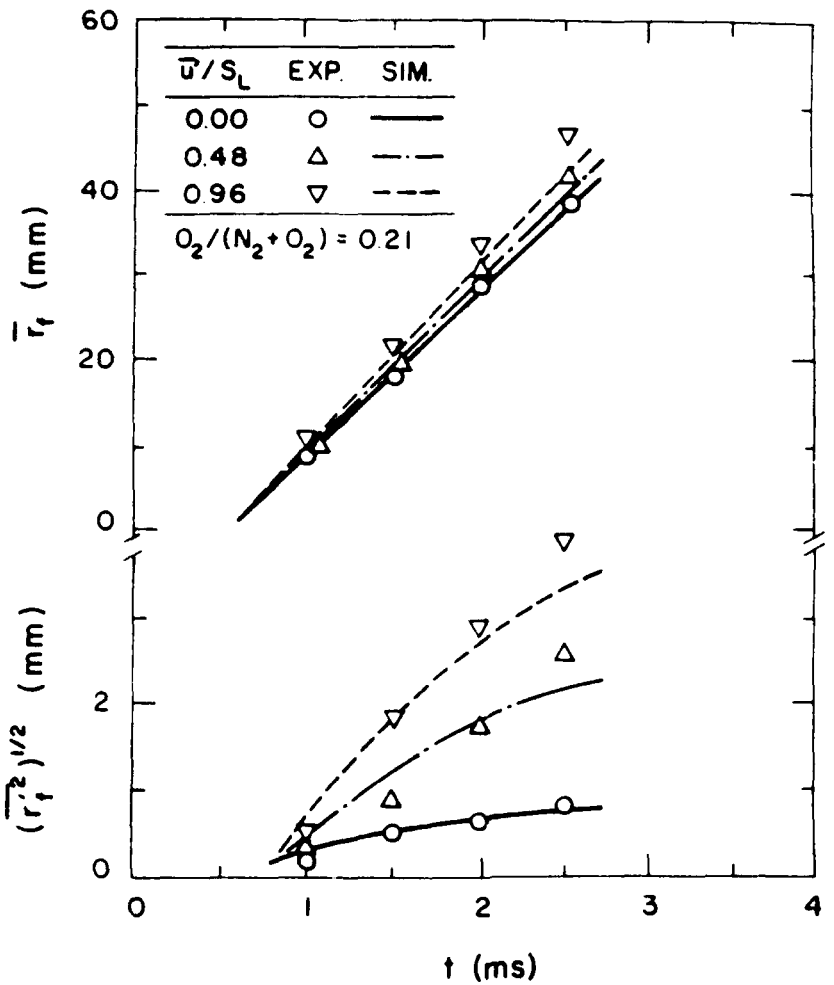
$\bar{u}'/S_L$ EXP. SIM.
0.00
0.48
0.96
$O_2/(N_2+O_2) = 0.21$
$\bar{r}_f$ (mm)
$(\overline{r_f'^2})^{1/2}$ (mm)
t (ms)

Fig. 8

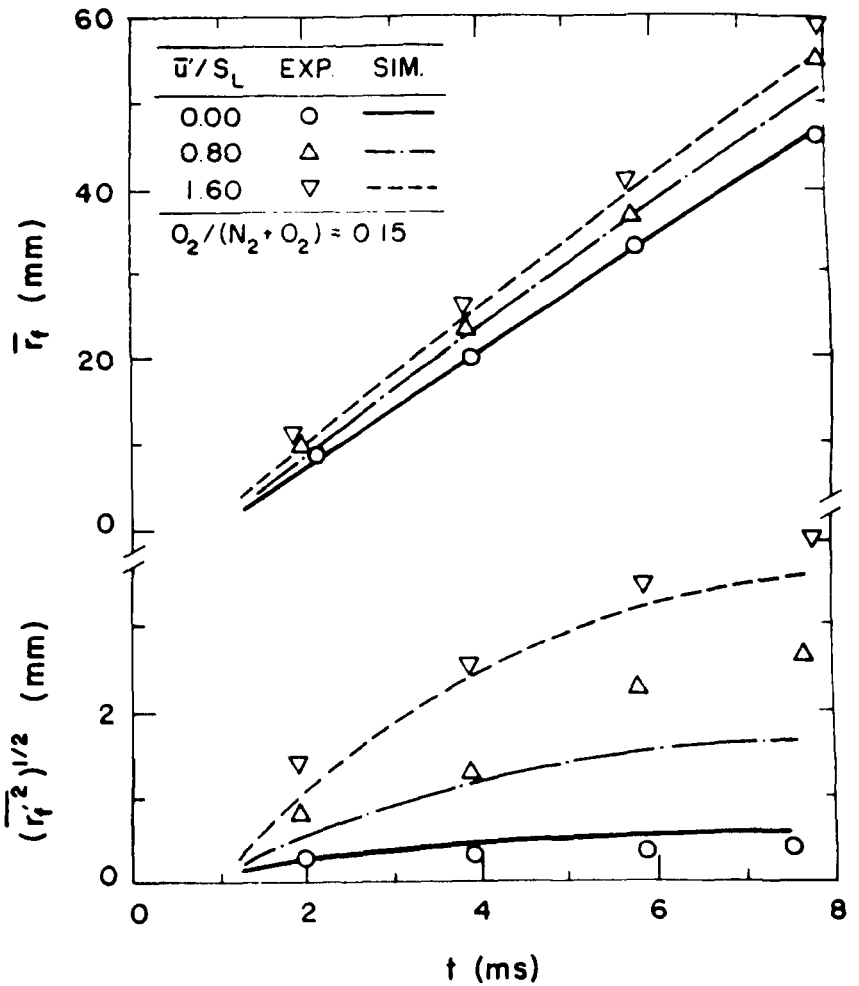
$\bar{u}'/S_L$ EXP. SIM.
0.00
0.80
1.60
$O_2/(N_2+O_2) = 0.15$
$\bar{r}_f$ (mm)
$(\overline{r_f'^2})^{1/2}$ (mm)
t (ms)

Fig. 3

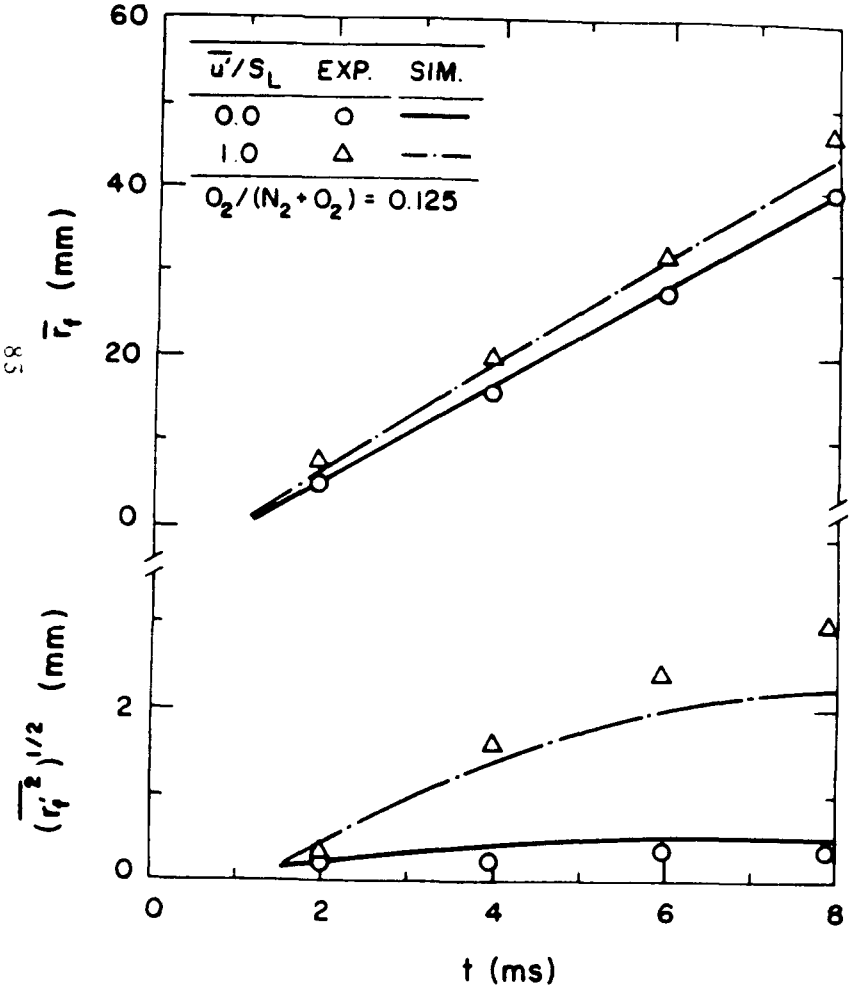
$\bar{u}'/S_L$ EXP. SIM.
0.0 ○ ——
1.0 △ —·—
$O_2/(N_2+O_2)$ = 0.125
$\bar{r}_f$ (mm)
$(\overline{r_f'^2})^{1/2}$ (mm)
t (ms)
0
2
4
6
8
20
40
60

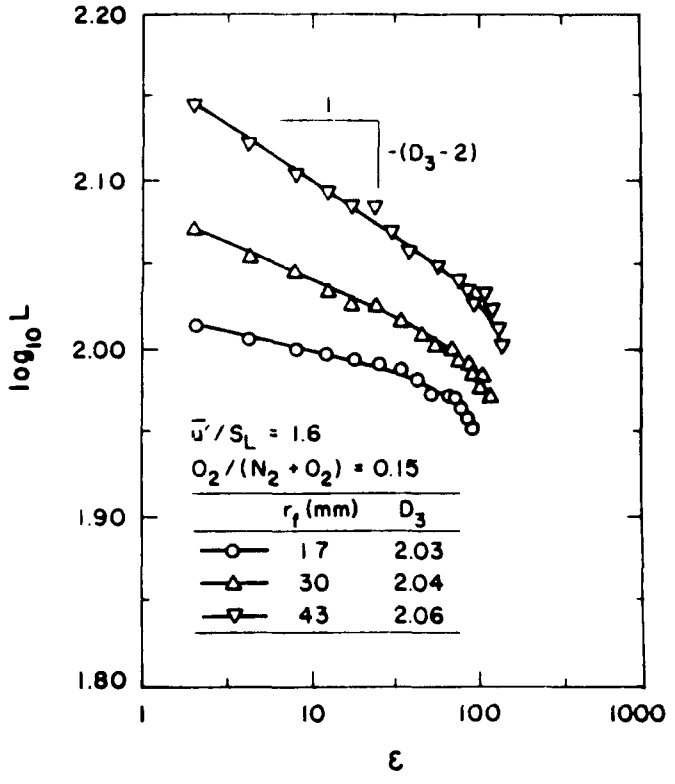
$\log_{10} L$
ε
1
$-(D_3-2)$
$\bar{u}'/S_L$ = 1.6
$O_2/(N_2+O_2)$ = 0.15
r_f (mm) D_3
17 2.03
30 2.04
43 2.06
2.20
2.10
2.00
1.90
1.80
1
10
100
1000

FIG 10

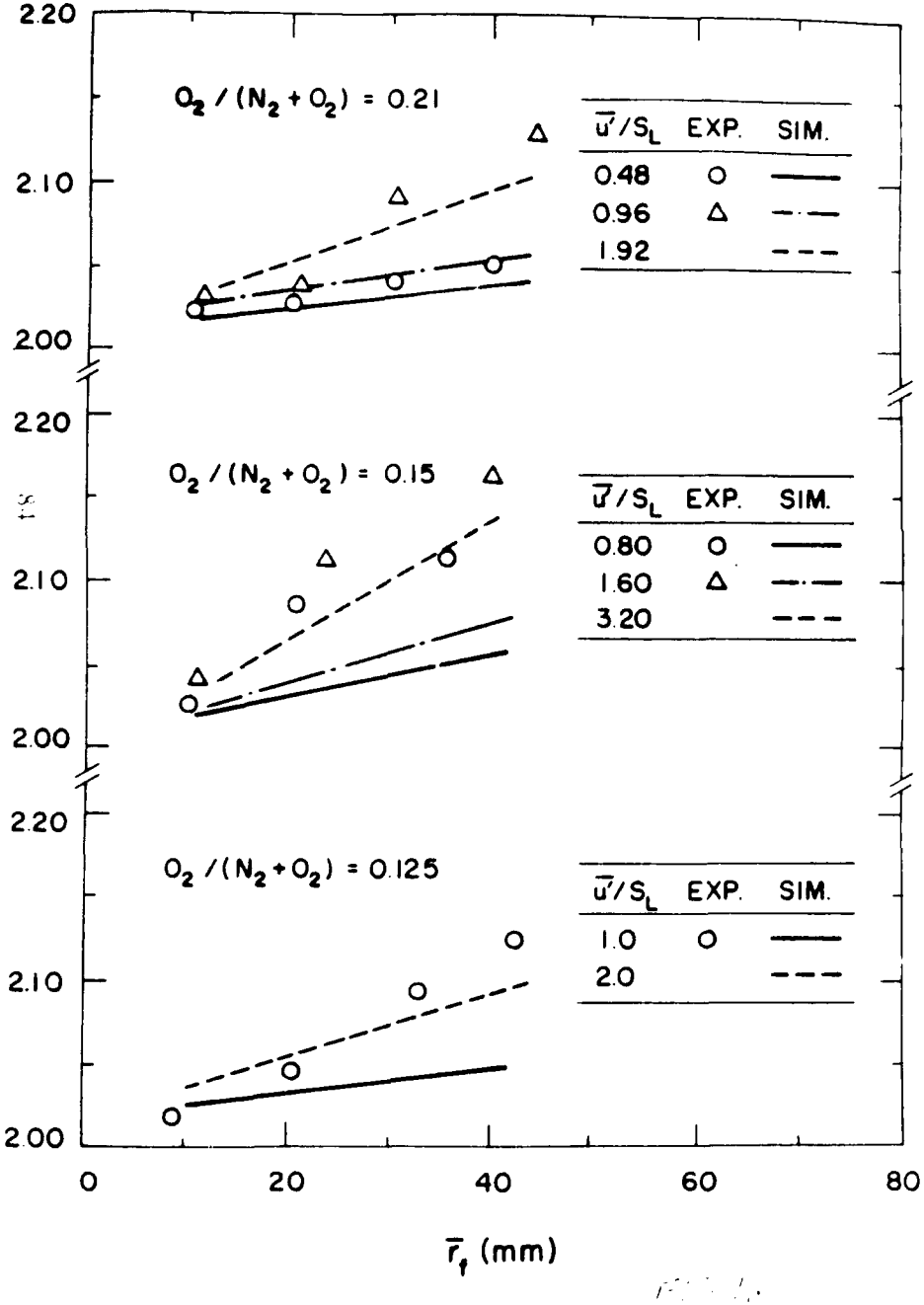
$O_2 / (N_2 + O_2) = 0.21$
$\bar{u}'/S_L$ EXP. SIM.
0.48 O
0.96 Δ
1.92
$O_2 / (N_2 + O_2) = 0.15$
$\bar{u}'/S_L$ EXP. SIM.
0.80 O
1.60 Δ
3.20
$O_2 / (N_2 + O_2) = 0.125$
$\bar{u}'/S_L$ EXP. SIM.
1.0 O
2.0
2.20
2.10
2.00
0
20
40
60
80
$\bar{r}_f$ (mm)

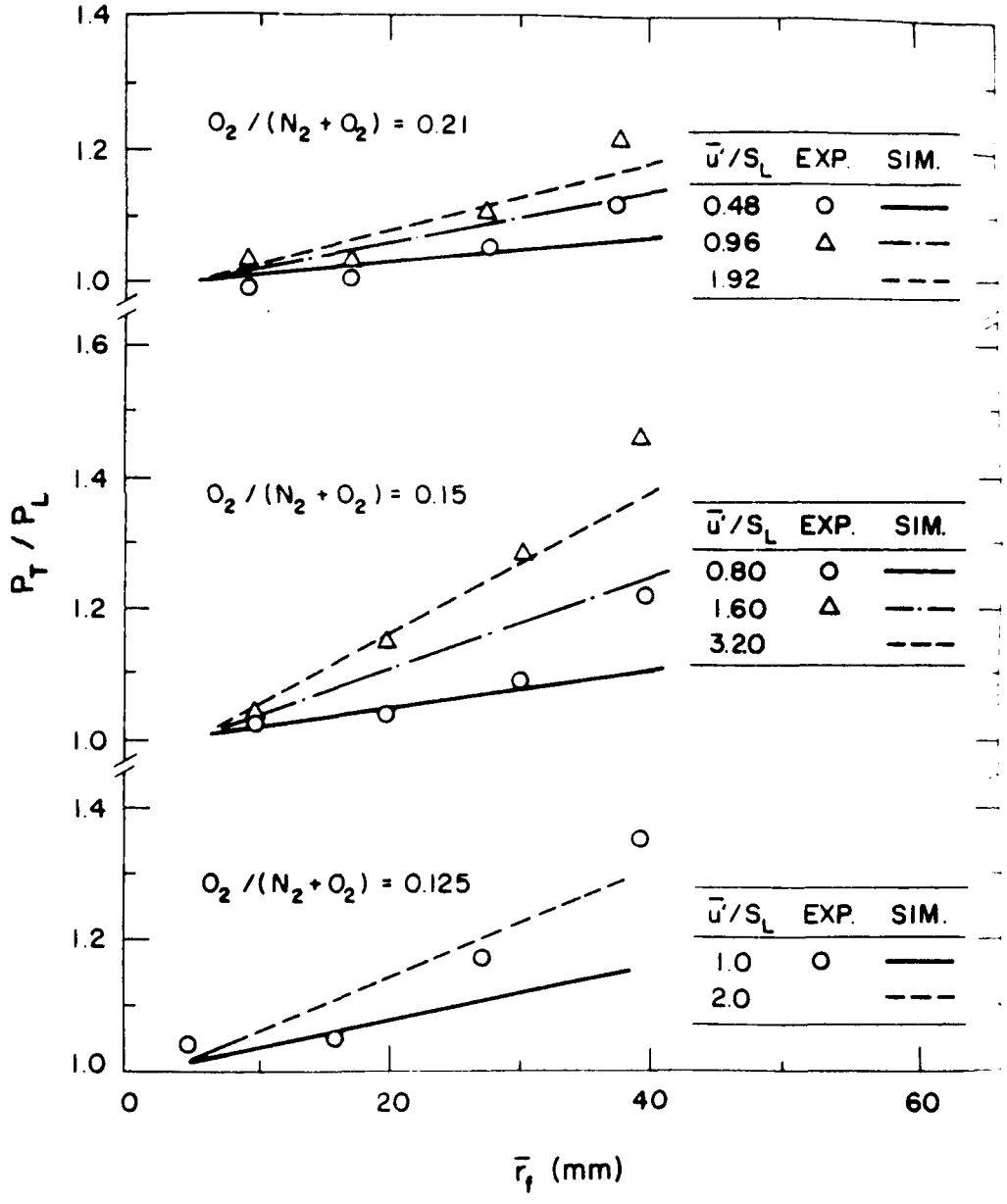
$O_2 / (N_2 + O_2) = 0.21$
$\bar{u}'/S_L$ EXP. SIM.
0.48 O
0.96 Δ
1.92
$O_2 / (N_2 + O_2) = 0.15$
$\bar{u}'/S_L$ EXP. SIM.
0.80 O
1.60 Δ
3.20
$O_2 / (N_2 + O_2) = 0.125$
$\bar{u}'/S_L$ EXP. SIM.
1.0 O
2.0
P_T / P_L
1.4
1.2
1.0
1.6
0
20
40
60
$\bar{r}_f$ (mm)

APPENDIX D: WU ET AL. (1991a)

Evaluation of Stochastic Simulations of Premixed Turbulent Jet Flames

M.-S. Wu, S. Kwon, J. F. Driscoll and G. M. Faeth

Department of Aerospace Engineering

The University of Michigan

Ann Arbor, MI 48109-2140

Abstract — A theoretical investigation of round premixed turbulent jet flames is described, limited to the thin laminar-flamelet regime at neutral preferential diffusion conditions. Flame surface properties were numerically simulated using a statistical time series simulation of unburned gas properties along the flame surface in conjunction with a two-dimensional flame advection and propagation algorithm. Predictions were evaluated using existing tomographic and Rayleigh scattering measurements of flame surface properties and mean unreactedness in round jet flames having burner exit Reynolds numbers in the range 7000-39200 and turbulence intensities relative to the laminar flame speed in the range 0.4-2.5. Simulated flame properties duplicated measured trends of the variation of flame surface properties and mean unreactedness with distance from the burner exit and relative turbulence intensity. However, effects of turbulence were underestimated — particularly near the flame tip — due to the limitations of a two-dimensional simulation.

NOMENCLATURE

C	reaction progress variable
d	burner exit diameter
F	value of streamwise spatial correlation coefficient at Δx
G	value of transverse spatial correlation coefficient at Δx
ℓ_i	integral length scale for velocity component in direction i
ℓ_k	Kolmogorov length scale
L_c	flame length based on a time-averaged reaction progress variable of one-half along the axis
r_f	radial distance to flame surface
Re_d	Reynolds number based on burner exit conditions, $u_{o,avg}d/\nu_o$
Re_t	turbulence Reynolds number, $u'_{o,avg}\ell_{uo}/\nu_o$
s'_u, s'_v	random shocks for u' and v' simulations
s^n_{uij}, s^n_{vij}	relative random shocks, s_{ij}/u', s'_v/v' at point $i\Delta x$, $j\Delta y$ and $n\Delta t$
S_L	laminar burning velocity
t	time
T	value of temporal correlation coefficient at Δt
u,v	streamwise and radial or crosstream velocity
u^n_{ij}, v^n_{ij}	relative instantaneous streamwise or crosstream velocity fluctuations, $u'/\bar{u}'$ or $v'/\bar{v}'$, at point $i\Delta x$, $j\Delta y$ and $n\Delta t$
x,y	streamwise and crosstream distance

Greek Letters

α	thermal diffusivity
δ_L	laminar flame thickness
Δt	time increment
$\Delta x, \Delta y$	streamwise and crosstream distance increments
ν	kinematic viscosity
ρ	density
τ	integral time scale
ϕ	fuel-equivalence ratio

Subscripts

avg	average value
c	centerline value

L	property from Laufer (1954)
max	*maximum* value
s	property used in simulation
o	burner exit condition

Superscripts

$(\tilde{\ }),(\bar{\ })'$	time-averaged mean and r.m.s. fluctuating property

INTRODUCTION

A theoretical investigation of premixed turbulent jet flames is described. The objectives were to extend an earlier approximate numerical simulation method that was reasonably successful for freely-propagating flames (Kwon et al., 1991) to jet flames; and to evaluate simulated flame surface properties using the measurements of Wu et al. (1990, 1991). These experiments involved hydrogen/air flames in the wrinkled thin flamelet regime at neutral preferential diffusion conditions and relatively high jet exit Reynolds numbers. Available experimental results included laser velocimeter measurements of unburned gas turbulence properties, flame-tomography measurements of flame surface statistics and Rayleigh-scattering measurements of mean unreactedness.

Only neutral preferential diffusion stability conditions were considered during the study, in order to simplify the simulation. In particular, Wu et al. (1990, 1991) show that effects of preferential diffusion enhance or retard turbulent distortion of flame surfaces, in the thin flamelet regime, even for high Reynolds number turbulent hydrogen/air jet flames. Thus, present conditions were limited to the maximum laminar burning velocity condition ($\Phi = 1.8$) where effects of preferential diffusion phenomena are suppressed.

Peters (1986) and Pope (1990) review models and simulations of premixed turbulent flames in the thin laminar-flamelet regime; therefore, discussion of past work will be brief. The most complete treatment of premixed turbulent flames involves direct numerical simulations of both hydrodynamic and flame propagation features, like those of

Ghoniem et al. (1980, 1982) and Ashurst and Barr (1983). Such simulations have the potential to provide a fundamental description of all aspects of premixed turbulent flames, however, they will not be computationally feasible for practical flames for some time to come (Pope, 1990). Thus, approximate numerical simulations that provide improved computational tractability are of interest.

Approximate numerical simulations generally involve stochastic simulation of the motion of flame surfaces in the presence of imposed turbulence having specified properties. This simplifies determination of fluid motion near the flame which is the most computationally intensive aspect of exact numerical simulations. Representative work along these lines includes Chate and Cant (1988), Said and Borghi (1988), Kwon et al. (1991) and references cited therein. The present approach is an extension of the method of Kwon et al. (1991) which was used to simulate flame surface properties for freely propagating flames in isotropic turbulence. This method involves a statistical time-series algorithm to simulate unburned gas velocities along the flame surface, assuming that effects of the flame on unburned gas turbulence properties are small, combined with a flame propagation algorithm to simulate the motion of the flame surface, assuming that the flame propagates relative to the local gas velocity at its laminar burning velocity and normal to its surface. The flame propagation algorithm was adapted from MIMOC (Ghoniem et al., 1983) which can provide only a two-dimensional time dependent simulation. This was a major limitation but past use of the approach for freely propagating flames has been encouraging (Kwon et al., 1991).

To summarize, the objectives of the present investigation were to extend the methods of Kwon et al. (1991) from unsteady freely-propagating flames in homogeneous isotropic turbulence to steady jet-stabilized flames in nonhomogeneous anisotropic turbulence, and to evaluate the simulations using the measurements of Wu et al. (1990, 1991). The limitation of a two-dimensional time-dependent simulation was maintained,

based on the flame propagation algorithm of Ghoniem et al. (1983), as a useful first st before committing resources to extend the method to treat three-dimensional effects.

The paper begins with descriptions of the test flame configuration and tl turbulence properties of the unburned gas. The numerical simulation of instantaneous g velocities along the flame surface, and its integration with the flame propagation algorithr are then described. The paper concludes with discussion of the comparison betwee simulations and measurements. The present description is brief, additional details and complete tabulation of computational and experimental data can be found in Wu (1991).

UNBURNED GAS PROPERTIES

Experimental Conditions

The experiments of Wu et al. (1990, 1991) involved a coaxial round jet burner wit an inner burner having a diameter of 11 mm and a tube length-to-diameter ratio of 50 i order to yield nearly fully-developed turbulent pipe flow at the burner exit. The oute burner had a diameter of 58 mm with the outer flame stabilized like a flat flame burne above a bed of beads and screens. The outer burner served primarily to stabilize the inne burner flame and no attempt was made to match the flow properties of the inner and oute burners, e.g. the outer burner had a fuel equivalence ratio of 0.3 and a burner exit velocit of 1 m/s, both of which are much lower than the corresponding properties of the inne burner. Nevertheless, the inner burner flames were well inside the mixing layer betwee the two flows (except at the point of flame attachment) and were not influenced by th properties of the outer burner flow (Wu et al., 1990, 1991).

Data from four flames at neutral preferential diffusion conditions were used t evaluate the simulations, see Table I for a summary of the test conditions. Flame surfac properties were available for $u'_{o,avg}/S_L$ = 0.9 and 2.5 while profiles of unreactedness were available for $u'_{o,avg}/S_L$ = 0.4 and 1.3 (Wu et al., 1990, 1991). Burner exit Reynold numbers were in the range 7000-39200 while turbulence Reynolds numbers based on streamwise velocity fluctuations and integral length scales at the center of the burner exit were in the range 200-1100. Taking the characteristic flame thickness to be $\delta_L = \alpha_u/S_L$, and the Kolmogorov length scale to be $\ell_k = \ell_{u0}/Re_t^{3/4}$ from Tennekes and Lumley (1972), ℓ_k/δ_L is in the range 0.9-3.5. This places present flows near the limit but still within the thin flamelet regime (Bray, 1980). Flame lengths, based on the condition where the time-averaged unreactedness at the axis was one-half, were in the range L_x/d = 1.7-5.3, therefore, the unburned gas was largely within the potential core of the jets where spatial variations of flow properties were modest.

Flow Properties

Certain properties of the turbulence within the unburned gas are needed as input to the simulation of the flame surface, as described in the next section. Measurements of unconditional mean and r.m.s. fluctuating streamwise velocities near the burner exit and along the axis are reported by Wu et al. (1991) for the full range of burner exit Reynolds numbers. Conditional measurements of turbulence properties in the unburned gas for $u'_{o,avg}/S_L$ = 0.9 are reported by Wu et al. (1991), however, findings at other conditions were similar (Wu, 1991).

Because the streamwise extent of the unburned gas was not very large, flow properties approximated fully developed pipe flow (Laufer, 1954; Nikuradse, 1932). The main difference was that the wake like flow due to the presence of the burner passage walls decayed and unburned gas flow properties became more uniform with increasing distance from the burner exit. The streamwise and radial velocity fluctuations satisfied Gaussian probability density functions (PDF). However, velocity fluctuations were anisotropic with u'/v' in the range 1.2-3.0, with the larger values observed near the edge of the flow.

The measured conditional temporal power spectra of streamwise velocity fluctuations approximated the spectra of an exponentially decaying autocorrelation function over the region that could be resolved. The spectra of crossstream velocity fluctuations were

similar, except for the appearance of a local maximum at low frequencies for positions near the axis and the burner exit. Laufer (1954) observed a similar spectral feature for turbulent pipe flow so that the effect is due to the origin of the flow. However, this feature decayed rapidly so that the spectra approximated spectra of exponentially decaying autocorrelations over most of the region of interest. Measured streamwise temporal integral scales were used to find the streamwise spatial integral scales using Taylor's hypothesis: ℓ_u/d was approximately 0.4 which is consistent with Laufer's (1954) measurements for turbulent pipe flow. Integral length scales in the crosstream direction are needed for the stochastic simulation but were not measured; therefore, ℓ_v was approximated as $\ell_u/4$, based on Laufer's (1954) measurements cited in Hinze (1975). Temporal integral scales in the crosstream direction were smaller than in the streamwise direction because the autocorrelation of v' has a negative portion at higher time delays (Laufer, 1954; Tennekes and Lumley, 1972).

STOCHASTIC SIMULATION

General Description

Turbulent flame propagation was numerically simulated using a statistical time series simulation of the velocity field of the unburned gas similar to Kwon et al. (1991), combined with the flame advection and propagation algorithm used in the MIMOC computer program of Ghoniem et al. (1983). As noted earlier, this algorithm only provides a two-dimensional time-dependent simulation. This is a major limitation; however, assessing the present approach is justified before undertaking the significant extension required to treat three-dimensional effects. At each grid point, velocity time series u(t) and v(t) are found using the algorithm described below. The algorithm is designed so that u(t) and v(t) satisfy the following properties of the given turbulent field: u, v, u', v', ℓ_x, ℓ_y, and τ. In addition, the velocity fluctuations must have Gaussian PDF's and their correlation functions must be exponentially decaying, as discussed previously. The flame

propagation algorithm, also discussed below, requires that each point on the flame surface is advected at velocity (u(t), v(t)) and propagates normal to the flame surface at a velocity S_L relative to the gas velocity.

Other major assumptions of the approximate numerical simulation are as follows: constant pressure turbulent deflagration wave, infinitely thin flame sheet, turbulence properties of the unburned gas are stationary and unaffected by the presence of the flame, the flame is attached to the rim of the burner exit, and the flame is neutrally stable with negligible effects of quenching (i.e., relative to the unburned gas, the flame propagates normal to its surface at the laminar burning velocity). The assumptions of constant pressure, thin flames, neutral stability, attachment points near the burner rim and turbulence properties of the unburned gas unaffected by the flame are all conditions of the experiments (Wu et al., 1990, 1991). Neglecting quenching also seems reasonable because the flames were at the maximum laminar burning velocity condition, well away from flammability limits, and values of $u'_{0,avg}/S_L$ were relatively small. Discussion of the approximations used for unburned gas turbulence properties will be taken up next.

Statistical simulations can be designed to satisfy any number of the statistical properties of turbulence. However, in order to control computation times, only variables found to be important by Kwon et al. (1991) were simulated, including: mean velocities, Gaussian PDF's of velocity fluctuations, and temporal and spatial correlations. Ignoring cross-correlations is less justified here than for the isotropic turbulence considered by Kwon et al. (1991), however, these correlations are still relatively small within a potential core region.

Other simulation approximations concern the treatment of spatial and temporal correlations. First of all, these correlations were approximated by exponential functions because this yields a Markov-like simulation that vastly simplifies computations (Box and Jenkins, 1976; Kwon et al., 1991). As noted earlier, the temporal and streamwise spatial correlations measured for the present experiments are fitted quite well by exponential

functions. Crosstream temporal correlations approximate exponential functions to a lesser degree near the burner exit, however, the discrepancy is not large in the region of the flame brush (Wu, 1991).

Another approximation involves treatment of two-point/two time correlations. Resolution of flame surfaces in space and time requires relatively small spatial and temporal increments in comparison to integral scales; therefore, values of the correlation coefficients between the important nearest neighbors in space and time, and the point being computed, all are near unity. Then it is reasonable to decompose two-point/two-time correlations along individual coordinate axes similar to stochastic simulations used to treat turbulent mixing (Kounalakis et al., 1991). Thus, given the following correlation coefficients for incremental steps in either of two orthogonal spatial directions or time

$$F = \exp(-\Delta x/\ell_x), \quad G = \exp(-\Delta y/\ell_y), \quad T = \exp(-\Delta t/\tau) \tag{1}$$

two-point/two-time correlation coefficients become

$$\overline{u^n_{i,j} u^{n+r}_{i+p,j+q}} = T^r F^p G^q \tag{2}$$

where $u^n_{i,j}$ is the instantaneous relative velocity fluctuation

$$u^n_{i,j} = u'(i\Delta x, j\Delta y, n\Delta t) / u'(i\Delta x, j\Delta y) \tag{3}$$

for stationary turbulence. Equation (2) is only formally correct in each coordinate direction. For example, for isotropic turbulence, Hinze (1975) shows that

$$\overline{u^n_{i,j} u^n_{i+1,j+1}} = (F^{\sqrt{2}} + G^{\sqrt{2}}) / 2,$$

rather than FG from Eq. (2). Nevertheless, the difference between the two expressions is less than 10% for F and G > 0.9 so that the error is acceptable in view of other approximations of the simulation.

A final matter involves the actual specification of the unburned gas flow properties. The measurements of Wu et al. (1990, 1991) were limited but generally indicated that flow properties within the unburned gas approximated the properties of turbulent pipe flow because the flames did not extend very far from the burner exit. Thus, in order to use well defined and accessible unburned gas velocity properties, the measurements of Laufer (1954) were used in the simulation at corresponding radial positions. This approach was feasible because the simulated motion of the flame surface never reached radial positions beyond the radius of the burner exit.

Velocity Simulation

An autoregressive time series process was used to simulate the velocity field, where the velocity fluctuation at a point to be computed is taken to be a weighted sum of velocity fluctuations computed earlier and a random shock (Box and Jenkins, 1976). The weighting factors of the process are chosen to satisfy correlations between points in space and time, while the properties of the random shock are chosen to satisfy the PDF of velocity fluctuations at the point being computed.

For stationary homogeneous turbulence, Gaussian PDFs, and exponential temporal and spatial correlations that can be decomposed according to Eq. (2), Kwon et al. (1991) find that an autoregressive process becomes a Markov like process (Box and Jenkins, 1976). Then only the seven nearest neighbors must be retained in the weighted sum in order to correctly simulate correlations for all space and time for a two dimensional time-dependent simulation. In order to exploit the computational efficiency of these properties for the present nonhomogeneous flow, the assumption of locally homogeneous turbulence was made. This implies that local properties, such as velocity fluctuations and integral length and time scales, are assumed to be constant for the eight neighboring points and their values are taken to be equal to those of the point being simulated. This assumption is reasonable because the variation of turbulence properties over the entire

region of interest was modest — generally less than 30%. Additionally, the small spatial increments used implied relatively high correlation coefficients between neighboring points so that changes of turbulence properties over these distances were negligible.

Under the present approximations, the autoregressive processes for streamwise and crosstream velocity fluctuations become (Kwon et al., 1991):

$$u^n_{i,j} = Fu^n_{i-1,j} + Gu^n_{i,j-1} + Tu^{n-1}_{i,j} - FGu^n_{i-1,j-1} - FTu^{n-1}_{i-1,j} - GTu^{n-1}_{i,j-1} + FGTu^{n-1}_{i-1,j-1} + s^n_{u,i,j} \quad (4)$$

$$v^n_{i,j} = Gv^n_{i-1,j} + Fv^n_{i,j-1} + Tv^{n-1}_{i,j} - FGv^n_{i-1,j-1} - GTv^{n-1}_{i-1,j} - FTv^{n-1}_{i,j-1} + FGTv^n_{i-1,j-1} + s^n_{v,i,j} \quad (5)$$

where F, G and T pertain to their associated velocity component and are to be found at the point $i\Delta x$, $j\Delta y$. The parameters $s^n_{u,i,j} = s'_u(i\Delta x, j\Delta y, n\Delta t)/\bar{u}'(i\Delta x, j\Delta y)$ and $s^n_{v,i,j} = s'_v(i\Delta x, j\Delta y, n\Delta t)/\bar{v}'(i\Delta x, j\Delta y)$ are uncorrelated Gaussian random variables (relative random shocks) with mean values of zero and variances:

$$(s^n_{u,i,j})^2 = (s^n_{v,i,j})^2 = 1 - F^2 - G^2 - T^2 + (FG)^2 + (FT)^2 + (GT)^2 - (FGT)^2 \quad (6)$$

where F, G and T are to be found for the appropriate velocity component at the point $i\Delta x$, $j\Delta y$ as before.

Initial conditions, t=0, and boundary points, e.g., x=0 or y=0, require corrected procedures because all seven points in Eqs. (4) and (5) are not available. In these cases, the unavailable points are simply deleted while dropping corresponding terms in Eq. (6) (note that the terms in Eq. (6) are simply the squares of the coefficients in Eqs. (4) and (5)). Given $u^n_{i,j}$ and $v^n_{i,j}$, the corresponding instantaneous velocity fluctuations were found and then added to the measured mean velocities in order to obtain the simulated instantaneous velocities at the point (however, v was neglected for present computations because it is small in comparison to $\bar{v}'$).

The autoregressive process was tested for typical conditions (60 × 264 spatial grid, with F = 0.92, G = 0.73 and T = 0.95 (other specifications of the computations will be taken up later). After 4000 time steps, the simulated PDFs were Gaussian and r.m.s. velocity fluctuations and spatial and temporal correlations were reproduced within 15 and 30%, respectively — the latter for the region within two temporal and spatial integral scales (Wu, 1991). These discrepancies were largely due to sampling limitations over 4000 time steps and decreased when the number of time steps used for averages were increased. The flame propagation algorithm requires much more computer time than the velocity simulation so that the velocity field to the unburned gas was computed over the whole spatial grid, to simplify bookkeeping, even though this was wasteful because only the region near the flame surface was needed.

Flame Propagation Algorithm

Flame surface properties were found using the flame advection and propagation portion of MIMOC (Ghoniem et al., 1983). This involves the simple line interface calculation (SLIC) of Noh and Woodward (1976) to treat advection of the flame surface at $u = \bar{u} + u'$ and $v = v'$, and Chorin's (1980) use of Huygens' principle to propagate the flame relative to these velocities at its laminar burning velocity and normal to its surface.

The computations involved 264 and 60 grid points in the streamwise and crosstream directions with 0.25 mm grid spacing in both directions. The grid spacing was chosen to be comparable to the resolution used to measure flame surface statistics and the reaction progress variable (Wu et al., 1990, 1991). Notably, there is no requirement for small grid spacing for accuracy of the velocity simulation because adjacent points are only connected through their correlations and the autoregressive process will reproduce these correlations for a sufficient number of realizations (aside from the requirement that correlations be high between neighboring points so that the approximations of Eq. (2) and locally homogeneous turbulence are acceptable). The time increment was set to satisfy the

Courant condition for the flame propagation algorithm: $\Delta t < \Delta x / (2|u|_{max})$, see Noh and Woodward (1976). A typical run time for 4000 time steps on a DEC 5000 computer was four hours.

The effect of grid spacing on simulated flame surface properties was evaluated. Simulations were completed for grid sizes 1/2, 1 and 2 times the standard value and extrapolated to a grid spacing of zero to estimate numerical accuracy. Variations of mean and fluctuating flame radius, and flame perimeter, deviated from the standard values less than 4%. Similarly, increasing the number of time steps from 1200 to 4800 resulted in only a 4% variation of the same properties. Thus, the numerical accuracy generally exceeds other uncertainties of the simulations.

RESULTS AND DISCUSSION

Flame Realizations

Visualization of the flames by schlieren photography and flame tomography is presented by Wu et al. (1990, 1991). In general, the flames appear to have a wrinkled flame surface with the extent of wrinkling increasing with increasing $\bar{u}'_{o,avg}/S_L$ and distance from the burner exit. Discussion of the results will begin with realizations of flame surfaces from tomographs for vertical planes through the burner axis.

Numerical simulations were completed for the same conditions as the measurements as well as for enhanced velocity fluctuations, as follows: $\bar{u}'_s/\bar{u}'_L = \bar{v}'_s/\bar{v}'_L = 1$, 2 and 4, where $\bar{u}'_s$ and $\bar{u}'_L$, etc., denote values for the simulation and from Laufer's (1954) pipe flow measurements, respectively. This was done because two-dimensional simulations of freely-propagating flames in isotropic turbulence required velocity fluctuations roughly twice the actual values in order to obtain good quantitative agreement between simulated and measured flame surface statistics (Kwon et al., 1991). This behavior was attributed to the limitations of a two-dimensional simulation where effects of flame surface irregularities and velocity fluctuations in the plane normal to the tomograph are ignored. In particular, a

two-dimensional simulation implies that the flame is a ruled surface normal to the plane of the tomograph which reduces the potential for irregularities of surface properties in comparison to the true three-dimensional surface.

The general nature of the stochastic simulations is illustrated in Figure 1. A typical realization of a section of both the total and fluctuating velocity fields, as well as the flame surface, is illustrated. Flame conditions include $\bar{u}'_{o,avg}/S_L = 0.9$, $x/d = 0.5$ and $\bar{u}'_s/\bar{u}'_L = 2$, the last being the degree of enhancement of the simulation that yielded the best results for the freely propagating flames. Reference lengths for velocity scales as well as streamwise and crosstream integral length scales at the center of the burner exit, $\ell_{x,o}$ and $\ell_{r,o}$, are also shown on the plots.

The angle of the flame surface in Figure 1 is never far from the streamwise direction because streamwise velocities are relatively large in comparison to the laminar flame speed, roughly 30 m/s in comparison to 3.5 m/s. Nevertheless, the local velocity fluctuations have created a significant bulge in the flame surface. This action is best illustrated by the fluctuating velocity field where the outward bulge of the flame surface is associated with a region of outward velocity fluctuations of the unburned gas. The realization also exhibits integral-scale sized flow structures, having anisotropy of shape similar to the streamwise and crosstream integral scales, with corresponding length scales of the main distortion of the flame surface.

The overall behavior of the measured and simulated flame surface properties are illustrated in Figure 2, where realizations of instantaneous flame position are plotted for $\bar{u}'_{o,avg}/S_L = 0.9$. The measured flame brush thickness increases, and the flame surface becomes progressively more irregular, with increasing height above the burner exit. This behavior is somewhat analogous to turbulent dispersion, where the lateral spread of the dispersed phase progressively increases with increasing distance from the source. The measured flame becomes blunt and thickened in the streamwise direction, with islands of unreacted material appearing at times near the tip of the flame. Much of this behavior is due

to the deflection of the irregular conical shaped flame surface out of the plane of the tomograph, as will be discussed later.

The comparison between measured and simulated flame shapes in Figure 2 is disappointing in comparison to results obtained for freely propagating flames, where simulations for $\bar{u}'_s/\bar{u}'_L = 2$ looked very much like the measurements. The present simulated flame brush thicknesses for $\bar{u}'_s/\bar{u}'_L = 2$ approximate the measurements up to one to two burner exit diameters, however, other features of this simulation are deficient: the simulated flame brush is too long, it is too thin in both the streamwise and crosstream directions near the tip, and its sides are straight rather than outward curved and blunt like the measurements. Increasing $\bar{u}'_s/\bar{u}'_L$ to 4 improves the estimate of flame length somewhat but overestimates the thickness of the flame brush near the burner exit and still does not yield the measured blunt flame brush near the tip. These difficulties, as well as the poorer performance of the simulation for jet flames than for freely-propagating flames, can be attributed to the limitations of a two-dimensional simulation and the different geometry of freely propagating and jet flames, as discussed next.

Some of the problems of a two-dimensional simulation of a turbulent round jet flame are illustrated in Figure 3. Ignoring small-scale features, the three-dimensional flame surface is approximated by a smooth conical surface whose axis generally is not aligned with the burner axis. Then the intersection of the conical surface with the tomograph plane through the axis is a parabola. This implies more outward curvature at the base and a blunter tip region, for the tomographic image than the conical shape itself. Additionally, deflection of the cone axis causes a broader range of streamwise motion of the tip region on the tomograph plane than corresponding changes in the cone itself. Finally, crossings of the tip region with the tomograph plane can contribute to the appearance of island-like images. Thus, the two-dimensional simulation, which is more representative of the cone itself, cannot reproduce these effects because it cannot be deflected out of the plane normal to the figure. Naturally, these discrepancies are smallest near the base of the cone so that

simulation of the flame brush thickness for $\bar{u}'_s/\bar{u}'_L = 2$ is reasonably good in this region, much like the findings for freely propagating flames for the same enhancement of velocity fluctuations in the simulation.

The reason why the three-dimensional effects discussed in connection with Figure 3 were less evident for freely propagating spherical flames (Kwon et al., 1991) is that the region considered by Kwon et al. (1991) involved relatively large flame balls. Then effects of out-of-plane deflection of the flame balls were small because of their large radii of curvature, somewhat like the base region of the turbulent jet flames. Thus, the narrow tip of the flame surface of a jet flame amplifies the importance of three-dimensional effects and probably accounts for most of the problems near the tip region seen in Figure 1. Judged by the base region alone, there is adequate agreement between simulations for $\bar{u}'_s/\bar{u}'_L = 2$ and the measurements of flame brush thickness, which is comparable to findings for freely-propagating flames (Kwon et al., 1991).

Flame Surface Statistics

Results illustrated in Figures 4 and 5 provide a more quantitative evaluation of the simulation. Measured and simulated mean and r.m.s. fluctuating flame radii are plotted as a function of height above the burner for $u'_{o,avg}/S_L = 0.9$ and 2.5. As before, results for $\bar{u}'_s/\bar{u}'_L = 1$, 2 and 4 are illustrated for the simulations.

The main effect of changing $u'_{o,avg}/S_L$ on the measurements illustrated in Figures 4 and 5 is that the flame is longer for the larger $u'_{o,avg}/S_L$ (note that Figures 4 and 5 have different scales in the streamwise direction); in contrast, values of r'_f/d are comparable. The change in flame length is due to the manner that $u'_{o,avg}/S_L$ was varied. For turbulent pipe flow, $u'_{o,avg}/\bar{u}_{o,avg}$ is essentially constant so that increasing values of $u'_{o,avg}/S_L$ required increasing values of $\bar{u}_{o,avg}$; this implies smaller flame angles with respect to the axis and an accordingly longer flames as $u'_{o,avg}/S_L$ increases because S_L was constant.

Simulations of $\bar{r}_f/d$ illustrated in Figures 4 and 5 are not strongly influenced by $\bar{u}'/\bar{u}'_L$ and are in reasonably good agreement with the measurements. Exceptions include somewhat overestimating the rate of reduction of $\bar{r}_f/d$ near the burner exit, and predicting a long tail for $\bar{r}_f/d$ near the tip, which was not observed. Out-of-plane deflections of the flame surface helps explain these deficiencies, as discussed earlier. In contrast to $\bar{r}_f/d$, however, simulated values of $\bar{r}'_f/d$ significantly increase as $\bar{u}'/\bar{u}'_L$ is increased. Near the base of the flame, measurements and simulations for $\bar{u}'/\bar{u}'_L = 2$ are in good agreement, with the range of x/d where agreement is achieved being longer for the longer flame (scaling roughly with the flame length). This is consistent with the findings for the freely propagating flames (Kwon et al., 1991), for the reasons discussed earlier. Near the tip of the flames, however, measurements exceed simulated results even for $\bar{u}'/\bar{u}'_L = 4$ due to out of plane motion of the narrow tip region of the flame surface. Small flame balls for freely-propagating flames just after ignition would cause similar difficulties by deflection of the flame kernal out of the tomograph plane, however, this region was not considered by Kwon et al. (1991).

Mean Unreactedness

Plots of measured and simulated time averaged unreactedness along the axis, $(1-\bar{C})_c$ are illustrated in Figure 6 for $\bar{u}'_{o,avg}/S_L = 0.4$ and 1.3. Both measurements and simulations are based on the assumption of an infinitely-thin flame sheet, with C = 0 and 1 in the reactants and products, respectively. The experimental results were obtained from the Rayleigh-scattering measurements of Wu et al. (1990). Simulations are illustrated for $\bar{u}'/\bar{u}'_L = 1$, 2 and 4, as before.

As anticipated from the previous results, the simulated unreactedness in Figure 6 is generally greater than the measurements with flame lengths overestimated accordingly. Thus, simulated values of L_c are 24 and 67% too large for $\bar{u}'_{o,avg}/S_L = 0.4$ and 1.3, and $\bar{u}'/\bar{u}'_L = 2$, the latter being ratio that gives the best simulation of flame brush thicknesses

near the base of the flame. This behavior also is probably due to out of plane distortion of the flame surface. In particular, the larger error for the larger $\bar{u}'_{o,avg}/S_L$ is consistent with anticipated capabilities of a long narrow flame surface to be deflected out of the tomographic plane. In spite of the limitations of a two-dimensional simulation, however, present predictions of both trends with respect to increasing $\bar{u}'_{o,avg}/S_L$, and the values of L_c, are still in better agreement with measurements than estimates Wu et al. (1990) obtained using a relatively sophisticated turbulence model.

CONCLUSIONS

The major conclusions of the study are as follows:

1. The present two-dimensional simulation successfully predicted the trends of flame properties with height above the burner and $\bar{u}'_{o,avg}/S_L$. Quantitative accuracy of the simulation was also reasonably good near the base of the flames using the artifice of doubling $\bar{u}'/S_L$ to compensate for the limitations of a two-dimensional time-dependent simulation, this performance is similar to the findings of Kwon et al. (1991) for freely-propagating flames in isotropic turbulence using the same approach.
2. In contrast, the present two-dimensional simulation was not effective near the flame tip where flame surface properties are very sensitive to out-of-plane deflection of the narrow tip region. The two dimensional simulations of freely propagating flames would probably encounter similar difficulties of out-of-plane deflections of small flame kernals; however, this region was not considered by Kwon et al. (1991).
3. Three-dimensional time dependent simulations are needed to definitively evaluate the effectiveness of the present numerical simulations. Fortunately, extension to three dimensions should be tractable even for high Reynolds number flames due to the computational efficiency of the velocity simulation. Three dimensional time-dependent results are particularly needed to determine whether simulating moments, PDFs, spatial correlations and temporal correlations of the unburned gas is adequate

to treat effects of flame surface distortion by turbulence. Issues of modification of unburned gas turbulence properties by the flame, quenching and preferential diffusion also need to be addressed; the present algorithm represents a promising framework to consider these modifications because it simulates the instantaneous flame surface from which local flame curvature and stretch can be computed.

ACKNOWLEDGEMENTS

This research was supported by the Office of Naval Research, Contract No. N00014-87-K-0698 with S. Ramberg serving as Scientific Program Officer.

REFERENCES

Ashurst, W. T., and Barr, P. K. (1983). Stochastic calculation of wrinkled laminar flame propagation via vortex dynamics. *Combust. Sci. and Tech.* 34, 227.

Box, G. P., and Jenkins, G. M. (1976). *Time Series Analysis*, Holden-Day, San Francisco, CA, pp. 47-66.

Bray, K. N. C. (1980). Turbulent flows with premixed reactants. In P. A. Libby and F. A. Williams (Eds.), *Turbulent Reacting Flows*, Springer, Berlin, pp. 115-183.

Chate, H., and Cant, R. S. (1988). Relevant scales in the corrugated flamelet regime, *Combust. Flame* 74, 1.

Chorin, A. J. (1980). Flame advection and propagation algorithm. *J. Comp. Phys.* 35, 1.

Ghoniem, A. F., Chorin, A. J., and Oppenheim, A. K. (1980). Numerical modeling of turbulent combustion in premixed flames. *Eighteenth Symposium (International) on Combustion*, The Combustion Institute, Pittsburgh, pp. 1375-1393.

Ghoniem, A. F., Chorin, A. J., and Oppenheim, A. K. (1982). Numerical modeling of turbulent flow in a combustion tunnel. *Trans. Roy. Soc. London* A304, 303.

Ghoniem, A. F., Marek, C. J., and Oppenheim, A. K. (1983). Modeling interface motion of combustion (MIMOC). NASA Technical Paper 2132.

Hinze, J. O. (1975). *Turbulence*, McGraw-Hill, New York, 2nd edition, Chapt. 3 and 4.

Kounalakis, M. E., Sivathanu, Y. R., and Faeth, G. M. (1991). Infrared radiation statistics of non-luminous turbulent diffusion flames. *J. Heat Trans.*, in press.

Kwon, S., Wu, M.-S., Driscoll, J. F., and Faeth, G. M. (1991). Flame surface properties of premixed flames in isotropic turbulence: measurements and numerical simulations. *Combust. Flame*, in press.

Laufer, J. (1954). Cited in Hinze, J. O. (1975). *Turbulence*, McGraw-Hill, New York, 2nd edition, pp. 720-724.

Nikuradse, J. (1932), Cited in Hinze, J. O. (1975). *Turbulence*, McGraw-Hill, New York, 2nd edition, pp. 725-727.

Noh, W. T., and Woodward, P. (1976). SLIC (simple line interface calculation). In A. I. Vooren and P. J. Zandenbergen (Eds.), *Fifth International Conference on Numerical Methods in Fluid Dynamics*, Springer-Verlag, Berlin, pp. 330-339.

Peters, N. (1986). Laminar flamelet concepts in turbulent combustion. *Twenty-First Symposium (International) on Combustion*, The Combustion Institute, Pittsburgh, pp. 1231-1250.

Pope, S. B. (1990). Computations of turbulent combustion: progress and challenges. *Twenty-Third Symposium (International) on Combustion*, The Combustion Institute, Pittsburgh, in press.

Said, R., and Borghi, R. (1988). A simulation with a "cellular automaton" for turbulent combustion modeling. *Twenty-Second Symposium (International) on Combustion*, The Combustion Institute, Pittsburgh, pp. 569-577.

Tennekes, H., and Lumley J. L. (1972). *Turbulence*, M.I.T. Press, Cambridge, MA, pp. 67.

Wu, M.-S., Kwon, S., Driscoll, J. F., and Faeth, G. M. (1990). Turbulent premixed hydrogen/air flames at high Reynolds numbers. *Combust. Sci. and Tech.* 73, 327.

Wu, M.-S., Kwon, S., Driscoll, J. F., and Faeth, G. M. (1991). Preferential diffusion effects on the surface structure of turbulent premixed hydrogen/air flames. *Combust Sci. and Tech.*, in press.

Wu, M.-S. (1991). The surface structure of turbulent premixed hydrogen/air rim-stabilized flames at high Reynolds number. Ph.D. Thesis, The University of Michigan, Ann Arbor, Michigan.

Table I. Summary of Test Flames[a]

$\bar{u}'_{o,avg}/S_L$	0.4	0.9	1.3	2.5
$\bar{u}_{o,avg}$ (m/s)	15.7	31.1	45.0	88.0
$\bar{u}'_{o,avg}$ (m/s)	1.6	3.1	4.5	8.8
$Re_d = \bar{u}_{o,avg}d/\nu_0$	7000	13900	20000	39200
$Re_t = \bar{u}'_{o,avg}\ell_{uo}/\nu_0$	200	390	560	1100
ℓ_k (μm)	58	35	27	16
ℓ_k/δ_L	3.4	2.1	1.6	0.9
L_o/d	1.7	2.6	3.3	5.3

[a]Hydrogen (99.95% purity)/air flames at a fuel-equivalence ratio of 1.8 and atmospheric pressure: d = 11 mm, ℓ_{uo} = 3.1 mm, S_L = 3.5 m/s, δ_L = 17 μm.

LIST OF FIGURES

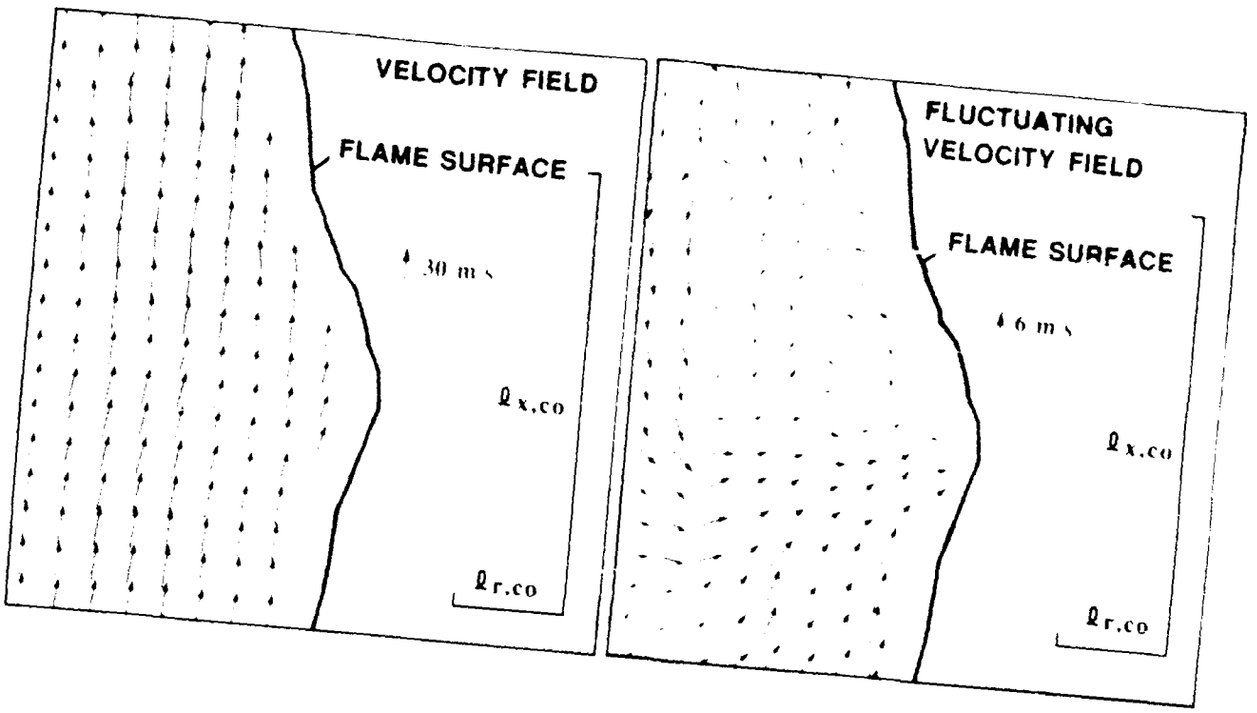
VELOCITY FIELD
FLAME SURFACE
30 m s
ℓx,co
ℓr,co
FLUCTUATING
VELOCITY FIELD
FLAME SURFACE
6 m s
ℓx,co
ℓr,co

Fig. 1

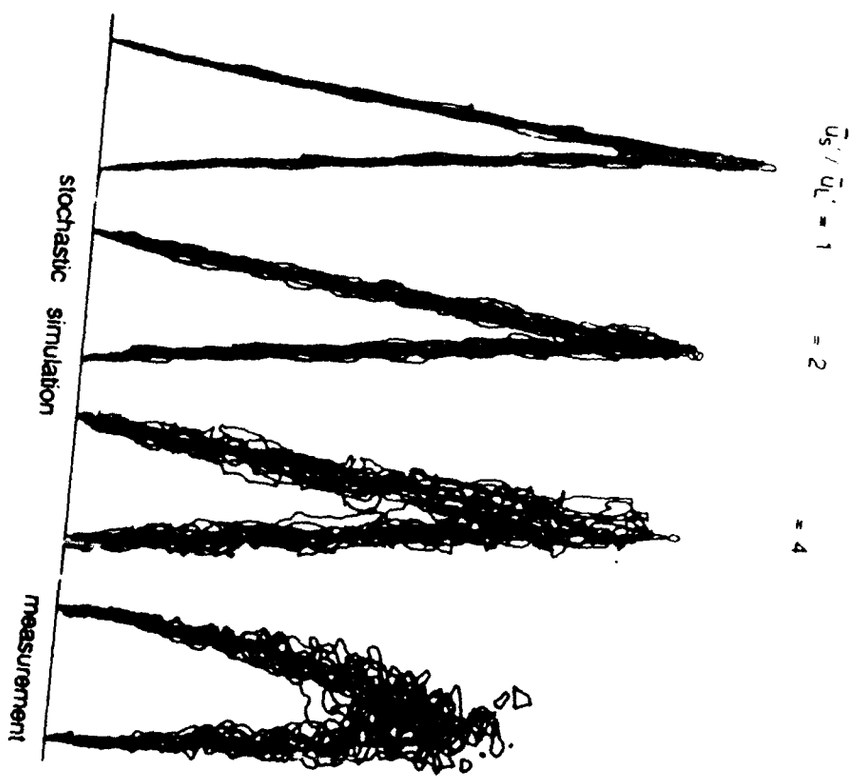
stochastic simulation
measurement
u's/u'L = 1
= 2
= 4

Fig. 2

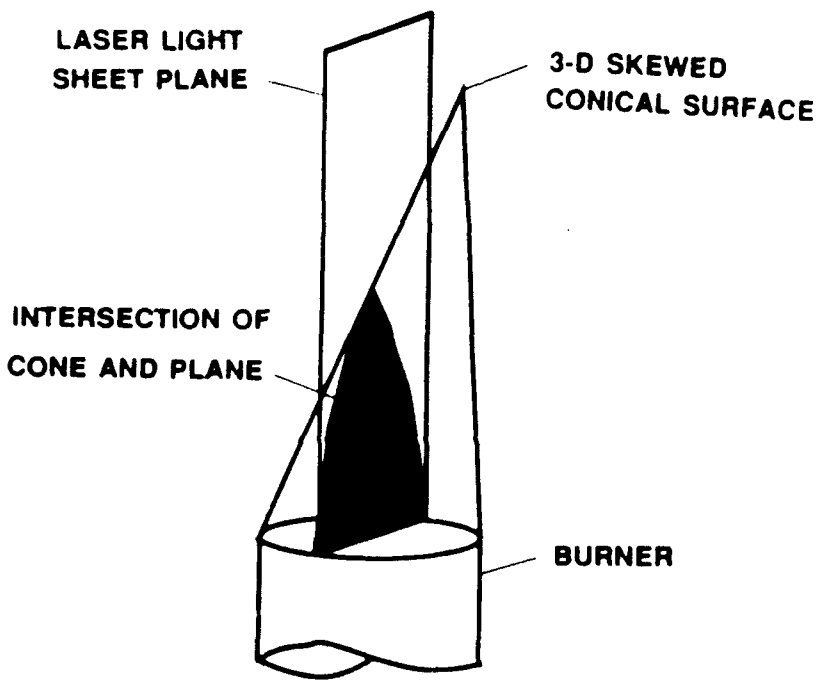
LASER LIGHT
SHEET PLANE
3-D SKEWED
CONICAL SURFACE
INTERSECTION OF
CONE AND PLANE
BURNER

FIG. 3

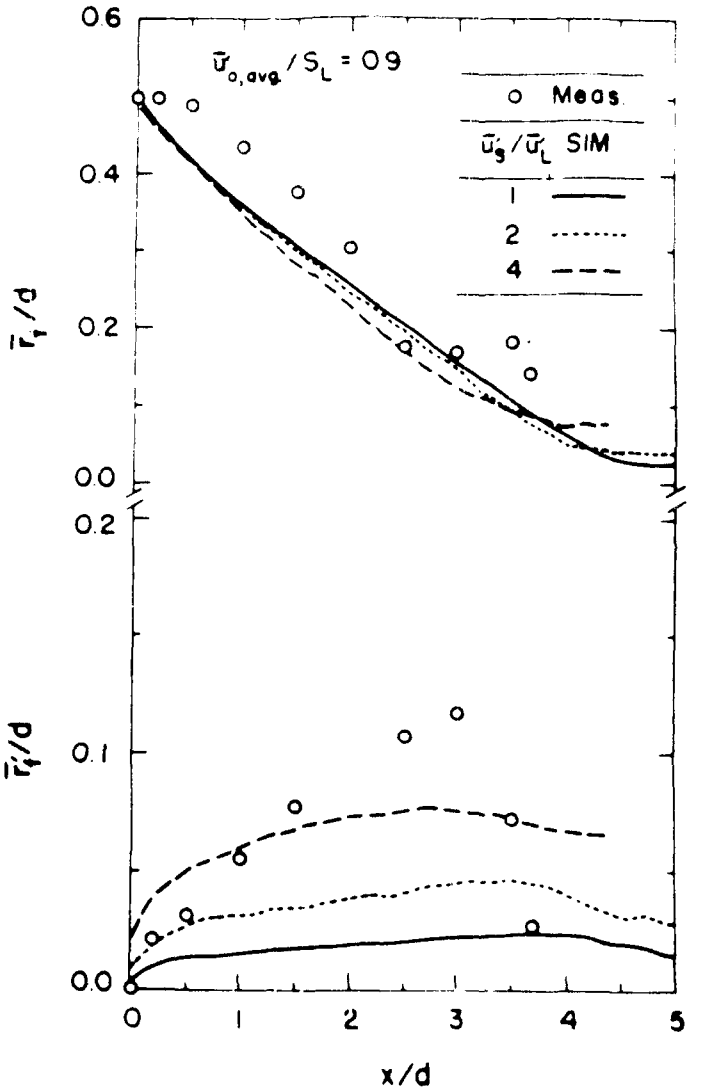
$\bar{u}_{o,avg}/S_L = 09$
o Meas.
$\bar{u}_g/\bar{u}_L$ SIM
1
2
4
$\bar{r}_f/d$
0.6
0.4
0.2
0.0
0.2
0.1
0.0
0
1
2
3
4
5
x/d

FIG. 4

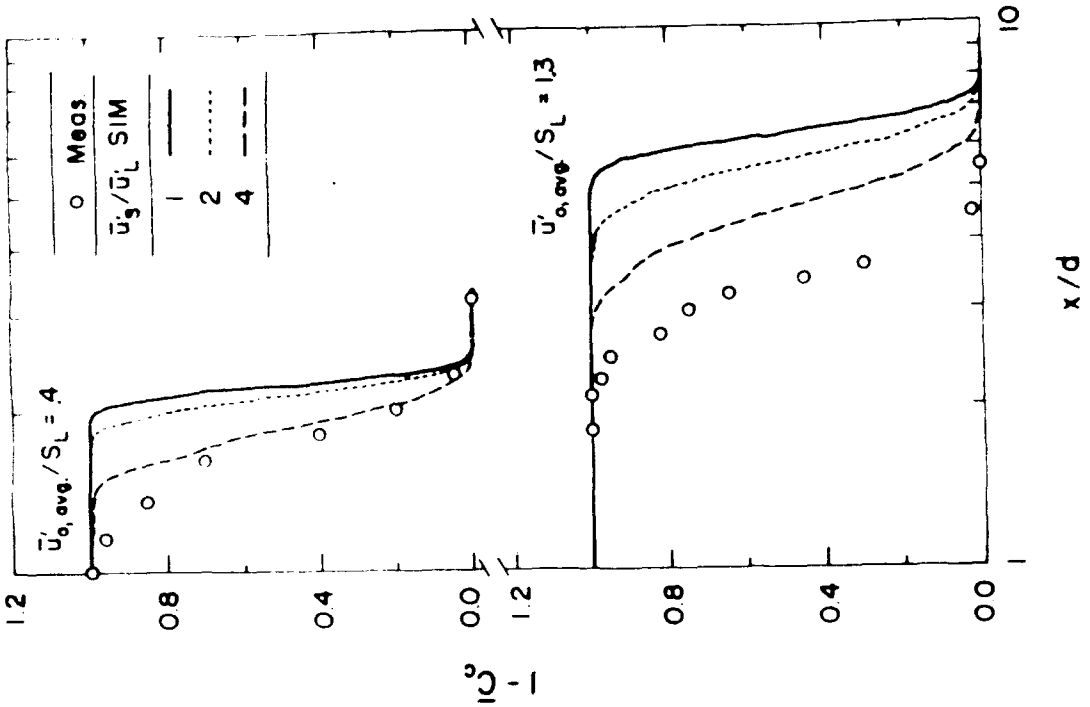
Meas.
$\bar{u}'_s/\bar{u}'_L$ SIM
1
2
4
$\bar{u}'_{o,avg}/S_L = 4$
$\bar{u}'_{o,avg}/S_L = 1.3$
1.2
0.8
0.4
0.0
10
x/d

Fig. 1 - 3

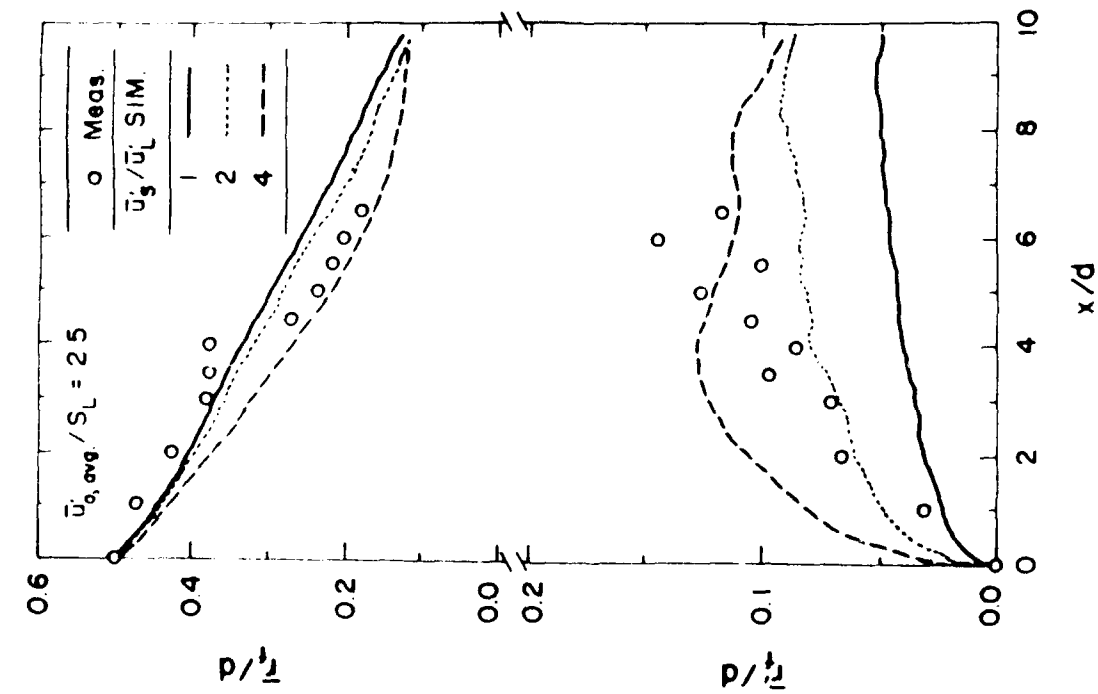
Meas.
$\bar{u}'_s/\bar{u}'_L$ SIM
1
2
4
$\bar{u}'_{o,avg}/S_L = 2.5$
0.6
0.4
0.2
0.0
0.2
0.1
0.0
$\bar{r}'_f/d$
$\bar{r}'_f/d$
0
2
4
6
8
10
x/d